University of Florida
Civil and Coastal Engineering

University of Florida
Civil and Coastal Engineering

Final Report **June 2008**

BEHAVIOR OF STANDARD HOOK ANCHORAGE MADE WITH CORROSION RESISTANT REINFORCEMENT

Principal investigator:
H. R. Hamilton III

Research assistants:
Gianni G. Ciancone
Antonis P. Michael

Department of Civil and Coastal Engineering
University of Florida
P.O. Box 116580
Gainesville, Florida 32611

Sponsor:
Florida Department of Transportation (FDOT)
Marcus H. Ansley, P.E. – Project Manager

Contract:
UF Project No. 00005766
FDOT Contract No. BD 545-40

DISCLAIMER

The opinions, findings, and conclusions expressed in this publication are those of the authors and not necessarily those of the State of Florida Department of Transportation.

Technical Report Documentation Page

1. Report No.	2. Government Accession No.	3. Recipient's Catalog No.

4. Title and Subtitle	5. Report Date
Behavior of Standard Hook Anchorage with Corrosion Resistant Reinforcement	June 2008
	6. Performing Organization Code
7. Author(s)	8. Performing Organization Report No.
G. G. Ciancone, A. P. Michael, and H. R. Hamilton III	00051711
9. Performing Organization Name and Address	10. Work Unit No. (TRAIS)
University of Florida Department of Civil & Coastal Engineering P.O. Box 116580 Gainesville, FL 32611-6580	11. Contract or Grant No. BD 545-40
12. Sponsoring Agency Name and Address	13. Type of Report and Period Covered
Florida Department of Transportation Research Management Center 605 Suwannee Street, MS 30 Tallahassee, FL 32301-8064	Final Report
	14. Sponsoring Agency Code

15. Supplementary Notes

16. Abstract

The objective of this study was to evaluate the behavior of standard hooks that are made using corrosion resistant reinforcement, which typically have higher yield and ultimate strengths than that of ASTM A615 Grade 60 reinforcement. Two steel types were evaluated in this research. The stainless steel was 316LN, which is a low-carbon austenitic stainless steel that has been nitrogen strengthened. The mechanical properties conformed to ASTM A955. The corrosion resistant bar was a low-carbon steel bar with chromium added and conformed to ASTM A1035. The impetus is that the current ACI/AASHTO equations for the development length of standard hooks do not directly address the use of high-strength steel bars that do not have a well-defined yield point or a relatively flat post-yield slope.

Hooked reinforcement is typically used to develop reinforcement in a relatively short distance and is usually associated with a nodal region of a strut and tie system. A test setup was devised that uses the strut and tie behavior of hooked anchorage to impose forces similar to those occurring in the structure. The specimen configuration and test setup were arranged to promote a splitting tension failure of the concrete in the plane of the hook, which is the typical behavior of hooked anchorage without ties. Single #5 and #7 bars were tested with either 90- or 180-deg standard hooks. Grade 60 reinforcement was first tested to ensure that the desired failure mode was achieved and that the ACI and AASHTO development length equations for hooks did indeed ensure that the reinforcement reached yield before the concrete failed. Stainless steel reinforcement with a yield strength over 100 ksi and corrosion resistant reinforcement with a yield strength over 120 ksi were also tested. Anchorage capacity ratios (ultimate load/specified yield load) were calculated for each of the specimens to determine the effectiveness of the development lengths. In addition, strain ductility ratios (strain at ultimate capacity/yield strain from bare bar tension test) were determined for each specimen to provide a basis for comparison. Finally, recommendations for adjusting the equation for hook development length were developed.

G17. Key Word	18. Distribution Statement
Development Length, Standard Hook, Anchorage Capacity, Bond Strength, Ductility, Stainless Steel Reinforcement	No restrictions. This document is available to the public through the National Technical Information Service, Springfield, VA, 22161

19. Security Classif. (of this report)	20. Security Classif. (of this page)	21. No. of Pages	22. Price
Unclassified	Unclassified	111	

Form DOT F 1700.7 (8-72) Reproduction of completed page authorized

ACKNOWLEDGMENTS

The authors would like to thank Florida Department of Transportation (FDOT) State Materials Office and Structural Lab for their support in materials testing and bar bending. Special thanks go to the University of Florida-Structural Laboratory personnel.

The authors would also like to thank VALBRUNA stainless steel, MMFX Technologies Corp, FLORIDA ROCK Industries, and BARSPLICE Products Inc. for their contributions to this research.

EXECUTIVE SUMMARY

The objective of this study was to evaluate the behavior of standard hooks that are made using corrosion resistant reinforcement, which typically have higher yield and ultimate strengths than that of ASTM A615 Grade 60 reinforcement. Two steel types were evaluated in this research. The stainless steel was 316LN, which is a low-carbon austenitic stainless steel that has been nitrogen strengthened. The mechanical properties conformed to ASTM A955. The corrosion resistant bar was a low-carbon steel bar with chromium added and conformed to ASTM A1035. The impetus is that the current ACI/AASHTO equations for the development length of standard hooks do not directly address the use of high-strength steel bars that do not have a well-defined yield point or a relatively flat post-yield slope.

Hooked reinforcement is typically used to develop reinforcement in a relatively short distance and is usually associated with a nodal region of a strut and tie system. A test setup was devised that uses the strut and tie behavior of hooked anchorage to impose forces similar to those occurring in the structure. The specimen configuration and test setup were arranged to promote a splitting tension failure of the concrete in the plane of the hook, which is the typical behavior of hooked anchorage without ties. Single #5 and #7 bars were tested with either 90- or 180-deg standard hooks. Grade 60 reinforcement was first tested to ensure that the desired failure mode was achieved and that the ACI and AASHTO development length equations for hooks did indeed ensure that the reinforcement reached yield before the concrete failed. Stainless steel reinforcement with a yield strength over 100 ksi and corrosion resistant reinforcement with a yield strength over 120 ksi were also tested. Anchorage capacity ratios (ultimate load/specified yield load) were calculated for each of the specimens to determine the effectiveness of the development lengths. In addition, strain ductility ratios (strain at ultimate capacity/yield strain from bare bar tension test) were determined for each specimen to provide a basis for comparison. Finally, recommendations for adjusting the equation for hook development length were developed.

TABLE OF CONTENTS

List of Figures

List of Tables

1 INTRODUCTION

Corrosion of steel reinforcement causes premature deterioration of concrete structures that are exposed to environments containing high chloride levels. Corrosion can drastically reduce the service life of the structure requiring costly repairs or even replacement early in the life of the structure. One potential solution that has been explored in recent years is to either treat the reinforcement with coatings such as zinc or epoxy or to use a corrosion resistant steel to manufacture the bar. Corrosion resistant steels tend to have higher yield and ultimate strength than that of ASTM A615 bars. They may also have different post-yield behavior.

Current concrete structural design specifications (ACI or AASHTO) do not clearly address the use of these materials. Furthermore, FDOT construction specifications limit bar reinforcement to ASTM A615, effectively limiting the specified yield strength to 60 ksi. Equations used to calculate the development length of standard hooks were developed using test data from ASTM A615 bars. These equations need to be evaluated to determine their applicability when used to calculate hook development lengths for high-strength and corrosion resistant steel bars.

2 LITERATURE REVIEW

This literature review covers the background of the current development length equations, which were based on ASTM A615 bars. It was found that limited research has been conducted dealing with the behavior of standard hook anchorages made with high-strength reinforcement.

2.1 HOOK BEHAVIOR AND GEOMETRY

The *AASHTO LRFD Bridge Design Specifications* (2004) (AASHTO) and *ACI Building Code Requirements for Structural Concrete* (2005) (ACI) are formulated to ensure that steel reinforcement will yield before the concrete crushes when the nominal strength of a reinforced concrete element is reached. Development of the yield strength of a reinforcing bar requires that a sufficient length of bond is available on both sides of the critical section where capacity is expected to occur. In locations where space is limited, insufficient length may be available to ensure full development. In these cases, it is common to bend the bar to form either a 90-degree or 180-degree hook. Figure 1 gives an example of one possible situation where a concentrated load is located near the end of a cantilever beam. The critical section for flexural strength is located at the face of the support. If the required straight development length is longer than the cantilever, then the bar would protrude from the concrete. The typical method to deal with this situation is to turn the bar down into the section, creating a 90-degree hook.

The required length to develop the hook is shorter due to the mechanical advantage provided by the concrete located along the inside radius of the bend. Figure 2 shows the normal bar stresses in a #7 90-degree hook as reported by Marques and Jirsa (1975). The stresses in the bar increase dramatically around the bend of the hook (from 13 ksi to 57 ksi), indicating that the bearing of the inside of the hook against the concrete provides a significant portion of the anchorage. These bearing stresses cause transverse tensile stresses, which can result in a splitting failure when confinement reinforcement is not present.

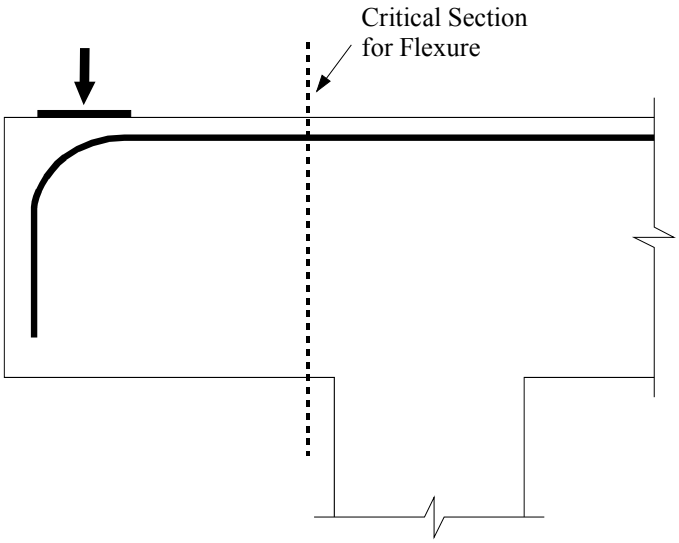

Figure 1. Hook used to develop bar in cantilever beam

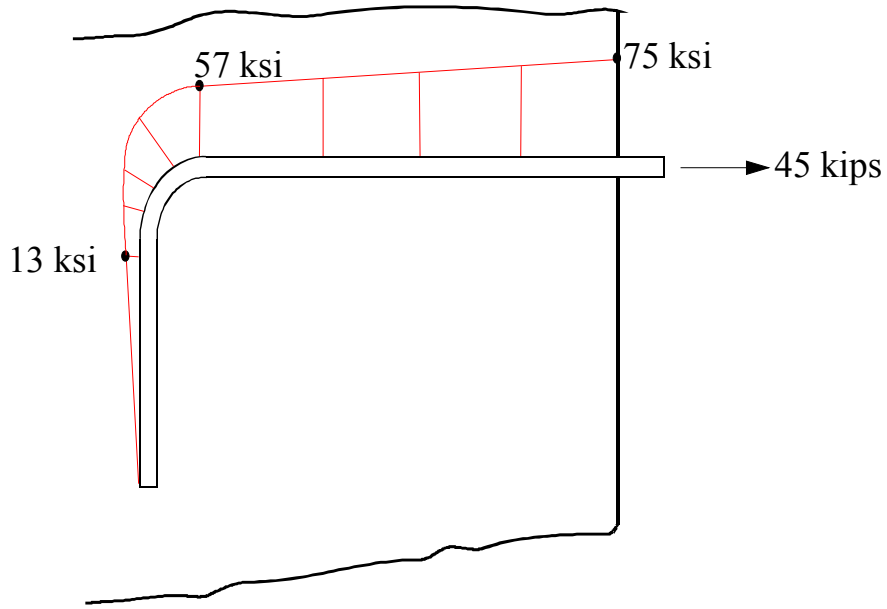

Figure 2. Tensile stresses in #7 bar with 90 deg. standard hook. (Marques and Jirsa (1975))

Standard bend radii and tail lengths are specified in AASHTO because the development length equation was derived empirically from test data. Figure 3 shows the dimensions for "standard hooks" that are the same in both ACI and AASHTO. The development length approach was first proposed by Pinc, Watkins, and Jirsa (1977). Table 1 shows the minimum hook dimensions proposed in this research.

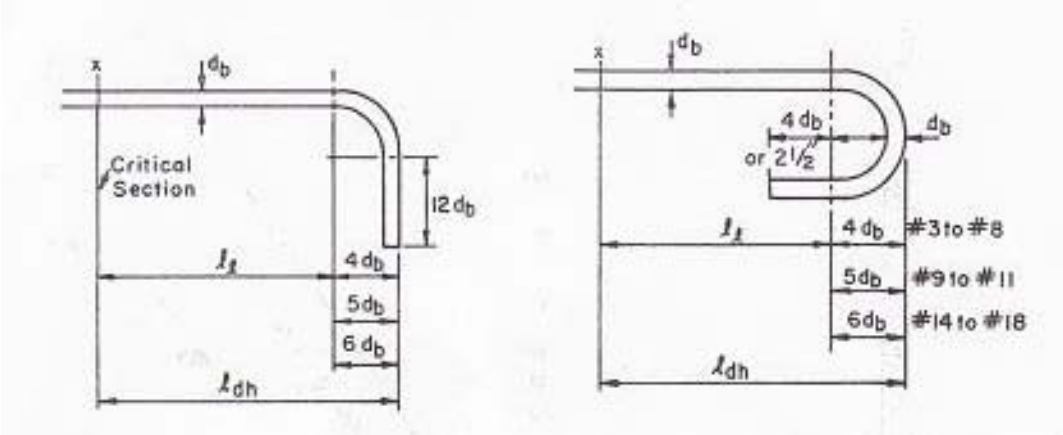

Figure 3. Standard hook details.

Table 1. Minimum dimensions for standard hooks.

Bar No.	d_b (in)	180 degree Diameter (in.) $6d_b$	180 degree Head (in.) $4d_b$	90 degree Extension (in.) $4d_b$	90 degree Tail (in.) $12d_b$	90 degree Ratio (in.) $3d_b$
5	0.625	3.75	2.50	2.50	7.50	1.88
7	0.875	5.25	3.50	3.50	10.50	2.625
16 mm	0.629	3.77	2.52	2.52	7.55	1.89
20 mm	0.787	4.72	3.15	3.15	9.44	2.36

2.2 CURRENT HOOK DESIGN PRACTICE

Standard hook anchorages are currently designed using the following equations:

$$l_{dh} = \frac{0.02\psi_e \lambda d_b f_y}{\sqrt{f_c'}} \qquad \text{Equation 1}$$

$$l_{dh} = \frac{38 d_b}{\sqrt{f_c'}} \frac{f_y}{60} \qquad \text{Equation 2}$$

where l_{dh} is the hook development length in in., ψ_e is the coating factor, λ is the lightweight aggregate concrete factor, d_b is the bar diameter in in., f'_c is the specified concrete strength in psi for Equation 1 and ksi for Equation 2, and f_y is the specified yield strength of the bar in psi.

Equation 1 is from ACI and Equation 2 is from AASHTO. These provisions were developed in the early 1970's and were finally implemented into the code in their present form in 1979.

Minor and Jirsa (1975) studied the factors that affect the anchorage capacity of bent deformed bars. Specimen geometry was varied to determine the effect of bond length, bar diameter, inside radius of bend, and angle included in the bend. Slip between the bar and the concrete was measured at several points along the bar as load was applied. Load-slip curves were used to compare different bar geometries. The results indicated that most of the slip occurred in the straight and curved portion of the hook, with little occurring in the tail.

Marques and Jirsa (1975) investigated the anchorage capacity of hooked bars in beam-column joints and the effect of the confinement on development. The variables included bar size, hook geometry, embedment length, confinement, and column axial load. Full scale beam-column specimen used #7 or #11 hooked bars made from ASTM A615 bars. Slip of the bar relative to the surrounding concrete was measured at five points along the anchored bar (see Figure 4). The slip measured on the tail of the hook was small in comparison with slip measured at 1H and 2H. The slip measured at the lead was greatest in most of the cases. Also, the slip at point (2H) was similar to the slip at point (1H) when the straight portion of the hook was short.

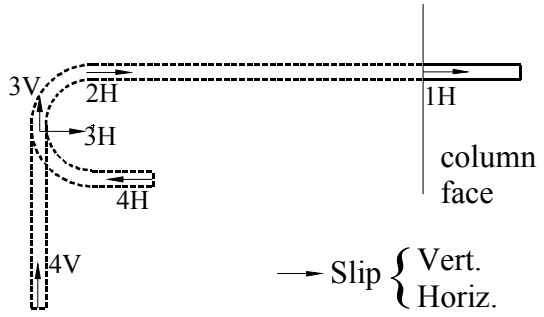

Figure 4. Points where slip was measured in research by Marques and Jirsa (1975).

Marques and Jirsa (1975) found that the equations from ACI 318-71 underestimated the anchorage capacity of the hooks. They found that for their test specimens the tensile stress in the bar when the bond capacity was reached was:

$$f_h = 700(1 - 0.3d_b)\psi\sqrt{f_c'} \qquad \text{Equation 3}$$

where f_h is the bar stress and can not be greater than f_y in psi, d_b is the diameter of the bar in in., f'_c is the average concrete strength in psi, and ψ is a coefficient factor which depends on the size of the bar, the lead straight embedment, side concrete cover and cover extension of the tail. It was also found that the straight lead embedment length (l_l) (shown in Figure 3) between the critical section and the hook could be expressed as follows:

$$l_l = [0.04 A_b (f_y - f_h) / \sqrt{f'_c}] + l' \qquad \text{Equation 4}$$

where l' is $4d_b$ or 4 in., whichever is greater, A_b is the bar area in sq. in., f_y the yield strength of the bar in psi, f_h the tensile stress of the bar in psi, and f'_c is the average concrete strength in psi.

Pinc, Watkins, and Jirsa (1977) also studied beam-column joints to determine the effect of lead embedment and lightweight aggregate concrete on the anchorage capacity of the hook. The first approach consisted in examining the hook and lead embedment separately. Variables $f_l/f'^{0.5}_c$ and l_l/d_b were correlated to obtain the lead embedment ultimate stress (f_l):

$$f_l = 67(l_l / d_b - 3)\psi\sqrt{f'_c} \qquad \text{Equation 5}$$

The bar stress at failure (f_u) can be obtained by summing Equation 3 and Equation 5 to obtain:

$$f_u = 550(1 - 0.4d_b + 0.8l_l / d_b)\psi\sqrt{f'_c} \qquad \text{Equation 6}$$

In an alternative approach the following equation resulted when the hook and lead length were examined together using $f_u/f'^{0.5}_c$ and l_{dh}/d_b:

$$f_u = 50\psi l_{dh}\sqrt{f'_c} / d_b \qquad \text{Equation 7}$$

An equation is needed that provides a length necessary to develop the yield stress in the bar (not ultimate stress). Consequently, f_y is substituted for f_u in Equation 7 and the equation is rearranged as follows:

$$l_{dh} = \frac{0.02 d_b f_y}{\psi \sqrt{f_c'}}$$ Equation 8

where l_{dh} represents the development length for a hooked bar in in. and is measured from the critical section to the back of the hook (Figure 3).

The ACI 408.1R-79 document presented recommendations for standard hook provisions for deformed bars in tension based on the study reported by Pinc, Watkins, and Jirsa (1977), and those recommendations were discussed and explained by Jirsa, Lutz, and Gergely (1979). Based on the research and discussions, ACI committee 408 recommended the following basic development length equation:

$$l_{hb} = \frac{960 d_b}{\phi \sqrt{f_c'}}$$ Equation 9

where l_{hb} represents the basic development length for a hooked bar in in., d_b is the diameter of the bar in in., f'_c is the average concrete strength in psi, and ϕ represents the factor for anchorage which was incorporated in the design equation. The basic development length (l_{hb}) is then modified by the following factors: f_y/60,000 for reinforcement having yield strength over 60,000 psi, 0.7 for side cover, 0.8 for use of stirrups, 1.25 for use of lightweight aggregate, and A_{sr}/A_{sp} for reinforcement in flexural members in excess of that required for strength.

Figure 5 shows a comparison between the development length proposed by ACI Committee 408 and the provisions that were then current in ACI 318-77. The proposed development length was computed as a linear function of the diameter of the bar. The development length from ACI 318-77 underestimated development lengths for #3 through #8 bars and overestimated for bars greater than #8 in comparison with the proposed.

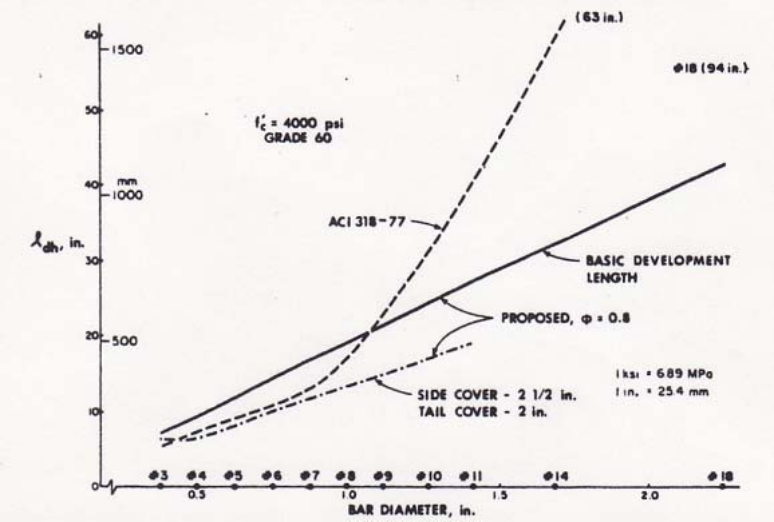

Figure 5. Comparison of hook provisions proposed by committee 408 with those in ACI 318-77.

ACI 318 adopted the recommendations by ACI Committee 408 and the development length equation and factors have not changed since that adoption in 1979. The epoxy-coated factor of 1.2 which was proposed by Hamad, Jirsa, and D'Abreu de Paulo (1993) was added in ACI 318-95.

Currently ACI hook development equation is:

$$l_{dh} = \frac{0.02\psi_e \lambda d_b f_y}{\sqrt{f'_c}} \qquad \text{Equation 10}$$

where ψ_e is the epoxy coated reinforcement factor, λ is the lightweight aggregate factor, d_b is the nominal bar diameter, f_y is the specified yield strength of the steel (psi), and $f'c$ is the specified compressive strength of the concrete (psi).

AASHTO requires the following hook development length:

$$l_{dh} = \frac{38.0 d_b}{\sqrt{f'_c}} \qquad \text{Equation 11}$$

where f'_c is the specified compressive strength of the concrete (ksi). An additional factor (fy/60) makes this equation identical to ACI's equation with the difference in the coefficient being due to the units conversion of f'_c under the radical. Further factors for cover, epoxy coating, and lightweight aggregate are also identical to ACI's factors.

2.3 STRUT AND TIE EVALUATION OF ANCHORAGE

Hooked reinforcement is typically required to provide anchorage for a tie in the disturbed region of a strut and tie system. The strut-and-tie method has been incorporated into the design specifications relatively recently. AASHTO adopted this method in 1994 and ACI included it as an alternative design method in 2002. Strut and tie analysis requires that the structural concrete system be idealized as a truss made up of a series of struts, ties, and nodal regions. The element is divided into B and D regions. The B-regions are based on the Bernoulli hypothesis which facilitates the flexural design of reinforced concrete structures by allowing a linear strain distribution for any loading stages (bending, shear, axial forces and torsional moments). D-regions (D for discontinuity, or disturbance) are portions of the element where the strain distribution is nonlinear. D-regions are typically characterized by geometrical discontinuities or concentrated forces.

Nodal regions connect struts and ties, requiring the transfer of large forces in relatively small areas. They are typically classified according to the sign of the forces. A C-C-C node represents three compressive forces, a C-C-T node represents two compressive forces and one tensile force, a C-T-T node represents two tensile forces and one compressive force, and a T-T-T node represents three tensile forces. Figure 6 shows a C-C-T node in which the external reaction and diagonal strut provide the two compressive forces. These are reacted by a tie composed of steel reinforcement that terminates in a standard hook. The length available to develop the hook (l_{dh}) is a function of the strut-and-tie geometry and is determined by finding the extended nodal zone. The anchorage provided by the hook must be of sufficient strength so that the yield strength of the bar is reached at the intersection of the extended nodal zone and the centroid of the tie. Figure 7 shows some examples of nodal regions in common structural elements that may contain standard hooks.

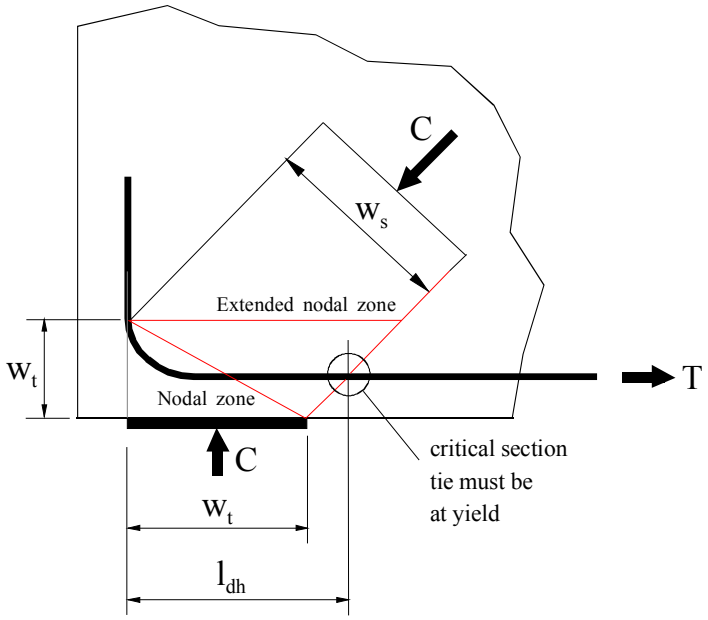

Figure 6. Extended nodal zone for standard hook anchorage.

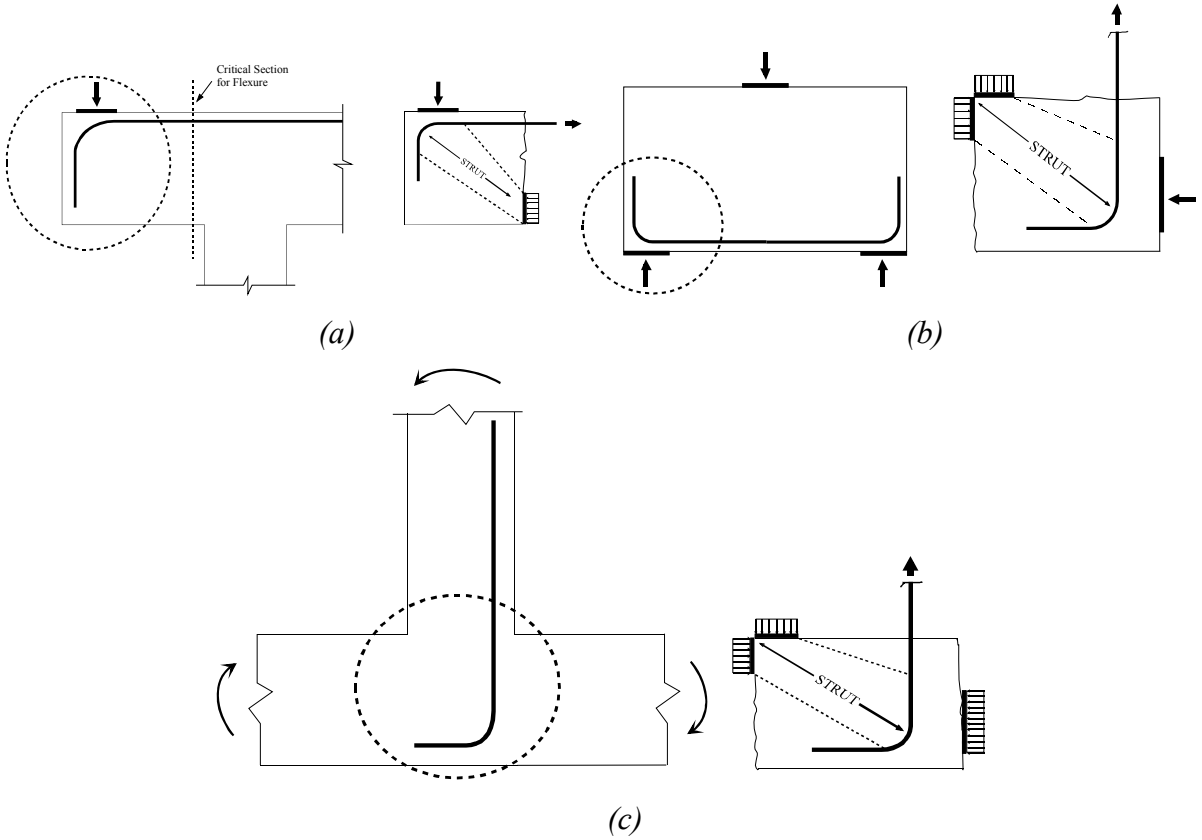

Figure 7. Schematic and strut and tie model of typical uses of a standard hook anchorage F.B.D (a) Pier Cap, (b) Deep Beam, and (c) Retaining Wall.

Although not explicitly addressed in their research, the beam-column specimen used for the original hook development research (Marques and Jirsa (1975)) can be modeled using the strut-and-tie approach. Figure 8 shows a free body diagram of the test specimen used in those tests. The region around the hooked bar can be modeled using strut and time. The reinforcement terminates in a C-C-T node where the compression reactions are provided by the eccentric axial force required to balance the couple created by tension in the bar. The distribution of this reaction is unknown.

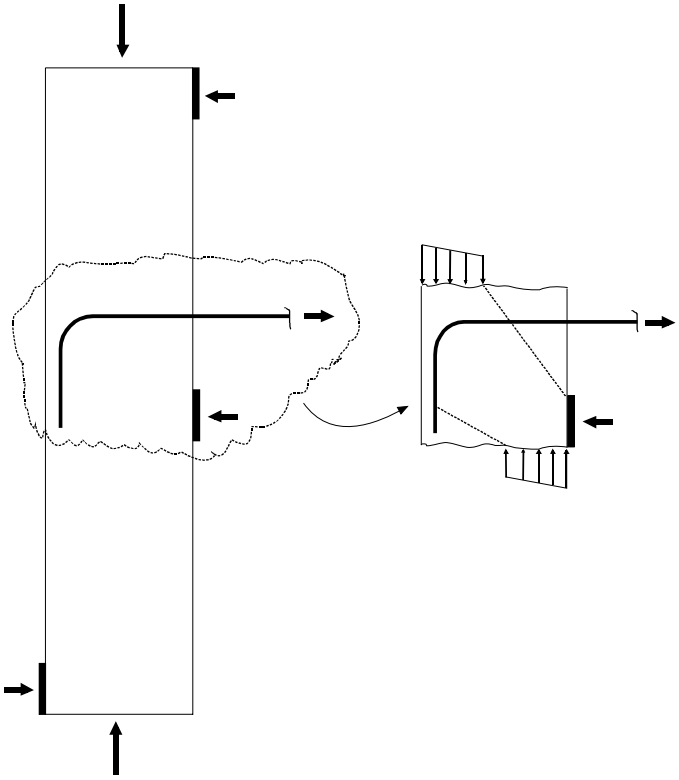

Figure 8. Specimen configuration and strut and tie model of specimen used in Marques and Jirsa (1975) research.

3 EXPERIMENTAL PROGRAM

The primary objective of the experimental program was to determine if the current development length equations would provide sufficient strength to ensure that the yield strength of the reinforcement was reached prior to failure of the concrete. Initially it was necessary to develop a test setup that gave agreeable results when testing ASTM A615 steel. Eventually a specimen taking advantage of the strut and tie modeling was chosen for this setup. Once this was complete then testing of unconfined specimens (with no transverse reinforcement) was conducted on A615 and high-strength steel bars to evaluate the efficacy of the development length equations.

3.1 SPECIMEN DESIGN

Initial testing was conducted with the specimen design shown in Figure 9a and b, which are denoted as unconfined and confined, respectively. The specimen configuration incorporated a single bar centered in a concrete block. The focus of this initial testing was to validate the test setup, specimen design, and loading configuration. Consequently, only ASTM A615 Grade 60 (hereinafter referred to as GR60) reinforcement was tested. Because the design complied with both design specifications, the expectation was that the specimens would be capable of reaching at least the yield strength of the GR60 reinforcement in both the confined and unconfined specimens. The test results, however, indicated that only the confined specimens could reach yield, but that the unconfined specimens were well below yield when the concrete failed. Furthermore, the failure was generally spalling of a corner section of concrete under the reaction at the outside of the hook, which was not the targeted splitting of the specimen in the plane of the hook.

The specimen configuration was then adjusted to simulate the strut and tie behavior of a hook in a C-C-T nodal region as shown in Figure 9c and d. The bearing over the hook was lengthened to ensure complete engagement of the bar over the design development length. It is likely that the bearing stress distribution varied along the length of the specimen as shown in the figure, but the setup did not allow this distribution to be determined quantitatively. This was not expected to affect the results significantly. Furthermore, any effect would likely be conservative since the provided development would be shortened due to the concentration of stresses near the

bend of the hook. The embedded portion of the bar beyond the design development length was debonded to ensure that only the bond under the bearing contributed to the hook development. The remainder of the testing was conducted with these two configurations using unconfined specimens.

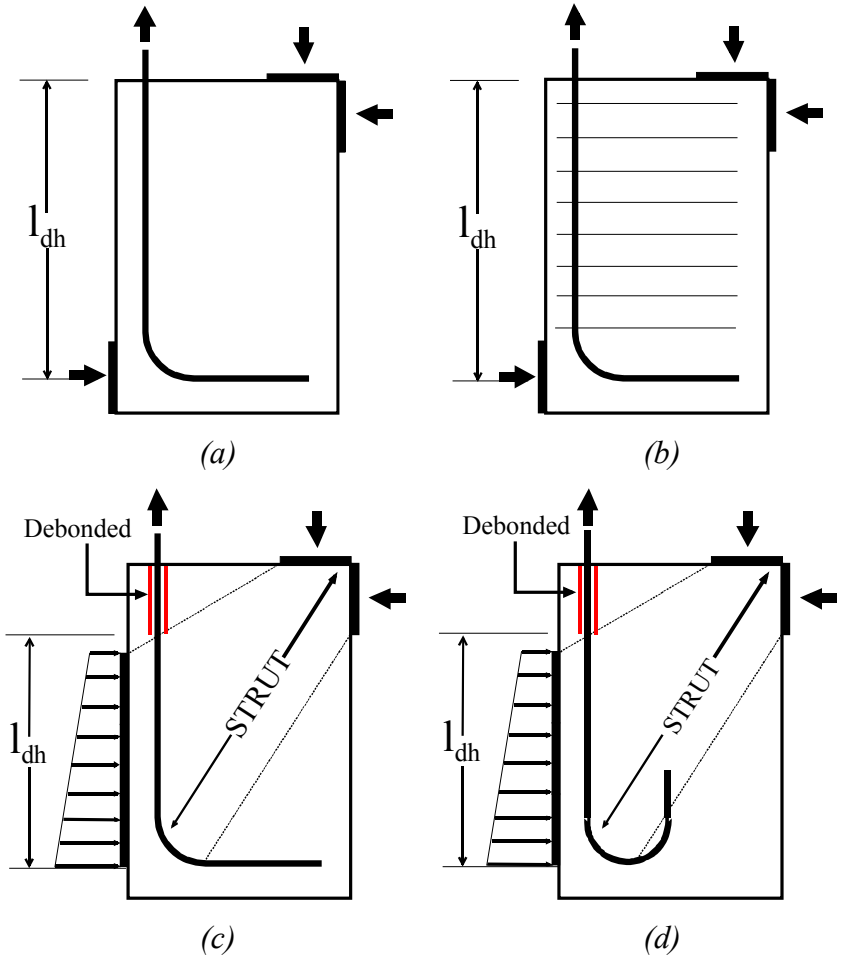

Figure 9. Specimen design with idealized boundary conditions (a) unconfined, (b) confined with stirrups, (c) 90 deg. hook, unconfined with debonded length, and (d) 180 deg. hook, unconfined with debonded length.

Forty eight specimens were cast and tested in five series, with each series representing the specimens cast with a single batch of concrete. The specimen details and testing configuration for the first series are given in Figure 10 and Table 2, which were designed to test GR60 steel. Clear cover and stirrup spacing complied with both AASHTO and ACI. The specimens were designed with side cover and cover on bar extension beyond hook not less than 2-1/2 in and 2 in., respectively. Confined specimens used #3 stirrups spaced at 1.88 or 2.63 in.

along the development length of the hook. This configuration was abandoned in favor of the strut and tie design used in series 2 through 5.

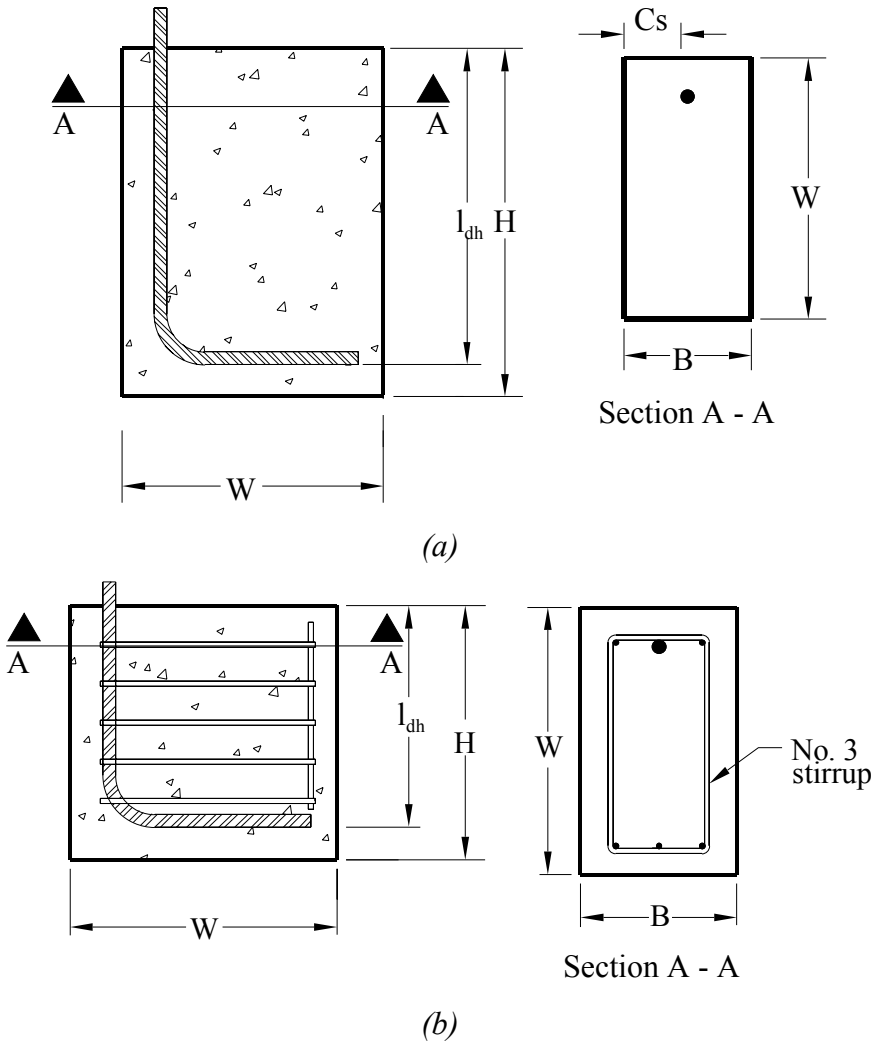

Figure 10. Specimen design details for series 1: (a) unconfined specimen details and (b) confined specimen details.

Table 2. Specimen design details for Series 1.

Specimen	W (in)	H (in)	B (in)	l_{dh} (in)
60_5_90_S	14.5	8.5	10	6
60_5_90_1	14.5	10.5	10	8
60_7_90_S	18.5	11.5	10	9
60_7_90_1	18.5	13.5	10	11

The remaining four series are detailed in Figure 11 and Table 3 and also complied with both AASHTO and ACI for clear cover. The specimen naming convention is as follows. The first term represents the type of steel where **60** indicates ASTM A615 Grade 60, **SS** indicates stainless steel, and **MM** indicates MMFX bars. The second term represents the bar size, #**5**, #**7**, **16** mm or **20** mm. The third term represents the hook bend angle of **90** or **180** degrees. The fourth term represents the strut angle **25**, **35** or **47** degrees, and the last term represents the replicate number.

The metric designation of the stainless steel bars was retained because they were manufactured in Italy under "hard" metric sizes. The 16 mm diameter and area are very near that of a U.S. Customary #5, the 20 mm has slightly smaller diameter and respective area than that of a #7.

The tables describe the specimen geometry including the development length of the hooked bar as measured from the back edge of the hook. The strut angles shown in the tables are a function of the specimen geometry and were varied in series 3 to determine the effect of the strut angle on the hook capacity. Results from series two indicated some minor differences in behavior between the two strut angles. The difference in strut angle, however, did not appear to have a significant effect on the specimen capacity. Therefore, a strut angle of 35 deg. was selected for use in series four and five.

Finally, because of the failure of SS and MM specimens to develop in earlier series the development lengths of the specimens in the later series were increased to determine if the bars could be developed.

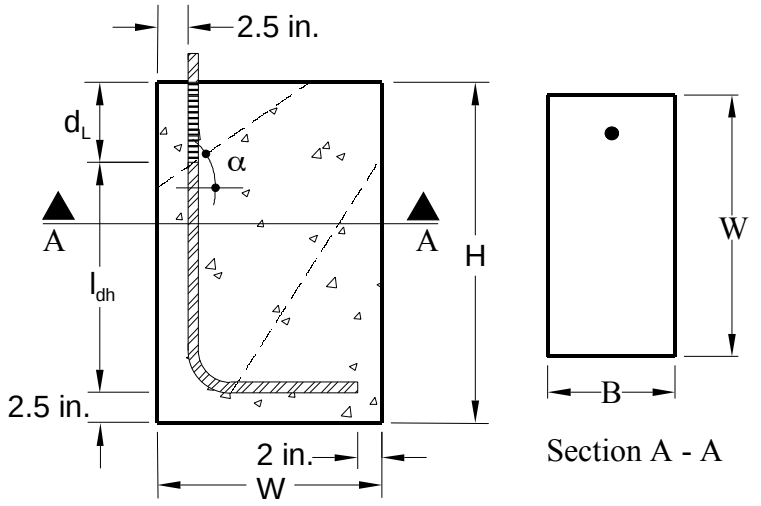

(a)

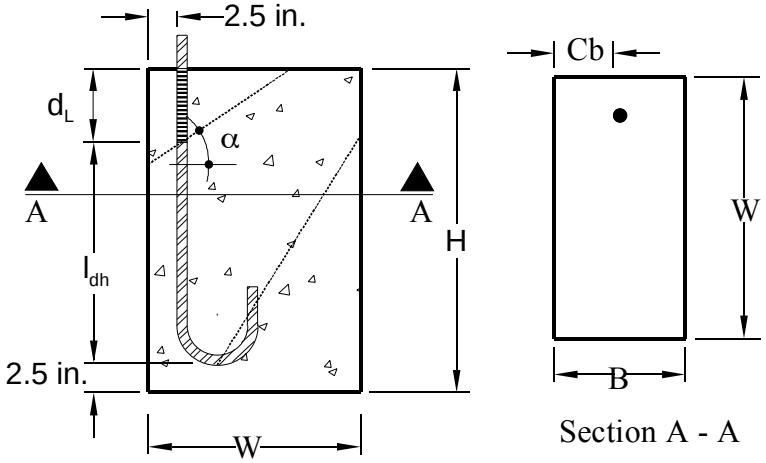

(b)

Figure 11. Specimen design for series 2 through 5: (a) unconfined specimen details for 90 degree bend and (b) unconfined specimen details for 180 degree bend.

Table 3. Specimen design details for series 2 through 5.

Series Number	Specimen	W (in)	H (in)	B (in)	α (deg.)	l_{dh} (in)	d_L (in)
Two	60_5_90_25_1	14.5	12.1	10	25	7	2.60
	60_5_90_25_2	14.5	12.1	10	25	7	2.60
	60_7_90_47_1	18.5	22.8	10	47	10	10.30
	60_7_90_47_2	18.5	22.8	10	47	10	10.30
Three	SS_16_90_25_1	14.5	17.1	10	25	12	2.60
	SS_16_90_25_2	14.5	17.1	10	25	12	2.60
	SS_16_90_35_1	14.5	18.4	10	35	12	3.90
	SS_16_90_35_2	14.5	18.4	10	35	12	3.90
	MM_5_90_25_1	14.5	19.1	10	25	14	2.60
	MM_5_90_25_2	14.5	19.1	10	25	14	2.60
	MM_5_90_35_1	14.5	20.4	10	35	14	3.90
	MM_5_90_35_2	14.5	20.4	10	35	14	3.90
	MM_7_90_25_1	18.5	27	10	25	20	4.50
	MM_7_90_25_2	18.5	27	10	25	20	4.50
	MM_7_90_35_1	18.5	29.1	10	35	20	6.60
	MM_7_90_35_2	18.5	29.1	10	35	20	6.60
Four	SS_16_180_35_1	14.5	17.4	10	35	11	3.90
	SS_16_180_35_2	14.5	17.4	10	35	11	3.90
	SS_16_180_35_3	14.5	18.4	10	35	12	3.90
	SS_16_180_35_4	14.5	18.4	10	35	12	3.90
	MM_5_180_35_1	14.5	18.4	10	35	12	3.90
	MM_5_180_35_2	14.5	18.4	10	35	12	3.90
	MM_5_180_35_3	14.5	20.4	10	35	14	3.90
	MM_5_180_35_4	14.5	20.4	10	35	14	3.90
	MM_7_180_35_1	18.5	26.1	10	35	17	6.60
	MM_7_180_35_2	18.5	26.1	10	35	17	6.60
	MM_7_180_35_3	18.5	29.1	10	35	20	6.60
	MM_7_180_35_4	18.5	29.1	10	35	20	6.60
Five	60_5_180_35_1	14.5	13.4	10	35	7	3.90
	60_5_180_35_2	14.5	13.4	10	35	7	3.90
	60_7_180_35_1	18.5	18.0	10	35	9	6.60
	60_7_180_35_2	18.5	18.0	10	35	9	6.60
	60_7_180_35_3	18.5	19.0	10	35	10	6.60
	60_7_180_35_4	18.5	19.0	10	35	10	6.60
	SS_20_90_35_1	17.0	21.1	10	35	13	5.60
	SS_20_90_35_2	17.0	21.1	10	35	13	5.60
	SS_20_90_35_3	17.0	22.1	10	35	14	5.60
	SS_20_90_35_4	17.0	22.1	10	35	14	5.60
	SS_20_180_35_1	17.0	21.1	10	35	13	5.60
	SS_20_180_35_2	17.0	21.1	10	35	13	5.60
	SS_20_180_35_3	17.0	22.1	10	35	14	5.60
	SS_20_180_35_4	17.0	22.1	10	35	14	5.60
	MM_7_90_35_3	18.5	29.1	10	35	20	6.60
	MM_7_90_35_4	18.5	29.1	10	35	20	6.60

3.2 CONCRETE MIXTURE DESIGNS

Five concrete batches were used to construct each of the five series. The batch for the first series was prepared at Florida Department of Transportation State Materials Office (SMO) in Gainesville, and the last four batches were prepared by Florida Rocks Industries, a local ready-mix concrete supplier. The concrete mixture proportions per cubic yard are shown in Table 4. All mixtures used a crushed limestone coarse aggregate with a maximum size of 3/8-in. (#89) and silica sand fine aggregate.

The size of the first batch was nine cubic feet (0.25 cubic meters), and for the last four batches was 81 cubic feet (2.29 cubic meter) per batch. Air-entrained admixture and high-range water reducer were included in the mixture proportions. The water to cement ratio was reduced in the last four batches by using a high-range water reducer (superplasticizer) obtain high concrete strengths at early age (14 days). Air-entraining admixture was also used to improve the workability of the concrete. The volume of concrete used in each batch included the specimens, extra examples and concrete for quality control testing.

About twenty standard cylinders 6 x 12-in (152 x 305-mm) were cast at the same time as the specimens, and vibrated in two layers by means of a vibrating table. The cylinders were cured at room temperature and under the same condition as the specimens for each concrete batch. Compressive tests were performed in accordance with the Standard Test Method for Compressive Strength of Cylindrical Concrete Specimens (ASTM C39–01). All cylinders were loaded at a load rate of 35 pound square inch per second to failure. The maximum load obtained from the universal testing machine was used to calculate the maximum compressive strength.

Table 4. Concrete mixture proportions (quantities are per cubic yard).

Materials	Series and Mixing Dates				
	1 2/1/2007	2 3/9/2007	3 4/9/2007	4 5/9/2007	5 6/8/2007
water/cementitious materials ratio (w/cm)	0.44	0.28	0.22	0.23	0.22
Cement (lb)	513	512	702	668	680
Fly Ash (lb)	145	145	145	152	150
Water (lb)	290	184	184	189	185
Fine Aggregate (lb)	1557	1607	1527	1527	1527
Coarse Aggregate (lb)	1309	1347	1360	1360	1360
Air-entrained (oz)	6.6	4.33	1	1.33	1
Admixture (oz)	39.5	100	156	155	155
Slump (in.)	5	7.5	7.5	8	7.25

3.3 SPECIMEN CONSTRUCTION

The formwork design, shown in Figure 12, consisted of a base, two side forms, one front form, one back form, and two 2 x 4 pieces. The front and back forms were kept between the side forms to allow adjustment in the specimen length. This flexibility in the specimen length allowed the formwork to be reused for differing specimen configurations. The front form was built in two pieces to ease bar placement. Three pieces of 2 x 4 were attached below the base to allow forms to be moved either with the crane or the forklift. The long pieces of plywood were clamped together with two 2 x 4 and two threaded rods. The 2 x 4 braces maintained the shape of the forms and dimensions of the specimen. The forms were sealed with a water-based adhesive caulk.

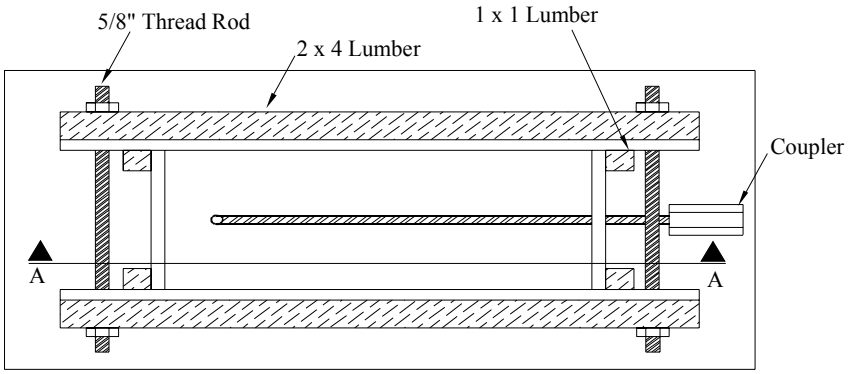

(a)

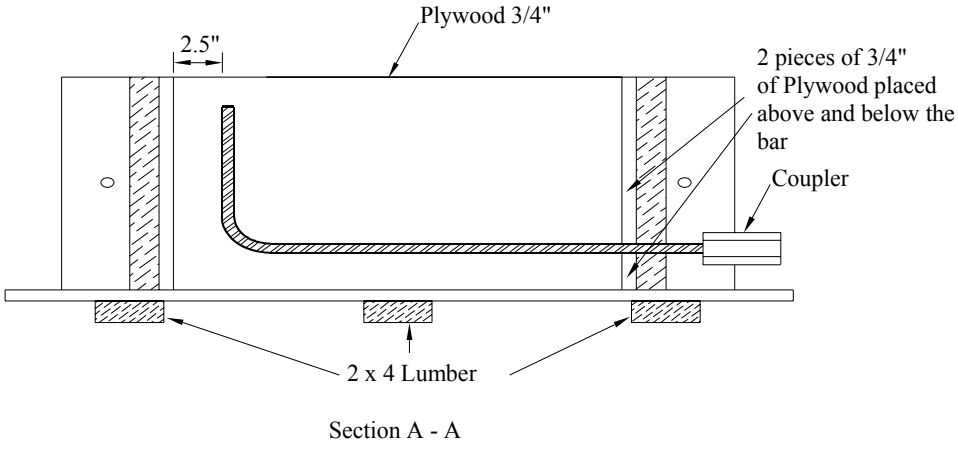

(b)

Figure 12. Formwork for casting specimens (a) plan view, and (b) section.

Figure 13. Photo of formwork ready for concrete placement.

Four specimens were cast in series one and two, twelve specimens in series three and four, and sixteen specimens in series five. All specimens were cast with the bar placed in the bottom of the forms with the tail of the bend pointed upward (see Figure 12b and Figure 13). A thin wire was attached to the side forms and to the tail of the hook to hold the bar level, and to maintain the side cover required. The debonded part of the bar was composed of a plastic tube which was sealed with electric tape to prevent cement paste from entering the tube.

Since most of the formwork was placed inside of University of Florida-Structural Laboratory, the concrete from the ready mix truck was poured directly to a galvanized steel container, which was then moved near the formwork (see Figure 14).

Figure 14. Ready-mixed concrete being discharged into the container for transporting.

To ensure that the instrumentation and bar position were not disturbed, concrete was delivered to the forms from the container by hand (see Figure 15a). Each specimen was cast in two lifts, which were compacted using mechanical vibrators. As concrete was placed in the forms, standard 6x12-in (152 x 305-mm) cylinders were cast, and also vibrated in two layers. Once finished with the casting procedure, the top surfaces of the specimens were smoothed with

a finishing trowel (see Figure 15b). Finally, a plastic sheet was placed over the specimens to minimize the evaporation of the water (see Figure 16). The specimens and cylinders were left to cure in the same environment until they were tested.

(a) *(b)*

Figure 15. Casting and compaction of the specimen (a), and finishing of specimens (b).

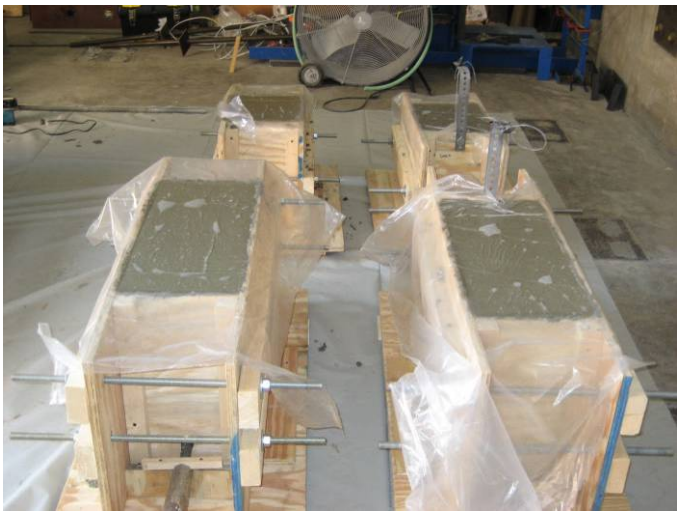

Figure 16. Curing of the specimens.

3.4 TEST SETUP

Figure 17 shows the test frame used to test all of the specimens. The concrete block was oriented in the frame to allow the bar to be tensioned vertically using a threaded rod inserted into the coupling on the reinforcing bar. A structural steel tube was placed between the frame and

block to react the vertical tension force. Rotation was restrained by the vertical portion of the frame.

The test frame was constructed with back-to-back structural channels. Each two structural channels were connected and stiffened by 0.5-in. thick plates. Back-to-back channels (C15x40) were connected to form a 90 degree frame. Each end of the frame was then welded to C12x30 shapes, which were attached to the strong floor and wall. Stiffeners were added to stiffen the frame against the heavy concentrated loads from the specimen (see Figure 17a, and Figure 17c).

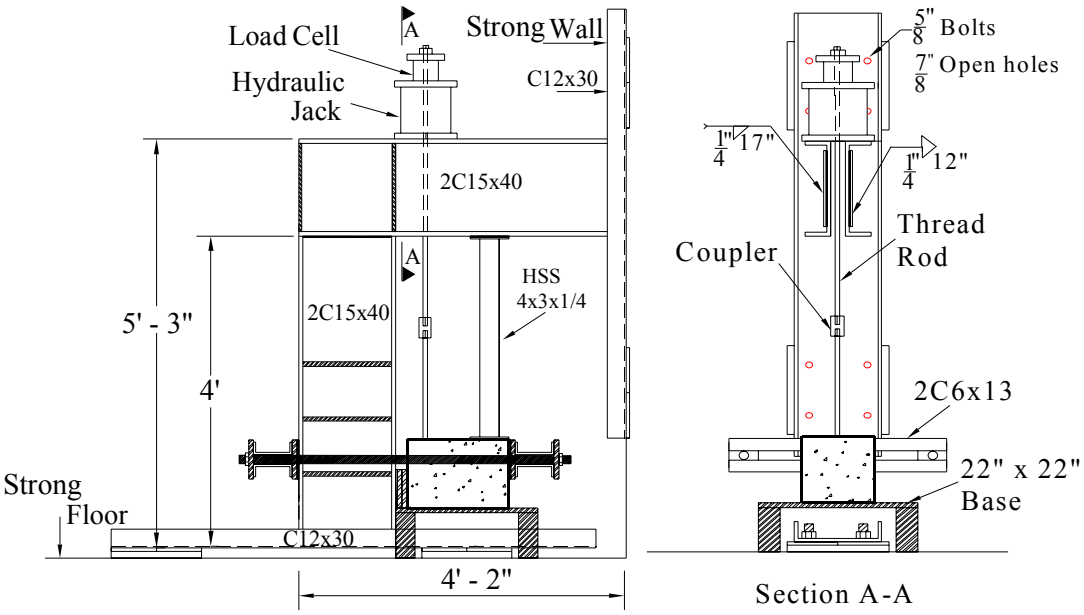

(c)

Figure 17. Load test setup (a) elevation, (b) section, and (c) photo.

After fabrication, the test frame was connected to the strong wall and floor by means of eight 5/8” bolts, and eight 1-1/4-in. diameter bolts respectively (see Figure 17b). The specimen was supported by a 22 x 22-in. steel base. Tension was applied to the bar extension by means of a center hole hydraulic jack. The threaded rod passed through the 2C15x40 beam, and the center hole hydraulic jack (see Figure 17b). A swaged coupler system was used to connect the anchored bar to a threaded rod (see Figure 18). This load was reacted with a strut placed between the specimen and the horizontal member of the reaction frame. The moment generated by the couple was reacted horizontally with the vertical member of the reaction frame. The reaction on the left face of the specimen shown in Figure 19 was distributed over the development length of the hook. The remaining portion above the bar was debonded to ensure that only the portion of the hook under the reaction contributed to the bar development.

Figure 18. Swaged coupler system.

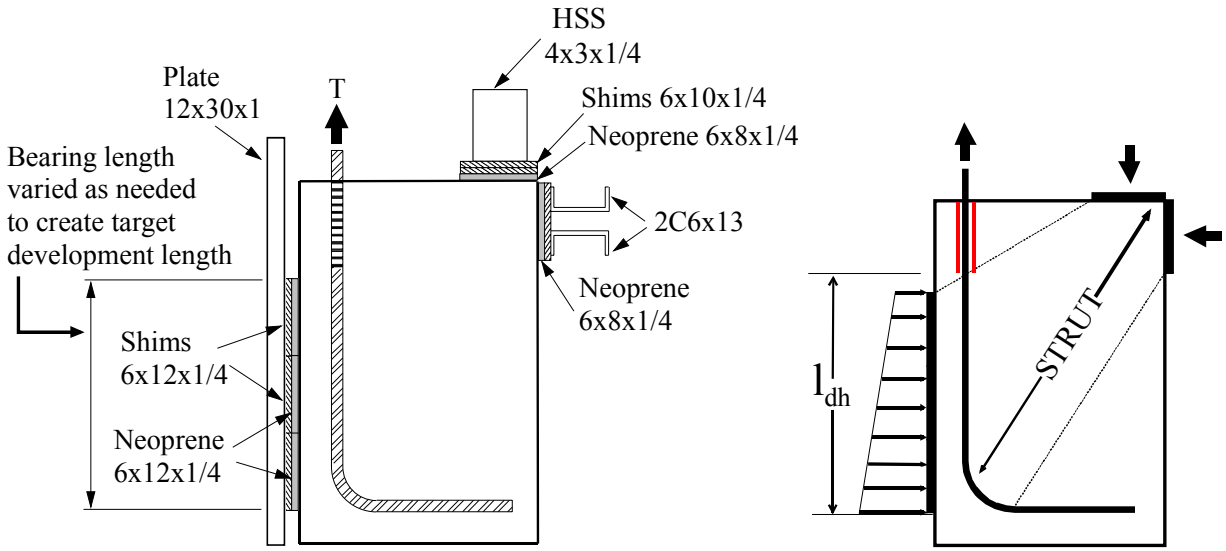

Figure 19. Details of support conditions.

3.5 DATA ACQUISITION SETUP

Relative slip between the bar and the concrete was measured by modifying a technique developed and used by Minor and Jirsa (1975). Figure 20 shows the locations along the hook where relative slip was measured. Location 1 was at the loaded end and location 2 was at the beginning of the bend. A 0.0625 in. diameter hole was drilled in the hooked bar. A 0.016 in. diameter wire was attached to the anchored bar at points 1 and 2 by inserting part of the wire to the ¼-in deep holes and securing with a small brass screw. The wire was placed inside of a thin plastic conduit of 0.042 in. diameter along the entire length in order to prevent bonding and to allow free movement of the wire relative to the surrounding concrete.

Figure 20. Positioning of slip wire in hooked bar.

The conduit containing the wire was extended from the bar attachment point through the concrete and exited the specimen on the side opposite to the straight portion of the bar. The exposed conduit and wire was then connected to a linear pot placed in a 1 x 1-in. frame (see Figure 21b). The linear pots were used to measure the relative movement between the wire and the conduit, which is nearly a direct measure of the relative movement of the bar and concrete at attachment point of the wire. Bar displacement was also measured relative to the top side of the specimen using a linear pot clamped to the bar (see Figure 21a, Figure 22). The purpose of this linear pot was to measure the strain of the debonded portion of the bar and any slip that might occur before failure.

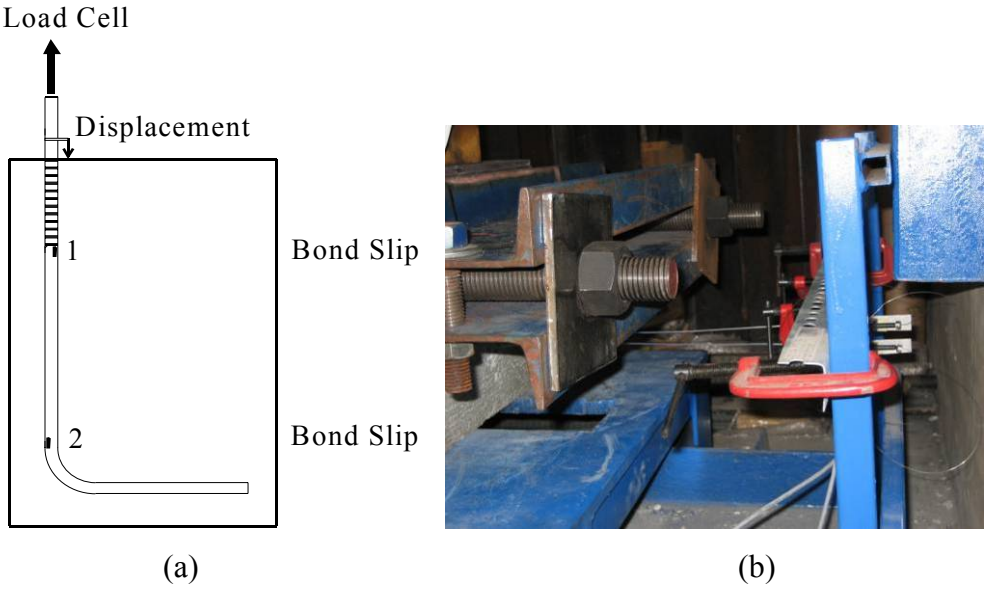

Figure 21. Bond slip instrumentation (a) displacement and slip position, (b) linear potentiometers.

Figure 22. Linear potentiometer placement to measure bar strain.

The data acquisition system consisted in a LabView virtual instrument which was programmed to read and record data points from linear pots, and a load cell (Figure 23).

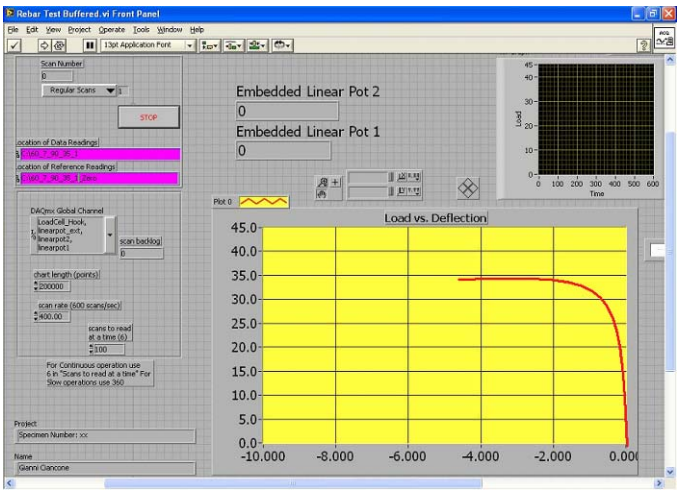

Figure 23. Data acquisition system.

4 RESULTS AND DISCUSSION

4.1 MATERIAL PROPERTIES

About twenty standard cylinders 6 x 12-in (152 x 305-mm) per batch were tested in accordance with the Standard Test Method for Compressive Strength of Cylindrical Concrete Specimens (ASTM C39–01). Pull-out specimens and companion cylinders were cured uncovered in the laboratory to ensure similar curing conditions. Companion cylinder tests were conducted each day that pull-out tests were conducted to determine the concrete strength for that particular test within a 24-hour window. The cylinder strength data are included with the pull-out test results later in this section. For reference, the average of these compressive strengths for each batch is shown in Table 5. The first batch was mixed at Florida Department of Transportation State Materials Office (SMO) in Gainesville, and the last four batches were delivered by Florida Rock Industries, a local ready-mix concrete supplier. Compressive strengths were tested after 7, 14, 21, and 28 days of continuous lab cured for all the concrete mixes (see APPENDIX A).

Table 5. Average concrete compressive strength of each series.

	Series				
	1	2	3	4	5
Average Concrete Strength	5700	5520	6500	6180	6070
Coefficient of Variation (%)	4.8	3.8	3.3	3.4	3.7

Samples of each bar type were tested in accordance with ASTM A370 at Florida Department of Transportation State Materials Office (SMO) in Gainesville. Two samples were tested for each bar size and steel type. The load rate used was 0.20 inches per minute per in. of distance between the grips (in/min/in) until the yield point was reached. After yielding, the rate was adjusted to 3.5 in/min/in until bar rupture occurred.

ACI indicates that for bars exceeding a specified yield strength of 60 ksi (413 MPa), the yield strength is to be determined using the stress corresponding to a 0.35% strain. The 0.2% offset method (ASTM A370), however, is more generally applicable to high-strength steel that does not have a well-defined yield point. Consequently, for the SS and MM bars that do not have well-defined yield points, the 0.2% offset method (illustrated in Figure 24) was used in lieu

of the 0.35% strain method. Data gathered during tension tests included strain at 0.2% offset, load at 0.2% offset, and ultimate strength. Complete tension test results are given in Appendix A.

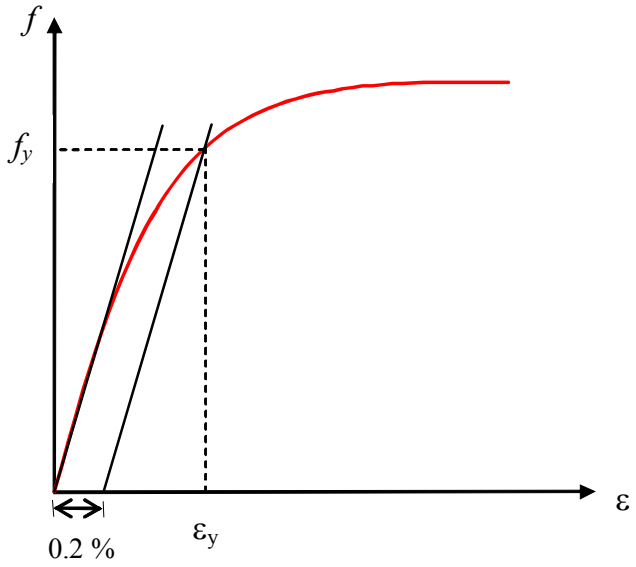

Figure 24. Stress-strain curve of steel with no well-defined yield point.

Grade 60 Steel

All GR60 bars were purchased locally at a building supply center and were thought to be from the same heat. As will be discussed later, test results for the specimens with #5 bars indicated that there may have been different heats in the batch of reinforcement tested. Table 6 shows the average results for the bar tests. The two samples of each size exceeded the GR60 requirements of minimum yield strength (60 ksi) and tensile strength (90 ksi).

Table 6. Tension test results for GR60 reinforcement.

Samples		Yield Strength at 0.35% strain (ksi)	Strain at 0.35% yield (in/in)	Load at 0.35% (kip)	Ultimate Strength (ksi)
#5	Ave.	62.8	0.00350	19.5	104.7
	COV (%)	< 1	< 1	< 1	< 1
#7	Ave.	63.7	0.00350	38.2	105.9
	COV (%)	< 1	< 1	< 1	< 1

Stainless Steel

The stainless steel 316LN bars were manufactured in Italy and were provided by Valbruna Stainless Steel. Table 7 shows the measured properties of the reinforcement. After testing was initiated it was noted that the 16 mm bars had two heats of steel, which are noted in the table. The yield and tensile strengths measured complied with the minimum yield strength of 75 ksi and minimum tensile strength of 100 ksi required for ASTM A955 and Valbruna product specifications.

Table 7. Tension test results for stainless steel (316LN) bars.

Samples		Yield Strength at 0.2% offset (ksi)	Strain at 0.2% offset yield (in/in)	Load at 0.2% offset (kip)	Ultimate Strength (ksi)
16 mm (0.625 in) Heat 1	Ave.	91.0	0.00555	28.2	114
	COV (%)	3	1	3	1
16 mm (0.625 in) Heat 2	Ave.	106	0.00615	32.9	124
	COV (%)	< 1	1	< 1	< 1
20 mm (0.787 in)	Ave.	100.8	0.0061	49.1	120
	COV (%)	< 1	3	< 1	< 1

MMFX Steel

The MMFX bars were provided by MMFX Steel Corporation of America. Table 8 shows the tested properties of the bars used in the specimens. The yield strength measured in the two samples of each size exceeded and complied with the minimum yield strength of 100 ksi and ultimate strength of 150 ksi required by ASTM A1035.

Table 8. Tension test results for MMFX bars.

Samples		Yield Strength at 0.35% strain (ksi)	Strain at 0.35% yield (in/in)	Load at 0.35% (kip)	Ultimate Strength (ksi)
#5	Ave.	122.4	0.00649	37.9	158.1
	COV (%)	< 1	< 1	< 1	< 1
#7	Ave.	128.0	0.00670	76.8	162.9
	COV (%)	< 1	2	< 1	< 1

4.2 TEST RESULTS

4.2.1 BEHAVIOR AND FAILURE MODES

Figure 25 shows the stress-strain plot of three pullout specimens to illustrate the typical behavior of each type of steel. Load-slip and stress-strain curves for all specimens are shown in Appendix B. The stress was obtained by dividing the measured load by the nominal area of the reinforcing bar. The strain was obtained by dividing the measured bar displacement by the debonded length.

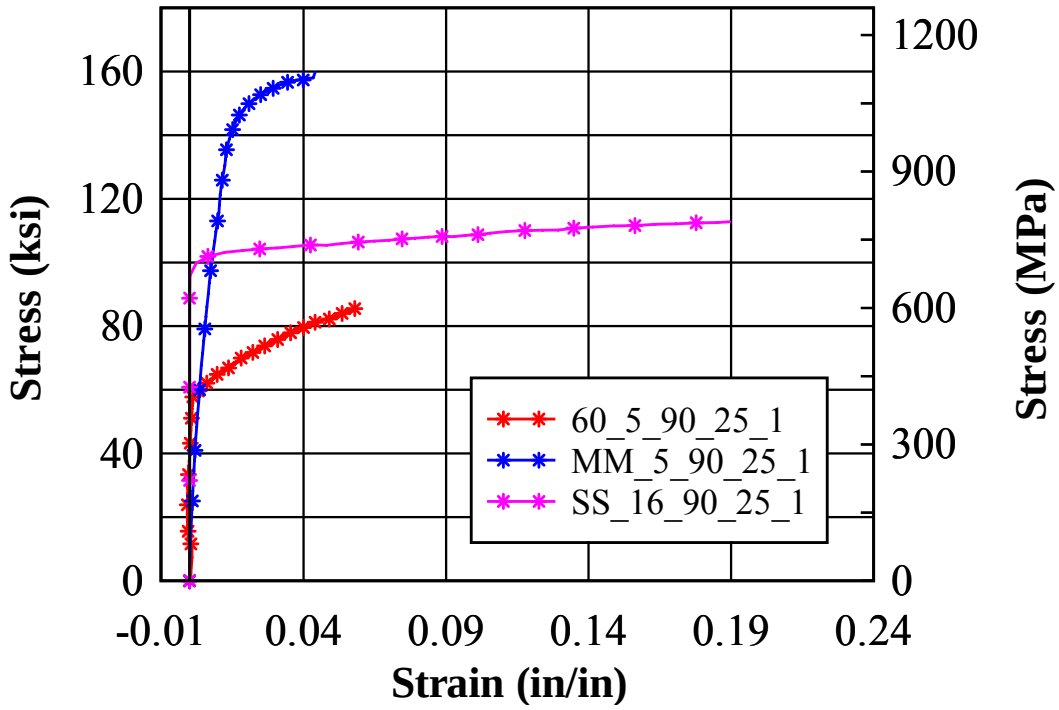

Figure 25. Comparison of stress strain curves for GR60, SS, and MM bars.

In general, as load was applied the specimen remained uncracked and linear elastic until the yield point was reached. In some of the specimens cracking occurred before the bar reached yield, which resulted in a loss of bond and a premature failure. This failure mode was deemed *concrete splitting,* which occurred suddenly when the peak load was reached. This type of failure was characterized by cracks that split the specimen from the front to the right face (see Figure 26a). Also, diagonal cracks formed on the right and left side of the specimen confirming the strut behavior of the specimens (Figure 26b). The front face of the specimen presented the

typical Y – crack which is seen in bond test using beam end specimens (Ahlborn and DenHartigh, 2002). The rear face exhibited an inverted Y – crack which split the specimen in three parts (see Figure 26c and d). Figure 27 shows a sketch of the crack pattern on each face.

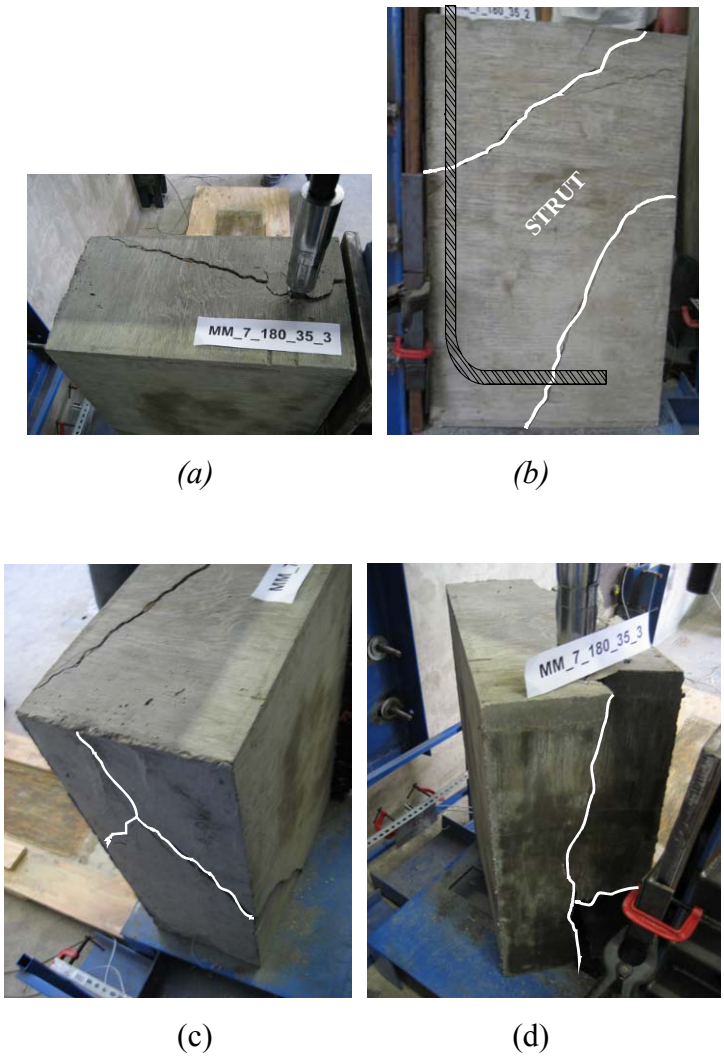

(a) *(b)*

(c) (d)

Figure 26. Photo of typical crack pattern after concrete splitting failure (a) top, (b) side, (c) rear, and (d) front faces. (MM_7_180_35_3)

After testing, a larger portion of the side cover was easy to remove. During the specimen examination, crushing of the concrete inside radius of the hook was noted. This kind of behavior was seen not only in 90 degree but also in 180 degree hooks (see Figure 28). Moreover, crushing of the concrete near to the radius of the bend was because of the large bearing stresses between

the bar radius and concrete resulting in loss of bond. This type of behavior was also observed and reported by Marques and Jirsa (1975) and Hamad, Jirsa, and D'Abreu de Paulo (1993).

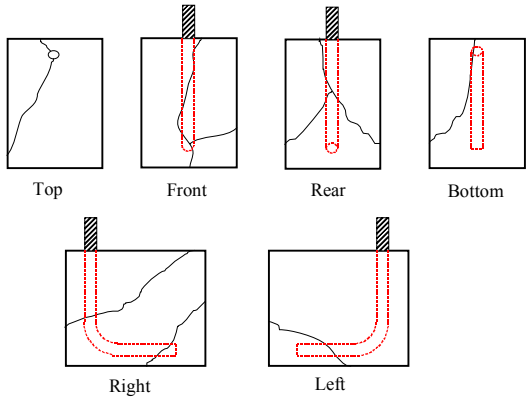

Figure 27. Drawing of typical crack pattern after concrete splitting failure. (MM_7_180_35_3)

(a) (b)

Figure 28. Crushed concrete inside of bend radius (a) 90 deg. hook and (b) 180 deg. hook.

If the specimen was able to sustain load beyond yield, one of two possible failure modes occurred. The *bar yield with concrete splitting,* occurred after the bar had yielded indicating that the anchorage was able to hold load at least to the yield point. Crack patterns were similar to the concrete splitting failure.

Bar yield was characterized by continued deformation of the bar without concrete splitting or bar rupture. This typically occurred on the SS specimens when the hydraulic jack stroke limit was reached. Specimens SS_16_90_25_1, SS_16_90_25_2, SS_16_90_35_1, SS_16_90_35_2, SS_16_180_35_1, and SS_16_180_35_4 were loaded until the stroke of the hydraulic jack reached its limit, which was well beyond the yield point. After testing, no cracks were noted on the faces of the specimens.

Finally, several specimens failed due to *bar yield and rupture*. This occurred when the full rupture strength of the bar was reached before the concrete failed. The bar yield and rupture failure was mainly observed in #5 MM specimens.

4.2.2 ASTM A615 GRADE 60 SPECIMENS

In this section the detailed results of the GR60 steel specimens are presented and discussed. Failure modes for each specimen are documented as well as the load displacement and load slip behavior.

Figure 29 shows the load displacement behavior for all of the #5 and #7 GR60 steel specimens. The plots for each are shown with different scales to accentuate the differences in behavior among the specimens with the same size bar. The 25-degree strut specimens appear to have a larger initial stiffness than that of the 35-degree strut specimens when comparing the results for the #5 bar. This is likely due to the manner in which the displacements were measured. The linear potentiometer was attached to the bar at the point where it exits the concrete and measured the relative movement between the bar and concrete. The 25-degree strut specimens had shorter debonded lengths than that of the 35-degree strut specimens resulting in larger elastic deformations under the same load.

The sudden change in slope of the load displacement plots indicates yielding of the bars. The #5 bars appear to exhibit two slightly different yield points while all of the #7 bars appear to be near the same yield point. The average yield points measured in the bare bar tests are plotted as a horizontal line denoted with P_{yt}. The #7 bar tests appear to very consistent and to agree with the results of the bare bar test. The #5 bars, however, appear to have two distinctly different yield points when specimens 60_5_90 1 and 60_5_90_S are ignored. The bare bar results seem to better match the lower yield point. This may indicate that there were two different steel heats tested in the GR60 #5 bars.

Post-yield slopes are not likely to provide useful information because the measurement of bar displacement was made relative to the concrete surface around the bar. Microcracking was likely to occur near yield, which would result in movement of the concrete along with the bar as ultimate strength is approached. This behavior is described more fully when the slip data are presented in a later section.

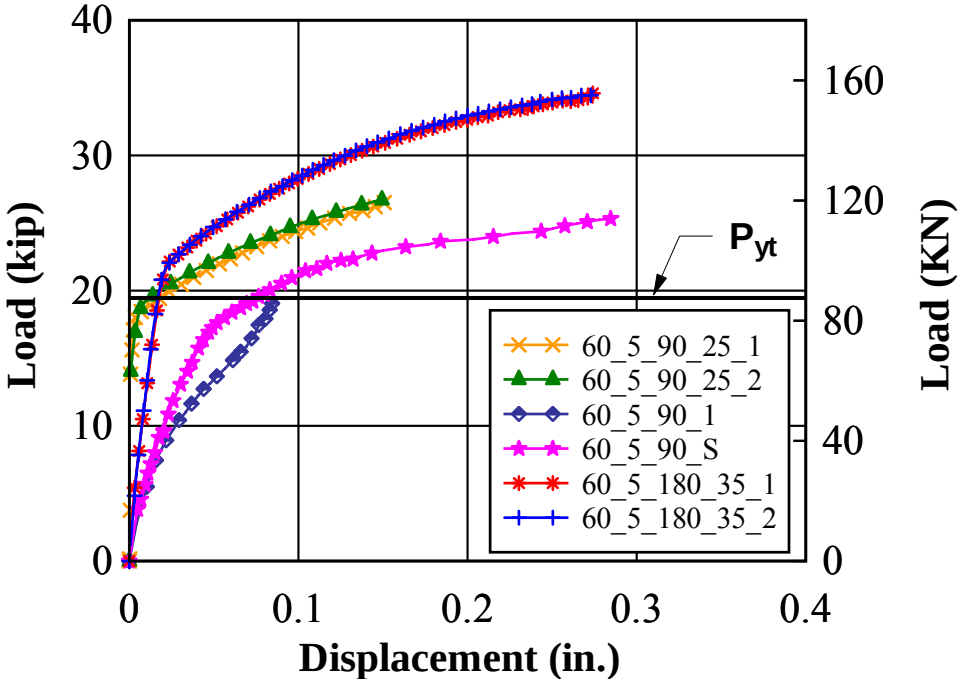

(a))

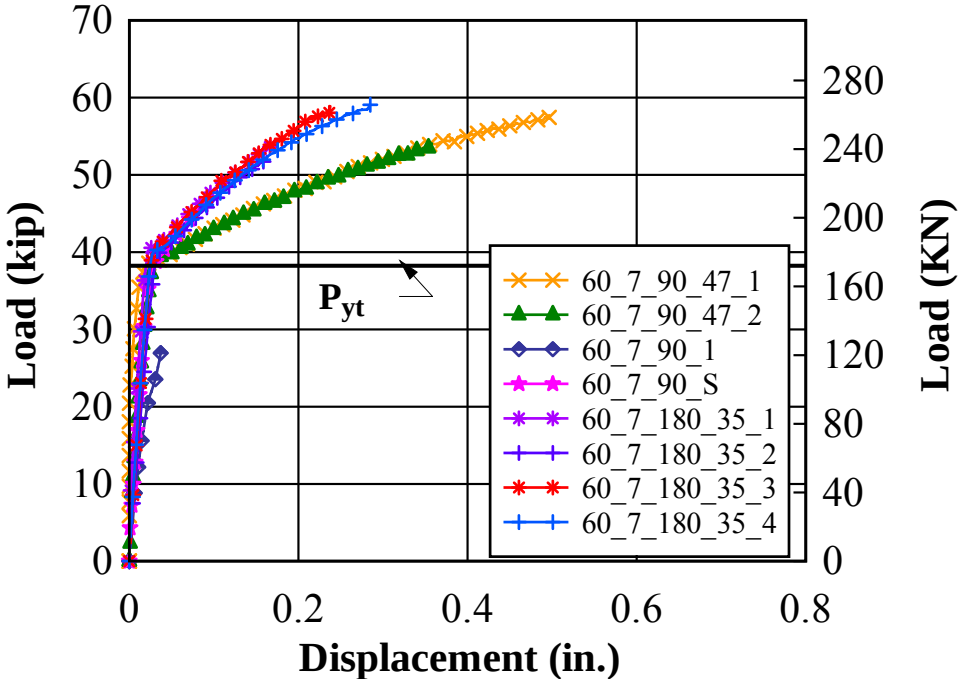

(b)

Figure 29. Load-displacement plot for GR60 (a) #5, and (b) #7.

The complete test results for GR60 steel specimens are shown in the Table 9. f'_{cr} is the average concrete strength of the specimen concrete as tested on the day of the pullout test. P_u is

the peak measured load applied to the bar. To allow comparison of the peak measured loads among the specimens that contained varying concrete strength, P_u was normalized to the square root of the ratio of the design strength (5500 psi) to the measured strength. P_y is the load in the bar at a measured strain of 0.35%. Δ_u is the displacement corresponding to P_u and Δ_y is the displacement corresponding to P_y. The bar stress based on the peak measured load is also given (P_u / A_b). D1 and D2 represent the total measured slip of the bar when the load in the bar is P_u.

Table 9. Test results for GR60 #5 and #7 specimens.

Specimen notation	f'_{cr} (psi)	P_u (kips)	P_y (kips)	Δ_u (in)	Δ_y (in)	$D1_u$ (in)	$D2_u$ (in)	P_u/A_b (ksi)	$P_u\sqrt{\frac{5500}{f'_{cr}}}$ (kips)	Failure Modes
60_5_90_1	5700	20.2	N.A	0.085	NA	0.162	0.152	63.8	19.8	Bar yield with concrete splitting
60_5_90_S	5700	25.5	N.A	0.289	NA	0.117	0.074	80.8	25.0	Bar yield and rupture
60_5_90_25_1	5490	26.5	18.7	0.151	0.009	NA	NA	85.6	26.5	Bar yield with concrete splitting
60_5_90_25_2	5490	27.0	19.1	0.150	0.009	0.167	0.132	87.1	27.0	Bar yield with concrete splitting
60_5_180_35_1	6330	34.6	18.9	0.274	0.017	0.178	0.081	106.0	32.9	Bar yield and rupture
60_5_180_35_2	6330	34.8	18.9	0.275	0.016	0.157	0.074	106.5	33.0	Bar yield and rupture
60_7_90_1	5700	27.8	N.A	0.037	N.A	0.102	0.097	45.4	27.3	Concrete splitting
60_7_90_S	5700	47.0	N.A	0.089	N.A	0.099	0.019	77.0	46.2	Bar yield with concrete splitting
60_7_90_47_1	5490	58.1	38.9	0.497	0.036	N.A	N.A	97.0	58.2	Bar yield
60_7_90_47_2	5490	54.1	39.5	0.358	0.036	0.249	0.164	90.2	54.1	Bar yield
60_7_180_35_1	6330	54.4	40.8	0.172	0.023	0.166	0.158	84.6	50.7	Bar yield with concrete splitting
60_7_180_35_2	6330	52.4	31.2	0.163	0.023	0.251	0.226	81.5	48.9	Bar yield with concrete splitting
60_7_180_35_3	6330	58.9	36.5	0.238	0.023	0.174	0.085	91.5	54.9	Bar yield with concrete splitting
60_7_180_35_4	6330	59.1	36.9	0.285	0.023	0.401	0.263	91.8	55.1	Bar yield with concrete splitting

Figure 30 shows two graphs that compare the confined and unconfined #5 bar specimens from the first series of testing. Recall that this testing was conducted with the original test configuration. It is readily apparent that the unconfined specimen (which did not reach yield) has a shallower load-slip slope than that of the confined specimen with stirrups, indicating that the lack of stirrups allowed greater bar movement prior to reaching ultimate capacity. This confirms observations by Hamad, Jirsa, and D'Abreu de Paulo (1993) when evaluating beam-column joints with GR60 steel and epoxy-coated hooked bars. They found that for #7 uncoated specimens with 90 degree hooks, the anchorage strength increased about 51% when stirrups were added. This compares well with results of this research in which a 69% increase was found when stirrups were added.

Further examination of the plots indicates that the slip at D1 is greater than that of D2 until higher loads are reached where the plots cross. This occurs in both the confined and unconfined specimens. D1 was expected to remain greater than D2 up to failure since the bar exits the specimen near where D1 is measured. The cross-over of the plots is likely due to cracking late in the loading process and is a function of the slip measurement technique and not an indication of peculiar behavior. Figure 31 shows the idealized location of cracks in unconfined and confined specimens, which are similar to those observed during and after the testing. As load is applied, the slip at D1 is greater than that of D2. As additional load is applied, diagonal cracks form perhaps along line 2-3. When these cracks occur, a spall in the shape of 1-2-3 forms and moves with the bar as further load is applied resulting in zero bond stress in this area. Because the slip measurement device measures relative movement between the concrete and steel, less (or zero) slip will register after the spall occurs. These cracks likely form when the specimen is near capacity, which confirms the crossing locations in the plots.

For unconfined specimens, initial slip located at D1 was greater than slip located at D2 until diagonal cracks formed as shown in Figure 31a. For confined specimens, the use of transverse reinforcement not only improved the anchorage capacity of the hooked bar but also controlled crack propagation. The inclusion of transverse reinforcement was sufficient to yield the bar and to achieve the bar rupture failure.

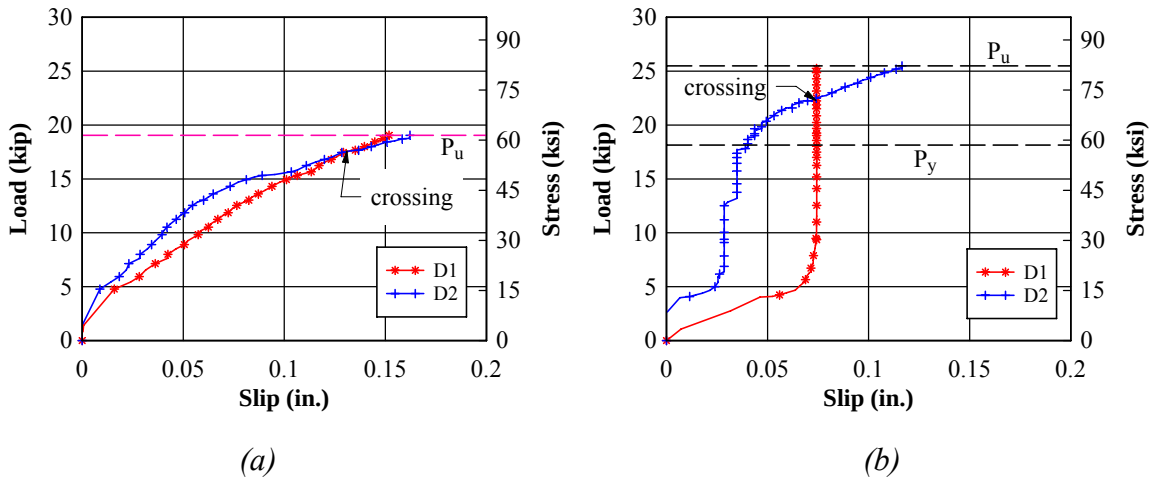

Figure 30. Load-slip plot for specimens (a) 60_5_90_1 and (b) 60_5_90_S.

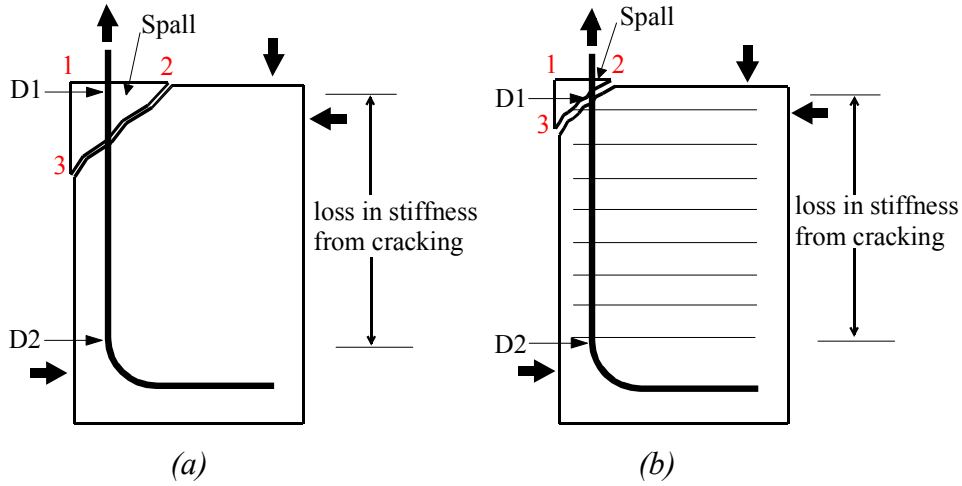

Figure 31. Locations where relative slip was measured for (a) unconfined, and (b) confined with stirrup.

Figure 32 shows the relative behavior of the confined and unconfined #7 tests. The unconfined test is similar to that of the #5 with failure occurring before bar yield and with a crossing of the slip plots near the specimen ultimate capacity. In contrast, however, the confined specimen never exhibits the cross-over of the slip plots. This is probably due to the confinement restricting the formation of the spall in the region of D1.

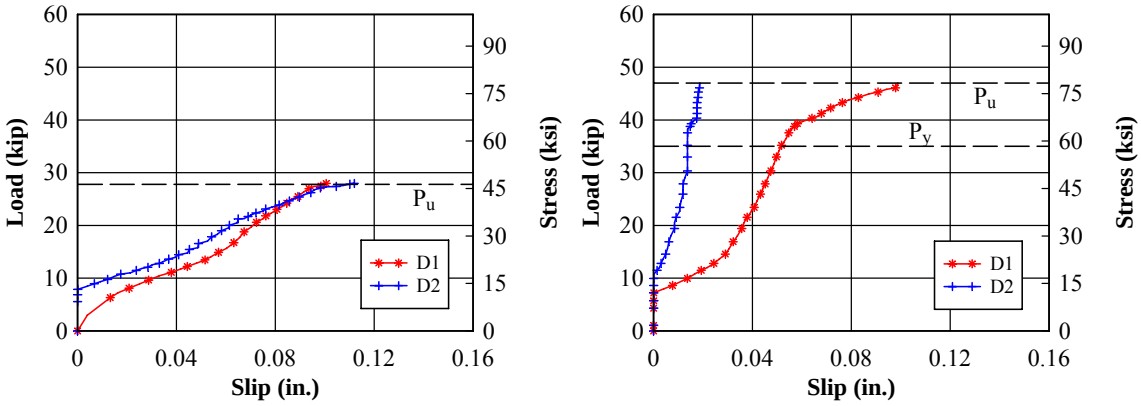

Figure 32. Load-slip plot for specimen (a) 60_7_90_1 and (b) 60_7_90_S.

Slip behavior of the series 2 through 5 tests was similar to that of the unconfined specimen from series 1 except that most of the specimens tested with the revised setup reached yield before failure. Figure 33 provides an example of the load slip behavior for a #5 bar with a 180-deg. hook. As expected, D1 remained greater than D2 for the entire test, and never crossed D2 as the load approached capacity. Recall that the slip D1 was measured at the end of the debonded length (d_L), which placed it closer to the bend than in the previous test setup (Figure 34). Figure 34 shows two possible locations where diagonal cracks formed at the edge of the strut. Crack 2-3 is shown above D1 and Crack 4-5 is shown below. It is believed that the reason there was no cross-over is that the cracking occurred primarily along line 2-3, which formed spall 1-2-3 and allowed the relative slip D1 to continue to be measured up to failure. Furthermore, the D2 plot shows a plateau forming while D1 remains linear up until failure of the concrete indicating that the bar was well beyond its yield point at D1.

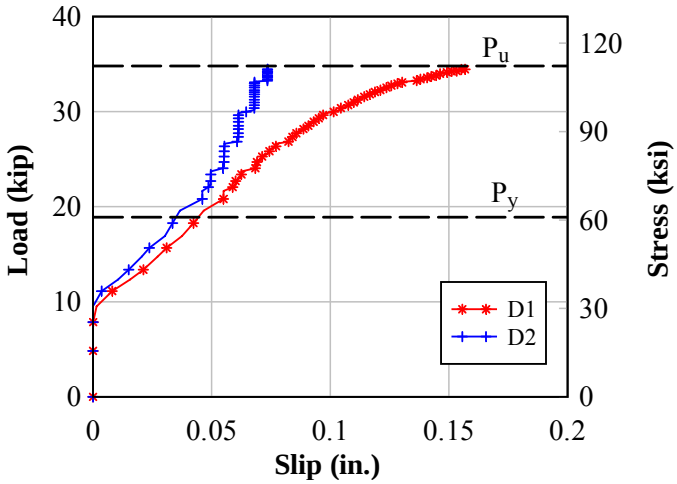

Figure 33. Typical load-slip behavior for #5 GR60 steel specimens with 180-degree hook (60_5_180_35_2 shown).

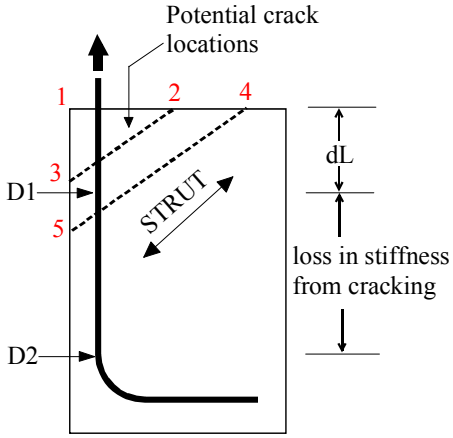

Figure 34. Relative slip at locations D1 and D2 for unconfined specimens with debonded length.

Typical behavior of a #7 GR60 steel bar with a 180-degree hook is shown in Figure 35. The behavior illustrated is similar to that of the #5 specimen in that D1 remains larger than D2 until failure.

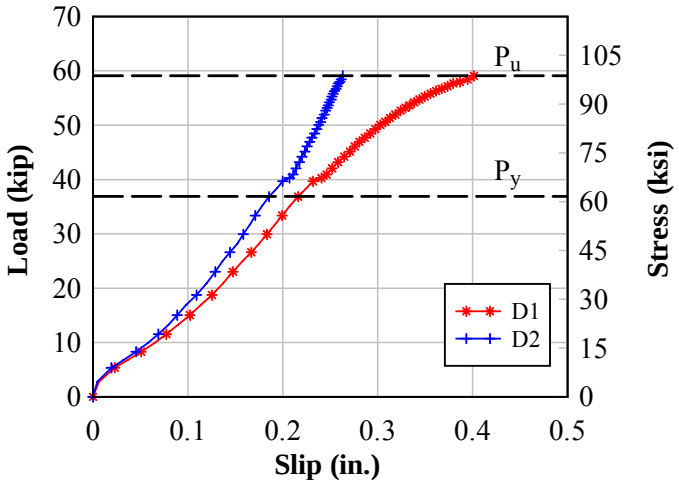

Figure 35. Typical load-slip behavior for #7 GR60 steel specimens with 180-degree hook (60_7_180_35_4 shown).

4.2.3 STAINLESS STEEL SPECIMENS

Figure 36 shows the load displacement behavior for all of the 16 and 20-mm SS specimens. Also, Figure 36 shows the yield load when testing the bar only (P_{yt}) for 16mm and 20mm, which confirms that the bars reached yield. The plots for each are shown with different scales to accentuate the differences in behavior among the specimens with the same size bar. All of the specimens with 16 mm bars reached their yield point with no bar rupture. In many cases, the test was terminated when the stroke of the hydraulic jack reached its limit. In contrast, most specimens with 20 mm bars reached their yield point but then failed by splitting of the concrete. During this portion of the testing program it was discovered that SS bars from two different heats had used (P_{yt1} and P_{yt2}), which explains the difference in the yield loads exhibited in Figure 36a for the 16 mm bars. A second tensile test was conducted on the remaining reinforcing bar. The results of the tests on the two heats were reported earlier.

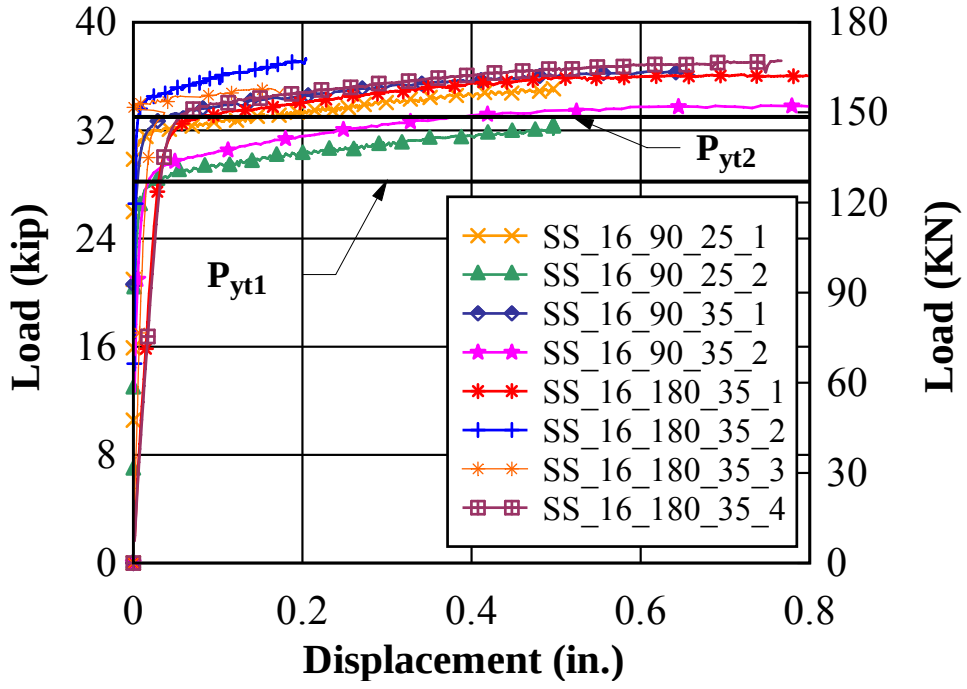

(a)

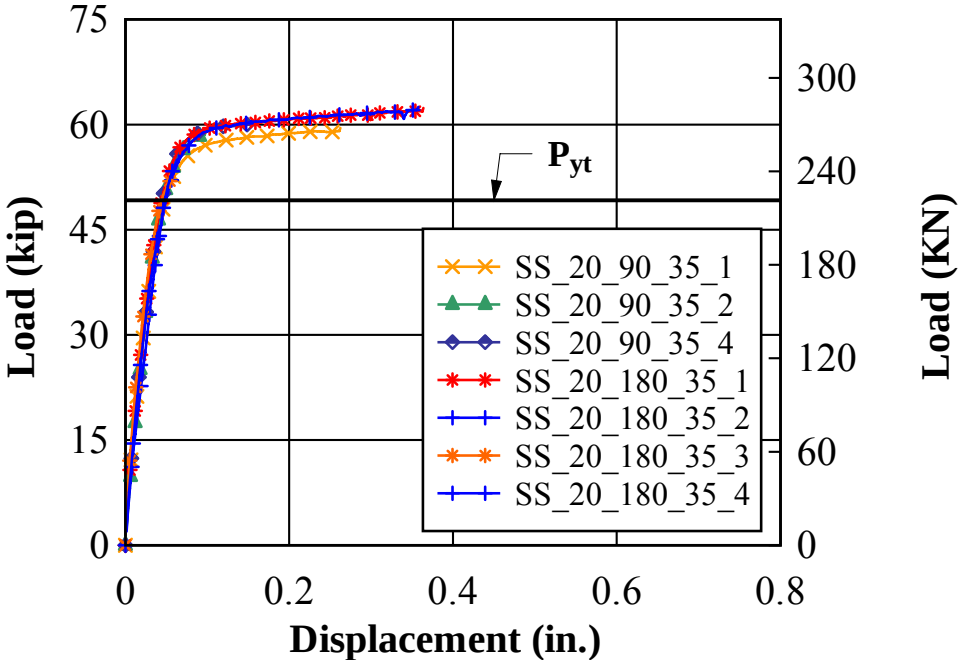

(b)

Figure 36. Load - displacement plot for SS (a) 16 mm, and (b) 20 mm.

The test results for SS specimens are shown in the Table 10. $\dot{f}_{cr}$ shows the average concrete strength of the specimen concrete as tested on the day of the pullout test. P_u is the peak

measured load applied to the bar. To allow comparison of the peak measured loads among the specimens that contained varying concrete strength, P_u was normalized to the square root of the ratio of the design strength (5500 psi) to the measured strength. P_y is the load at which the bar yielded using the 0.2% offset strain. Δ_u is the displacement corresponding to P_u and Δ_y is the displacement corresponding to P_y. The bar stress based on the peak measured load is also given (P_u / A_b). D1 and D2 represent the total measured slip of the bar when the load in the bar is P_u.

Table 10. Test results for SS 16 mm and 20 mm specimens.

Specimen notation	f'_{cr} (psi)	P_u (kips)	P_y (kips)	Δ_u (in)	Δ_y (in)	$D1_u$ (in)	$D2_u$ (in)	P_u/A_b (ksi)	$P_u\sqrt{\frac{5500}{f'_{cr}}}$ (kips)	Failure Modes
SS_16_90_25_1	6350	35.4	32.15	0.497	0.036	0.287	0.186	105.7	33.0	Bar yield
SS_16_90_25_2	6350	33.3	27.44	0.497	0.015	0.265	0.126	99.2	31.0	Bar yield
SS_16_90_35_1	6350	36.7	32.84	0.658	0.024	0.446	0.235	109.6	34.2	Bar yield
SS_16_90_35_2	6350	33.6	28.98	0.729	0.022	0.413	0.148	100.2	31.3	Bar yield
SS_16_180_35_1	6100	36.3	22.62	0.882	0.022	0.400	0.882	110.4	34.5	Bar yield
SS_16_180_35_2	6100	37.3	34.89	0.204	0.024	0.207	0.108	113.5	35.4	Bar yield with concrete splitting
SS_16_180_35_3	6100	35.1	32.43	0.177	0.024	0.109	0.102	106.8	33.3	Bar yield and rupture
SS_16_180_35_4	6100	37.4	28.64	0.758	0.032	0.334	0.051	113.8	35.5	Bar yield
SS_20_90_35_1	6150	59.5	39.83	0.263	0.033	0.239	0.188	114.9	56.3	Bar yield with concrete splitting
SS_20_90_35_2	6150	59.1	39.75	0.099	0.032	0.193	0.146	114.0	55.9	Bar yield with concrete splitting
SS_20_90_35_3	6150	58.5	N.A	0.011	N.A	0.166	0.158	113.0	55.4	Bar yield with concrete splitting
SS_20_90_35_4	6150	60.4	39.38	0.150	0.032	0.077	0.041	116.5	57.1	Bar yield with concrete splitting
SS_20_180_35_1	6150	62.4	40.94	0.364	0.032	0.222	0.061	120.4	59.0	Bar yield with concrete splitting
SS_20_180_35_2	6150	62.5	35.15	0.358	0.031	0.146	0.043	120.6	59.1	Bar yield with concrete splitting
SS_20_180_35_3	6150	52.5	41.74	0.056	0.032	0.167	0.132	101.3	49.6	Bar yield with concrete splitting
SS_20_180_35_4	6150	55.6	38.03	0.066	0.032	0.152	0.079	107.2	52.5	Bar yield with concrete splitting

The 25-degree strut specimens had shorter debonded lengths than that of the 35-degree strut specimens, which resulted in larger elastic deformations under the same load (see Figure 37). As a result, it was found that the maximum slip for specimen SS_16_90_35_2 increased about 56% as the strut angle increased in comparison with the specimen SS_16_90_25_2 (see Table 10).

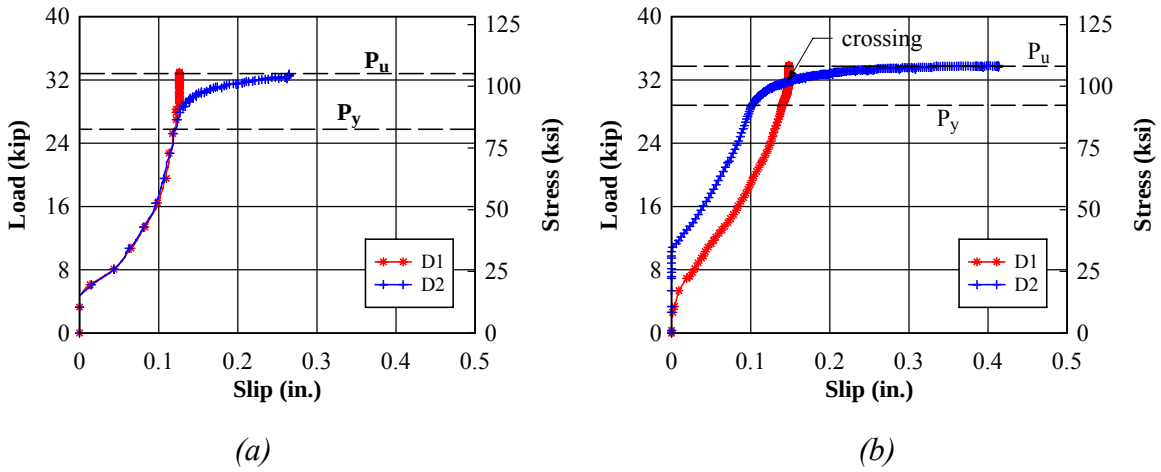

Figure 37. Load-slip behavior for specimens (a) SS_16_90_25_2 and (b) SS_16_90_35_2.

Typical load-slip behavior is illustrated in Figure 38 for 16 mm SS specimens. Initial slip is larger for D1 than for D2. As the load nears yield, however, the plots cross, indicating that the diagonal crack formed the 1-4-5 spall (Figure 34) in the debonded region of the bar.

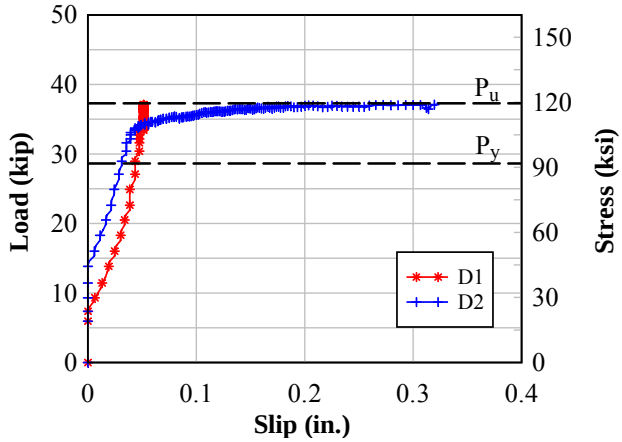

Figure 38. Typical load-slip behavior for 16mm SS specimens with both 90 and 180-degree hooks (SS_16_180_35_4 shown).

Figure 39 indicates that the 20 mm SS specimens behave more like the #7 GR60 steel specimens than that of the 16 SS specimens. This may be due to the difference in the failure mode. Recall that the 16 mm SS specimens did not split while both the #7 GR60 steel and 20 mm SS specimens yielded and then split.

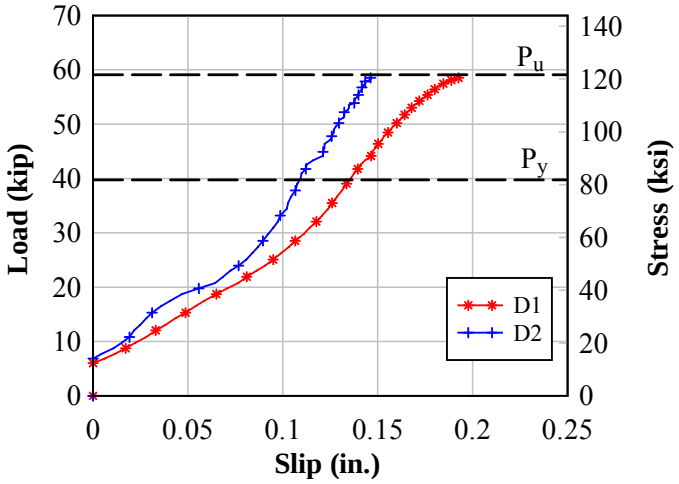

Figure 39. Typical load-slip behavior for 20mm SS specimens with both 90 and 180-degree hooks (SS_20_90_35_2 shown).

4.2.4 MMFX SPECIMENS

In this section the detailed results of the MMFX specimens are presented and discussed. Failure modes for each specimen are documented as well as the load displacement and load slip behavior.

Figure 40 shows the load displacement behavior for all of the #5 and #7 MM specimens. Also, Figure 40 shows the bar yield load (P_{yt}) for #5 and #7. The plots for each are shown with different scales to accentuate the differences in behavior among the specimens with the same size bar. All of the specimens with #5 bars reached yield, which appears to be at approximately the same load. In contrast, just a few specimens with #7 bars reached their yield point before failure by concrete splitting occurred, indicating that the bond strength was not sufficient to develop the #7 bars as fully as the #5 bars.

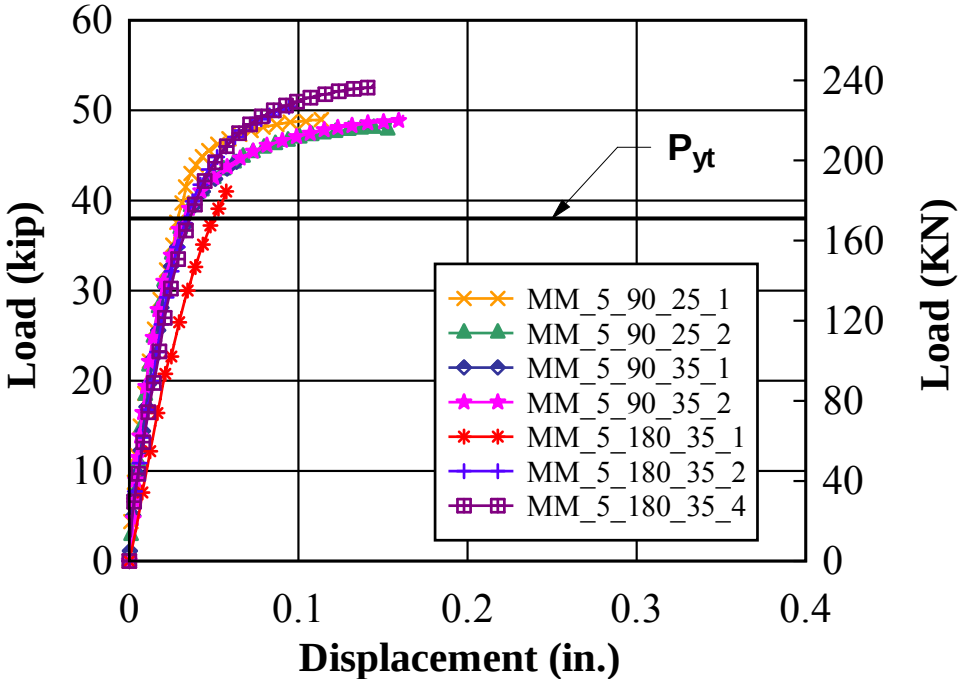

(a)

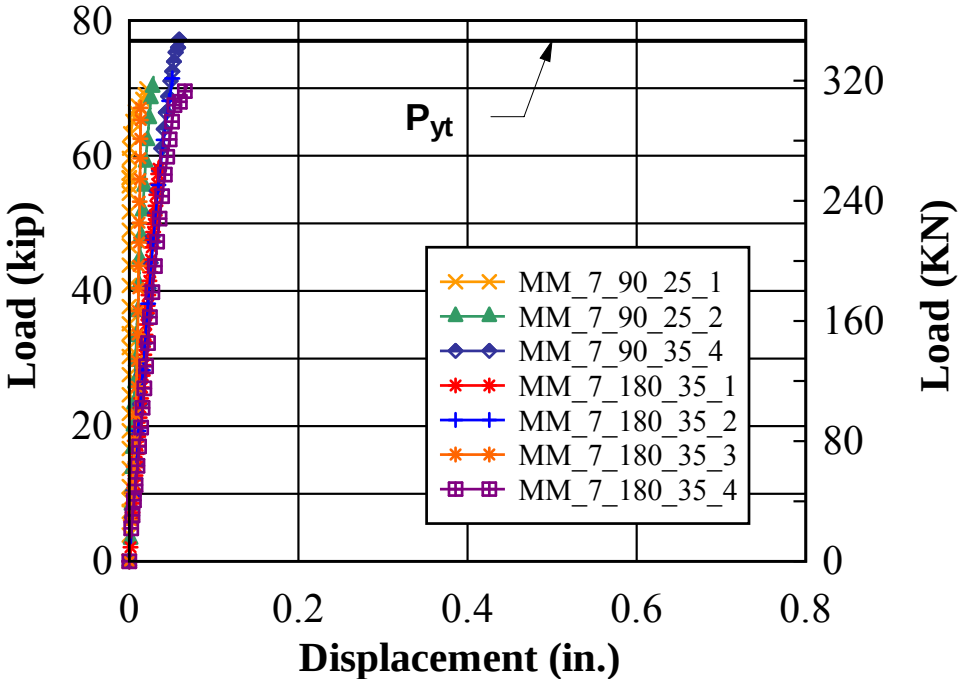

(b)

Figure 40. Load-displacement plot for MM specimens (a) #5, and (b) #7.

The test results for MM specimens are shown in the Table 11. f'_{cr} shows the average concrete strength of the specimen concrete as tested on the day of the pullout test. P_u is the peak measured load applied to the bar. To allow comparison of the peak measured loads among the specimens that contained varying concrete strength, P_u was normalized to the square root of the ratio of the design strength (5500 psi) to the measured strength. P_y is the load at which the bar yielded using the 0.2% offset strain. Δ_u is the displacement corresponding to P_u and Δ_y is the displacement corresponding to P_y. The bar stress based on the peak measured load is also given (P_u / A_b). D1 and D2 represent the total measured slip of the bar when the load in the bar is P_u.

.

Table 11. Test results for MM #5 and #7 specimens.

Specimen notation	f'_{cr} (psi)	P_u (kips)	P_y (kips)	Δ_u (in)	Δ_y (in)	$D1_u$ (in)	$D2_u$ (in)	P_u/A_b (ksi)	$P_u\sqrt{\frac{5500}{f'_{cr}}}$ (kips)	Failure Modes
MM_5_90_25_1	6450	49.5	27.6	0.115	0.017	0.071	0.067	159.7	45.7	Bar rupture
MM_5_90_25_2	6450	48.6	28.2	0.155	0.017	0.114	0.077	156.7	44.8	Bar rupture
MM_5_90_35_1	6450	44.9	33.3	0.064	0.025	0.145	0.057	144.9	41.5	Bar yield with concrete splitting
MM_5_90_35_2	6450	49.4	34.6	0.162	0.025	0.244	0.233	159.3	45.6	Bar yield with concrete splitting
MM_5_180_35_1	6320	41.0	23.1	0.057	0.025	0.019	0.014	132.3	38.2	Bar yield with concrete splitting
MM_5_180_35_2	6320	51.0	32.7	0.096	0.025	0.087	0.037	164.4	47.5	Bar yield with concrete splitting
MM_5_180_35_3	6320	47.4	44.8	0.051	0.025	0.199	0.197	153.0	44.3	Bar yield with concrete splitting
MM_5_180_35_4	6320	52.9	31.4	0.145	0.026	0.187	0.154	170.5	49.3	Bar rupture
MM_7_90_25_1	6600	69.9	N.A	0.021	N.A	0.379	0.291	116.5	63.8	Concrete splitting
MM_7_90_25_2	6600	71.7	N.A	0.029	N.A	0.044	0.018	119.4	65.4	Bar cast out of position
MM_7_90_35_1	6600	58.3	N.A	0.010	N.A	0.003	0.000	97.1	53.2	Bar cast out of position
MM_7_90_35_2	6600	65.8	N.A	0.029	N.A	0.284	0.150	109.6	60.0	Bar cast out of position
MM_7_90_35_3	6330	58.9	N.A	0.044	N.A	0.237	0.234	98.2	54.9	Concrete splitting
MM_7_90_35_4	6330	77.2	67.5	0.059	0.044	0.088	0.086	128.6	71.9	Bar yield with concrete splitting
MM_7_180_35_1	6170	59.3	N.A	0.035	N.A	0.171	0.126	98.8	56.0	Concrete splitting
MM_7_180_35_2	6170	71.4	65.3	0.051	0.044	0.077	0.052	119.1	67.5	Bar yield with concrete splitting
MM_7_180_35_3	6170	67.6	N.A	0.014	N.A	0.106	0.096	112.7	63.9	Concrete splitting
MM_7_180_35_4	6170	70.4	59.6	0.068	0.044	0.309	0.252	117.3	66.5	Bar yield with concrete splitting

Typical behavior of a #5 and #7 MM specimen with a 90 and 180-degree hooks is shown in Figure 41 and Figure 42. The behavior illustrated is similar to that of the #5 and #7 GR60 steel specimens with 180 degree hook in that D1 remains larger than D2 until failure. The maximum slip for specimen MM_5_90_35_2 increased about 114% as the strut angle increased in comparison with the specimen MM_5_90_25_2. Also, it was found that the maximum slip for specimen MM_5_180_35_2 increased about 116% as the development length increased in comparison with the specimen MM_5_180_35_4.

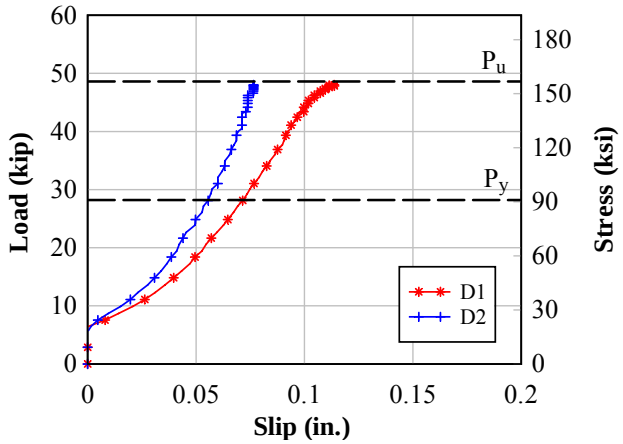

Figure 41. Typical load-slip behavior for #5 MM specimens with either 90 and 180-degree hooks (MM_5_90_25_2 shown).

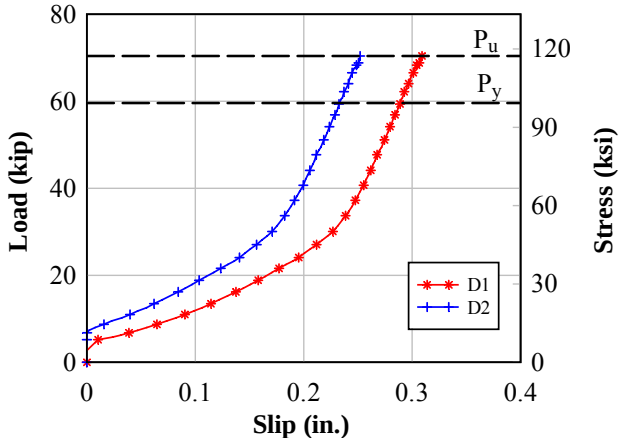

Figure 42. Typical load-slip behavior for #7 MM specimens with either 90 and 180-degree hooks (MM_7_180_35_4 shown).

5 ANALYSIS OF RESULTS

This chapter presents the results of several analyses that are intended to quantitatively analyze results of the hooked anchorage tests and determine the suitability of the current design equations.

5.1 EFFECT OF STRUT ANGLE

One of the variables examined in the series two tests was the angle of the diagonal strut, which is controlled by the length of the specimen. The average capacities of the two angles, 25 deg. and 35 deg., are compared in Figure 43. All specimens had 90-deg. bend angles to ensure that this did not cause a variation. The SS and MM specimens showed little effect from the difference in angle with the possible exception of #7 MM in which the larger angle appeared to cause a reduction in capacity. The 35-deg specimens had the hooks out of alignment, which may have contributed to the reduced capacity. Since the angle did not appear to make a significant difference in the results, 35-degrees was chosen to ensure that the specimen was a compact as possible for handling.

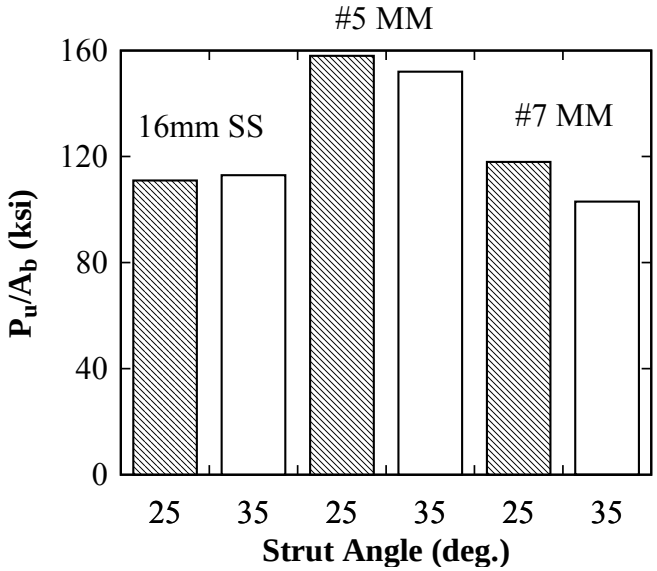

Figure 43. Influence of strut angle on ultimate capacity.

5.2 EFFECT OF BEND ANGLE

Figure 44 through Figure 46 provide a compare the capacity of 90-deg. bend against 180-deg. bends for each steel type. The #5 GR60 bars appear to have been affected by the bend angle with the 180-deg. angle providing a higher capacity than that of the 90-deg. bend. The remainder of the specimens, however, does not appear to be significantly affected by the bend angle. Consequently, the remainder of the analysis does not distinguish the bend angle.

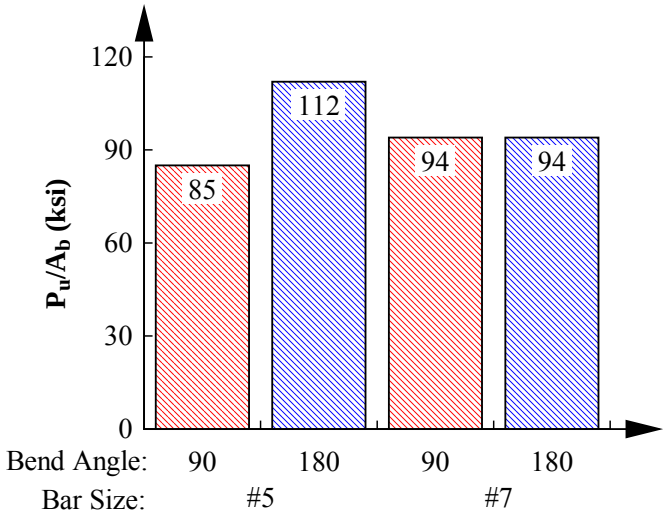

Figure 44. Comparison of bend angle for GR60 specimens.

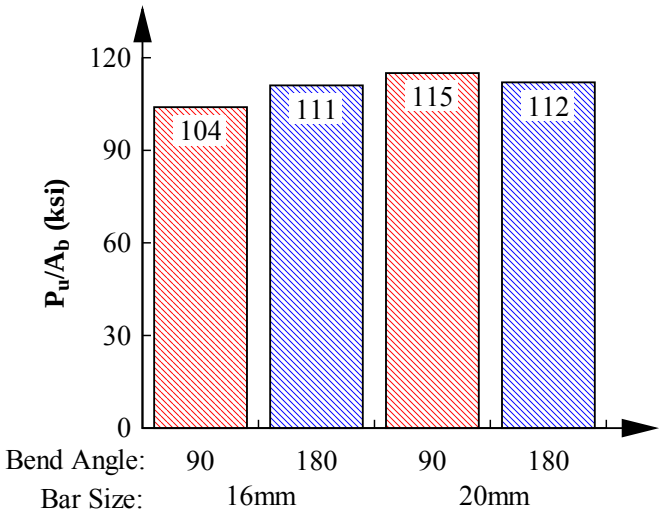

Figure 45. Comparison of bend angle for SS specimens.

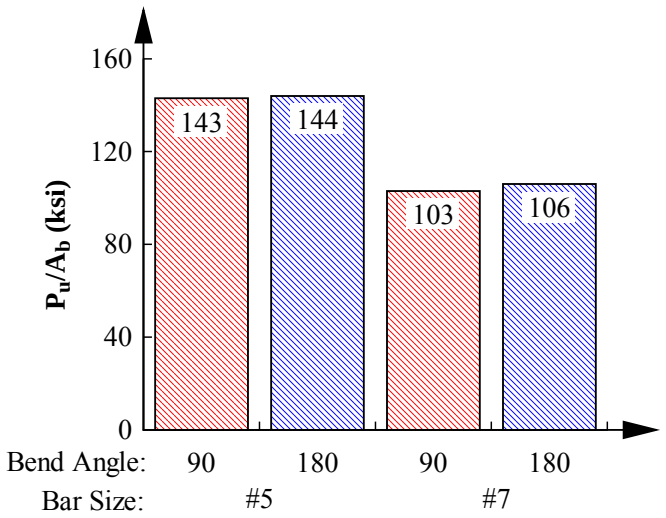

Figure 46. Comparison of bend angle for MM specimens.

5.3 ANCHORAGE CAPACITY

One method that can be used to compare the results of tests on high strength bars is the excess force capacity available beyond the yield point. Mechanical couplers are required to reach least 1.25 times the specified yield strength (f_y) of the bar when splicing reinforcement (ACI 318-05 Section 12.14.3.2). The rationale for this approach is not specified, but it has also been used by Marques and Jirsa (1975) and by Ueda, Lin, and Hawkins (1986) in evaluating the capacity and ductility of hooked bar anchorages that used GR60 steel. It is likely that this provides a factor of safety for the coupler should the reinforcing steel have a significantly higher actual yield strength than specified. The disadvantage of this approach, however, is that the current research is comparing steels that have higher yield strengths and different post-yield properties than that of GR60 steel. Consequently, the bars already vary in how much post-yield strength is available, both in the absolute and relative sense.

For the purposes of analyzing these pullout data, the Anchorage Capacity Ratio (Pu/Py) is defined as the ultimate capacity of the test specimen divided by the specified yield strength of the bar in terms of load. Note that the corrected ultimate strength value is used in these calculations to ensure that the comparison is made with specified values. Table 12 through Table 14 show the individual anchorage capacity ratios calculated for all of the specimens tested in the strut and tie test configuration.

Figure 47 compares the anchorage capacity ratios by bar size and type of steel. All steel types and bar sizes exceed the 1.25 mark except for #7 MM, which has a single value above 1.25. Judging the specimens by the 1.25 criteria, then all would be deemed acceptable except for the #7 MM.

Table 12. Anchorage capacity ratio - GR60 specimens

Specimen notation	P_u (kips)	$P_u\sqrt{\frac{5500}{f'_{cr}}}$ (kips)	P_y Load at f_y (kips)	Anchorage Ratio (P_u/P_y)
60_5_90_25_1	26.5	26.5	18.6	1.42
60_5_90_25_2	27.0	27.0	18.6	1.45
60_5_180_35_1	34.6	32.9	18.6	1.86
60_5_180_35_2	34.8	33.0	18.6	1.87
60_7_90_47_1	58.1	58.2	36	1.61
60_7_90_47_2	54.1	54.1	36	1.50
60_7_180_35_1	54.4	50.7	36	1.51
60_7_180_35_2	52.4	48.9	36	1.46
60_7_180_35_3	58.9	54.9	36	1.64
60_7_180_35_4	59.1	55.1	36	1.64

Table 13. Anchorage capacity ratio - SS specimens

Specimen notation	P_u (kips)	$P_u\sqrt{\frac{5500}{f'_{cr}}}$ (kips)	P_y Load at f_y (kips)	Anchorage Ratio (P_u/P_y)
SS_16_90_25_1	35.4	33.0	23.4	1.51
SS_16_90_25_2	33.3	31.0	23.4	1.42
SS_16_90_35_1	36.7	34.2	23.4	1.57
SS_16_90_35_2	33.6	31.3	23.4	1.44
SS_16_180_35_1	36.3	34.5	23.4	1.55
SS_16_180_35_2	37.3	35.4	23.4	1.60
SS_16_180_35_3	35.1	33.3	23.4	1.50
SS_16_180_35_4	37.4	35.5	23.4	1.60
SS_20_90_35_1	59.5	56.5	36.5	1.63
SS_20_90_35_2	59.1	56.1	36.5	1.62
SS_20_90_35_3	58.5	55.4	36.5	1.60
SS_20_90_35_4	60.4	57.3	36.5	1.65
SS_20_180_35_1	62.4	59.2	36.5	1.71
SS_20_180_35_2	62.5	59.4	36.5	1.71
SS_20_180_35_3	52.5	49.8	36.5	1.44
SS_20_180_35_4	55.6	52.8	36.5	1.52

Table 14 Anchorage capacity ratio - MM specimens

Specimen notation	P_u (kips)	$P_u\sqrt{\frac{5500}{f'_{cr}}}$ (kips)	P_y Load at f_y (kips)	Anchorage Ratio (P_u/P_y)
MM_5_90_25_1	49.5	45.7	31	1.60
MM_5_90_25_2	48.6	44.8	31	1.57
MM_5_90_35_1	44.9	41.5	31	1.45
MM_5_90_35_2	49.4	45.6	31	1.59
MM_5_180_35_1	41.0	38.2	31	1.32
MM_5_180_35_2	51.0	47.5	31	1.65
MM_5_180_35_4	52.9	49.3	31	1.53
MM_7_90_25_1	69.9	63.8	60	1.17
MM_7_90_25_2*	71.7	65.4	60	1.20
MM_7_90_35_1*	58.3	53.2	60	0.97
MM_7_90_35_2*	65.8	60	60	1.10
MM_7_90_35_3	58.9	54.9	60	0.98
MM_7_90_35_4	77.2	71.9	60	1.29
MM_7_180_35_1	59.3	56	60	0.99
MM_7_180_35_2	71.4	67.5	60	1.19
MM_7_180_35_3	67.6	63.9	60	1.13
MM_7_180_35_4	70.4	66.5	60	1.17

* Bars cast out of position.

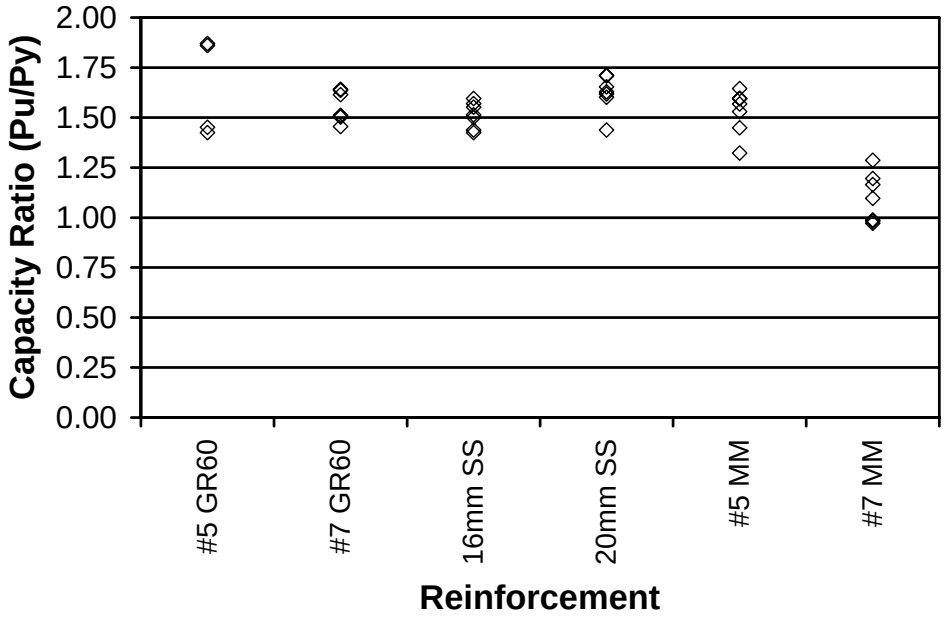

Figure 47. Anchorage capacity ratios for all sizes and steel types.

5.4 DUCTILITY

Previous researchers have used ductility as a means to evaluate the performance of reinforcement anchorage (Azizinamini et al. 1999). The focus was on lap splices of #8 and #11 bars in high-strength concrete. The test setup was four-point bending with the splice centered in the constant moment region. Displacement ductility was determined by dividing the displacement at ultimate capacity by the displacement at first yield.

In this research the strain measured in the debonded portion of the bar was used to determine a strain ductility ratio to compare hook anchorage performance when using a material other than GR60. This approach resolves the problem of the varying post-yield slopes that occur in various steel types.

The strain ductility ratio for each specimen was calculated as illustrated in Figure 48. The bar displacement was divided by the length of the debonded portion of the bar to obtain strain. The measured load was divided by the nominal bar area to obtain stress. The strain at ultimate capacity (ε_u) was determined from the strain measured at the ultimate load of each specimen and is shown in Table 15 through Table 17. The ultimate strain capacity was then divided by the yield strain (ε_y) measured in the bar tests corresponding to 0.35% for the GR60 bars and the 0.2% offset for the SS and MM specimens to form the ductility ratio shown in the tables ($\varepsilon_u/\varepsilon_y$).

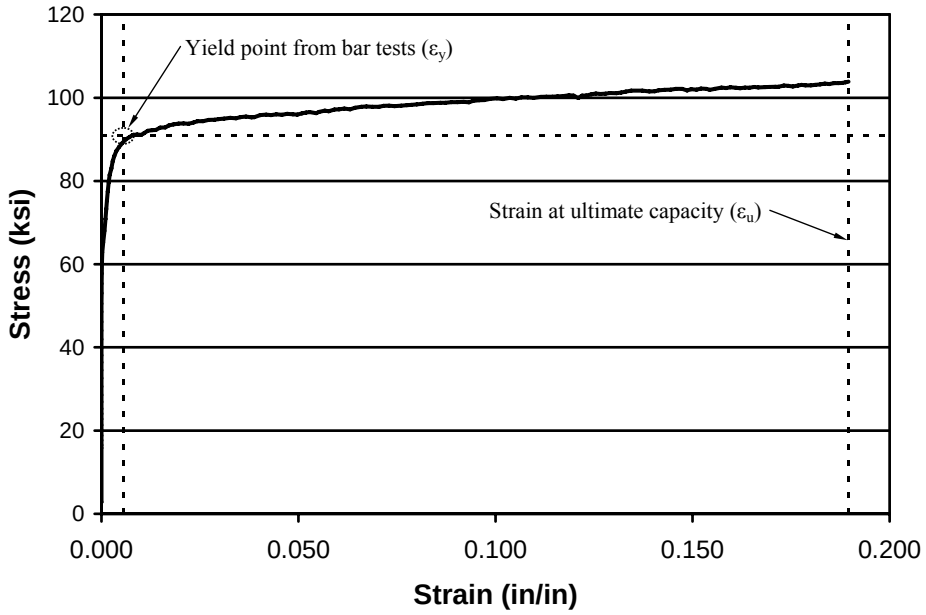

Figure 48. Method used to determine the ductility ratio for Specimen SS_16_90_25_2

Table 15. Ductility ratio for GR60 steel.

Specimen notation	ε_u [Strain at P_u] (in/in)	ε_y [Strain at 0.35%] (in/in)	Ductility Ratio ($\varepsilon_u/\varepsilon_y$)
60_5_90_25_1	0.0580	0.0035	16.6
60_5_90_25_2	0.0579	0.0035	16.6
60_5_180_35_1	0.0699	0.0035	20.0
60_5_180_35_2	0.0701	0.0035	20.0
60_7_90_47_2	0.0347	0.0035	9.9
60_7_180_35_1	0.0261	0.0035	7.5
60_7_180_35_2	0.0248	0.0035	7.1
60_7_180_35_3	0.0361	0.0035	10.3
60_7_180_35_4	0.0433	0.0035	12.4

Table 16. Ductility ratio for SS.

Specimen notation	ε_u [Strain at P_u] (in/in)	ε_y [Strain at 0.2% offset yield] (in/in)	Ductility Ratio ($\varepsilon_u/\varepsilon_y$)
SS_16_90_25_1	0.1856	0.0062	30.2
SS_16_90_25_2	0.1896	0.0056	34.2
SS_16_90_35_1	0.1682	0.0062	27.4
SS_16_90_35_2	0.2090	0.0056	37.7
SS_16_180_35_1	0.2256	0.0056	40.6
SS_16_180_35_4	0.1939	0.0056	34.9
SS_20_90_35_1	0.0466	0.0058	8.1
SS_20_90_35_2	0.0175	0.0058	3.0
SS_20_90_35_4	0.0266	0.0058	4.6
SS_20_180_35_1	0.0645	0.0058	11.2
SS_20_180_35_2	0.0635	0.0058	11.0
SS_20_180_35_3	0.0099	0.0058	1.7
SS_20_180_35_4	0.0116	0.0058	2.0

Table 17. Ductility ratio for MM specimens.

Specimen notation	ε_u [Strain at P_u] (in/in)	ε_y [Strain at 0.2% offset yield] (in/in)	Ductility Ratio ($\varepsilon_u/\varepsilon_y$)
MM_5_90_25_1	0.0440	0.0065	6.8
MM_5_90_25_2	0.0590	0.0065	9.1
MM_5_90_35_1	0.0165	0.0065	2.5
MM_5_90_35_2	0.0414	0.0065	6.4
MM_5_180_35_1	0.0147	0.0065	2.3
MM_5_180_35_2	0.0247	0.0065	3.8
MM_5_180_35_4	0.0130	0.0065	2.0
MM_7_90_25_1	0.0370	0.0065	5.7
MM_7_90_25_2	0.0052	0.0067	0.8
MM_7_90_35_1	0.0013	0.0067	0.2
MM_7_90_35_2	0.0038	0.0067	0.6
MM_7_90_35_3	0.0066	0.0067	1.0
MM_7_90_35_4	0.0089	0.0067	1.3
MM_7_180_35_1	0.0053	0.0067	0.8
MM_7_180_35_2	0.0077	0.0067	1.2
MM_7_180_35_3	0.0021	0.0067	0.3
MM_7_180_35_4	0.0103	0.0067	1.5

No clear trend is present when comparing the data from 90-deg and 180-deg hooks. Consequently, the data have been plotted in Figure 49 to provide a visual comparison across bar size and steel type. In addition, the mean ductility ratios are presented in Table 18. In all steel types, the ductility of the smaller bars is greater than that of the larger bars. For instance, #5 GR60 bars have nearly twice the ductility of the #7 bars, while the SS 16mm bars have nearly 6 times the ductility as that of the 20 mm bars. The large difference in the SS bars is likely due, at least partially, to the longer developments lengths provided for the 16mm bars than was required by the equation for the specified yield strength of the material (this will be discussed further in the next section). Finally, the #5 MM specimens have more than 3 times the ductility of the #7 bars. The larger ductility for the smaller bars is expected due to the lower bond stresses created by the larger surface-area-to-cross-sectional area ratio provided by smaller bars.

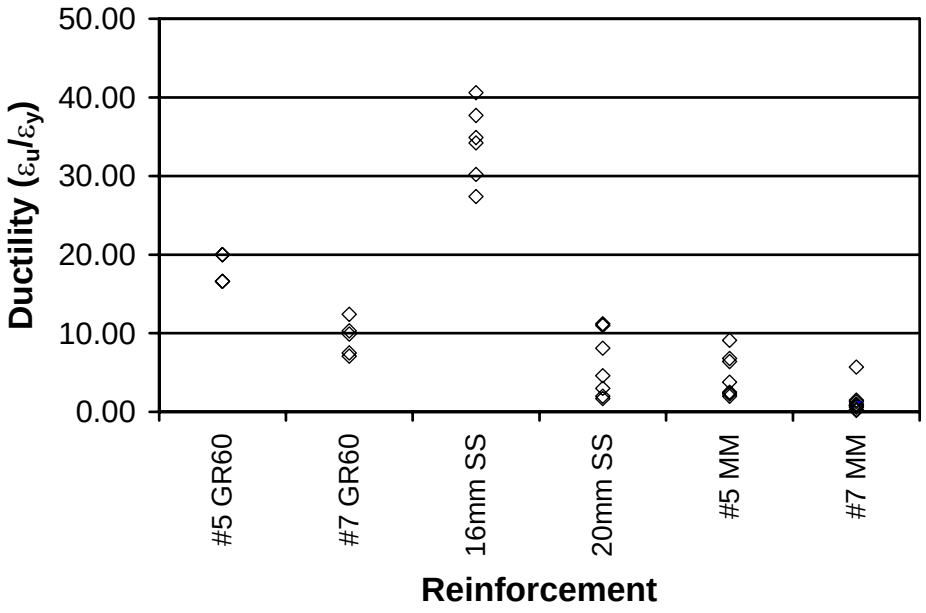

Figure 49. Comparison of ductility ratios.

Table 18. Mean ductility ratio for all steel types

Specimen	Bar Size	Mean Ductility Ratio ($\varepsilon_u/\varepsilon_y$)
GR60	#5	18
	#7	9.4
SS	16mm	34
	20mm	5.9
MM	#5	4.7
	#7	1.3

5.5 DEVELOPMENT LENGTH EQUATION

The ACI and AASHTO equations given in equations 1 and 2 give identical results for required development length. The ACI equation will be used here for convenience. The ACI equation can be rewritten to include the additional multipliers as:

$$l_{dh} = \frac{K d_b f_y}{\sqrt{f'_c}} \qquad \text{Equation 12}$$

where the K is the coefficient 0.02. Additional multipliers are needed for epoxy coating, lightweight aggregate concrete, and concrete cover. If the side cover and cover on bar extension beyond the hook are not less than 2-1/2 in. and 2 in., respectively for the specimens, then a 0.7 reduction factor is used. The specimens in this research met these criteria.

Equation 12 can be rearranged to allow the computation of the coefficient based on the test parameters used in this research:

$$K = \frac{l_{dh}\sqrt{f'_c}}{0.7 f_y d_b} \qquad \text{Equation 13}$$

where l_{dh} represents the tested development length, d_b is the nominal diameter of the bar, f_y is the specified yield strength, and f'_c is the average concrete strength. The yield strength was selected to calculate the coefficient because this is the value that would be used in design, not the actual steel strength. Furthermore, the actual concrete strength was used to ensure that the coefficients were conservative. They are conservative because this is the concrete strength needed to give the anchorage capacity measured. If the specified strength was used, then the coefficient would be unconservatively low. Table 19, Table 20, and Table 21 show the experimental K-factor obtained for each specimen.

The coefficients for GR60 steel are all within 10% of the code specified equation of 0.02, indicating that the test conditions for the GR60 steel bars, including tested development length, matched that required by the code equation. Development lengths were varied for the SS and MM specimens to determine if the longer development lengths could provide improved

performance. The SS coefficients varied from 0.0247 to a maximum of 0.0291. Note that larger coefficients indicate longer development lengths than required by code.

Table 19. K-factor for #5 and #7 GR60 specimens.

Specimen	f'_c (psi)	f_y (psi)	l_{dh} (in)	d_b (in)	K
60_5_90_25_1	5490	60000	7	0.625	0.0198
60_5_90_25_2	5490	60000	7	0.625	0.0198
60_5_180_35_1	6100	60000	7	0.625	0.0208
60_5_180_35_2	6100	60000	7	0.625	0.0208
60_7_90_47_1	5490	60000	10	0.875	0.0202
60_7_90_47_2	5490	60000	10	0.875	0.0202
60_7_180_35_1	6330	60000	9	0.875	0.0195
60_7_180_35_2	6330	60000	9	0.875	0.0195
60_7_180_35_3	6330	60000	10	0.875	0.0216
60_7_180_35_4	6330	60000	10	0.875	0.0216

Table 20. K-factor for 16 mm and 20 mm SS specimens.

Specimen	f'_c (psi)	f_y (psi)	l_{dh} (in)	d_b (in)	K
SS_16_90_25_1	6350	75000	12	0.625	0.0291
SS_16_90_25_2	6350	75000	12	0.625	0.0291
SS_16_90_35_1	6350	75000	12	0.625	0.0291
SS_16_90_35_2	6350	75000	12	0.625	0.0291
SS_16_180_35_1	6100	75000	11	0.625	0.0262
SS_16_180_35_2	6100	75000	11	0.625	0.0262
SS_16_180_35_3	6100	75000	12	0.625	0.0286
SS_16_180_35_4	6100	75000	12	0.625	0.0286
SS_20_90_35_1	6150	75000	13	0.787	0.0247
SS_20_90_35_2	6150	75000	13	0.787	0.0247
SS_20_90_35_3	6150	75000	14	0.787	0.0266
SS_20_90_35_4	6150	75000	14	0.787	0.0266
SS_20_180_35_1	6150	75000	13	0.787	0.0247
SS_20_180_35_2	6150	75000	13	0.787	0.0247
SS_20_180_35_3	6150	75000	14	0.787	0.0266
SS_20_180_35_4	6150	75000	14	0.787	0.0266

Table 21. K-factor for #5 and #7 MM specimens.

Specimen	f'_c (psi)	f_y (psi)	l_{dh} (in)	d_b (in)	K
MM_5_90_25_1	6450	100000	14	0.625	0.0257
MM_5_90_25_2	6450	100000	14	0.625	0.0257
MM_5_90_35_1	6450	100000	14	0.625	0.0257
MM_5_90_35_2	6450	100000	14	0.625	0.0257
MM_5_180_35_1	6320	100000	12	0.625	0.0218
MM_5_180_35_2	6320	100000	12	0.625	0.0218
MM_5_180_35_3	6320	100000	14	0.625	0.0254
MM_5_180_35_4	6320	100000	14	0.625	0.0254
MM_7_90_25_1	6600	100000	20	0.875	0.0265
MM_7_90_25_2*	6600	100000	20	0.875	0.0265
MM_7_90_35_1*	6600	100000	20	0.875	0.0265
MM_7_90_35_2*	6600	100000	20	0.875	0.0265
MM_7_90_35_3	6330	100000	20	0.875	0.0260
MM_7_90_35_4	6330	100000	20	0.875	0.0260
MM_7_180_35_1	6170	100000	17	0.875	0.0218
MM_7_180_35_2	6170	100000	17	0.875	0.0218
MM_7_180_35_3	6170	100000	20	0.875	0.0256
MM_7_180_35_4	6170	100000	20	0.875	0.0256

*Bars cast out of position

6 SUMMARY AND CONCLUSIONS

This research report covers testing of concrete reinforcement made with high strength steel and hooked to provide anchorage. Hooked reinforcement is typically used to develop reinforcement in a relatively short distance and is usually associated with a nodal region of a strut and tie system. A test setup was devised that uses the strut and tie behavior of hooked anchorage to impose forces similar to those occurring in the structure. The specimen configuration and test setup were arranged to promote a splitting tension failure of the concrete in the plane of the hook, which is the typical behavior of hooked anchorage without ties. Single #5 and #7 bars were tested with either 90- or 180-deg standard hooks. GR60 reinforcement was first tested to ensure that the desired failure mode was achieved and that the ACI and AASHTO development length equations for hooks did indeed ensure that the reinforcement reached yield before the concrete failed. Stainless steel reinforcement with a yield strength over 100 ksi and corrosion resistant reinforcement with a yield strength over 120 ksi were also tested. Anchorage capacity ratios (ultimate load/specified yield load) were calculated for each of the specimens to determine the effectiveness of the development lengths. In addition, strain ductility ratios (strain at ultimate capacity/yield strain from bare bar tension test) were determined for each specimen to provide a basis for comparison. The following conclusions are offered:

1. The test setup and the procedures using the strut and tie approach appear to provide an adequate basis to evaluate the unconfined anchorage capacities of GR60 hooked bars. The predominant failure mode generated using this test setup was splitting of the concrete in the plane of the hook. GR60 bars gave results consistent and agreeable with ACI and AASHTO requirements for development lengths. No clear trends indicated a performance difference between 90-deg. and 180-deg. hooks.
2. The anchorage capacity ratios were well above 1.25 for all specimens except #7 MM. The majority of the #7 MM specimens had anchorage capacity ratios below 1.25. This is an indication that development lengths longer than were tested in this program would be required for the #7 MM or that confinement reinforcement would be needed to ensure development, or both.
3. The mean strain ductility ratios of the GR60 bars were 18 and 9.4 for #5 and #7, respectively.

4. The mean strain ductility ratios of the SS bars were 34 and 6 for 16 mm and 20mm, respectively.
5. The mean strain ductility ratios of the MM specimens were 4.7 and 1.3 for #5 and #7, respectively.
6. Stainless steel #5 and #7 bars and the #5 MM specimens were able to resist loads beyond their respective yield points as indicated by the ductility ratios. Development lengths longer than that required by the current design equation, however, were needed to develop the necessary anchorage forces to attain the reported ductility.

7 RECOMMENDATIONS

A test approach and procedure by which hook development length can be tested has been developed. The test data indicate that the results are applicable for up to and including #7 bars. Although the tests were conducted on single bars causing a failure mode of concrete splitting in the plane of the hook, it is anticipated (but not experimentally validated) that multiple hooks placed in a row will be developed independently and that these results are applicable to those conditions, assuming code clearances and cover are maintained. Three methods of comparison were presented. The first was the capacity ratio, which measured the load beyond yield that the anchorage could sustain. The second was the strain ductility ratio, which is the ultimate bar strain divided by the yield strain measured in the bar tests. Finally, the development length equation was reorganized to allow the comparison of the coefficient, K. This coefficient is indicative of the geometry of the hook and the associated material properties.

Figure 50 shows the development length equations plotted against the capacity ratio for all test specimens. Figure 51 shows a similar plot with the ductility. Note that as the development length equation increases (K increases), there is no apparent increase in capacity or ductility, which may indicate that for larger bars increasing development length will not necessarily result in increased capacity or ductility. These results are similar to those found in lap splices in high performance concrete. Increasing the development did not really increase the splice capacity. In either case, transverse reinforcement may be required to ensure that the bars can be fully developed.

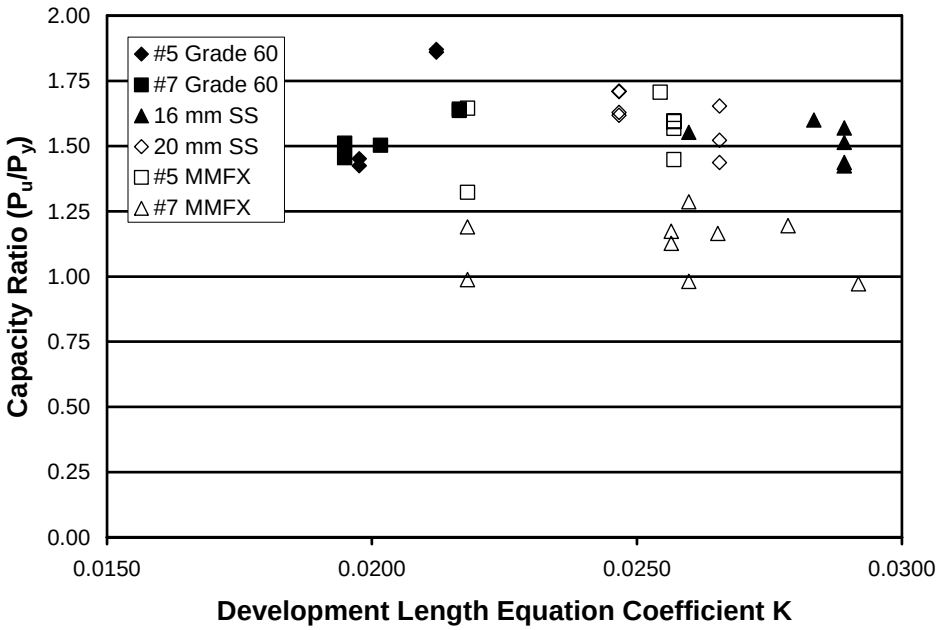

Figure 50. Comparison of equation coefficient with capacity ratio

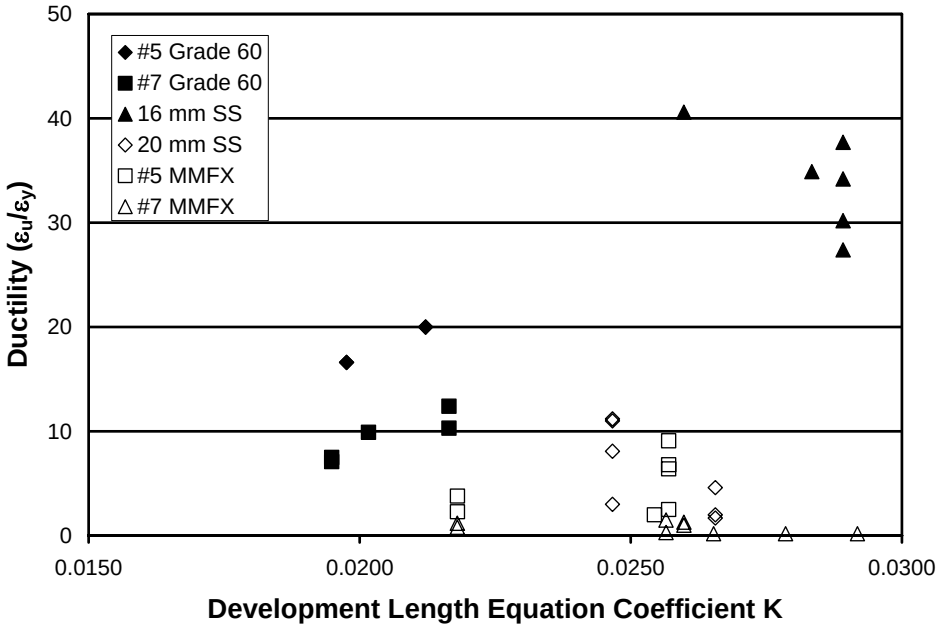

Figure 51. Comparison of ductility and development length equation coefficient.

Nevertheless, full development for some of the bars tested in this research was reached. Consequently, it is recommended that the following adjustment to the code equation be made to account for the higher strength steels. For bars up to #5 with f_y = 100 ksi and f_u = 150 ksi and up to #7 for steel with f_y = 75 ksi and f_u = 100 ksi the recommended change to the ACI Equation is:

$$l_{dh} = \frac{0.026\psi_e \lambda d_b f_y}{\sqrt{f_c'}}$$ Equation 14

Where ψ_e is the epoxy coated reinforcement factor, λ is the lightweight aggregate factor, d_b is the nominal bar diameter, f_y is the specified yield strength of the steel, and $f'c$ is the specified compressive strength of the concrete.

For bars up to #5 with f_y = 100 ksi and f_u = 150 ksi and up to #7 for steel with f_y = 75 ksi and f_u = 100 ksi the recommended change to AASHTO LRFD Specifications equation is:

$$l_{dh} = \frac{50 d_b}{\sqrt{f_c'}}$$ Equation 15

8 FUTURE RESEARCH

The research reported in this report presented a test procedure for determine the effectiveness of standard hook anchorage for concrete reinforcement. The variables studied in this research were limited to #5 and #7 bar sizes that were unconfined by transverse reinforcement. Although longer development lengths were attempted for the #7 MM specimens, full development of these bars was unsuccessful. Further research is required to determine if even longer lengths can develop these bars. If not, transverse reinforcement should be investigated to determine if the full development length can be reached. Another option might be to increase the radius of the bar bend to ease the bearing stresses on the inside of the bar. Finally, bars up to #11 should be tested to determine if these bars can be developed without transverse reinforcement.

9 REFERENCES

AASHTO (2001). " Standard Specifications for Highway Bridges." American Association of States Highway and Transportation Officials.

ACI 408.1R-79 (1979). "Suggested Development, Splice, and Standard Hook Provisions for Deformed Bars in Tension." American Concrete Institute.

ACI Committee 318 (1977). “Building Code Requirements for Reinforced Concrete (ACI 318-77).” American Concrete Institute.

ACI Committee 318 (1995). “Building Code Requirements for Reinforced Concrete (ACI 318-95).” American Concrete Institute.

ACI Committee 318 (2002). “Building Code Requirements for Reinforced Concrete (ACI 318-02).” American Concrete Institute.

ASTM A 370 (2007). “Standard Test Methods and Definitions for Mechanical Testing of Steel Products.” American Society for Testing and Materials.

ASTM A1035/A1035M (2007). “Standard Specification for Deformed and Plain, Low-carbon, Chromium, Steel Bars for Concrete Reinforcement.” American Society for Testing and Materials.

ASTM C 39 (1999). “Standard Test Method for Compressive Strength of Cylindrical Concrete Specimens.” American Society for Testing and Materials.

ASTM C 143 (2000). “Standard Test Method for Slump of Hydraulic Cement Concrete.” American Society for Testing and Materials.

Ahlborn, Tess and DenHarting Tim (2002). “A Comparative Bond Study of MMFX Reinforcing Steel in Concrete”. Michigan Technological University. Center for Structural Durability. Final Report CSD-2002-03.

Azizinamini, A., Darwin, D., Eligehausen, R., Pavel, R., and Ghosh, S. K. (1999) “Proposed Modifications to ACI 318-95 Tension Development and Lap Splice for High-Strength Concrete” *ACI Structural Journal*, 96(6), 822-827.

Hamad, B.S., Jirsa, J.O. and D’Abreu de Paulo, N.I (1993). “Anchorage Strength of Epoxy-Coated Hooked Bars.” *ACI Structural Journal*, 90(2), 210-217.

Jirsa, J.O., Lutz, L.A. and Gergely, P (1979). “Rationale for Suggested Development, Splice, and Standard Hook Provisions for Deformed Bars in Tension.” *Concrete International*, 79(7), 47-61.

Marques, J.L.G., and Jirsa, J.O (1975). “A Study of Hooked Bar Anchorages in Beam-Column Joints.” *ACI Journal*, 72(5), 198-209.

Minor, J., and Jirsa, J.O (1975). “Behavior of Bent Bar Anchorages.” *ACI Journal*, 72(4), 141-149.

Pinc, R.L., Watkins, M.D. and Jirsa, J.O (1977). “Strength of Hooked Bar Anchorages in Beam-Column Joints.” CESRL Report No. 77-3, Department of Civil Engineering, The University of Texas, Austin, Texas.

APPENDIX A

Table 22. Compressive concrete strength results –age (days)

Batches	Concrete Strength (psi) - Age (days)			
	7	14	21	28
1	4670	5850	6320	-
2	3490	4420	5050	5890
3	6350	6690	-	8060
4	5170	6320	6670	7160
5	4170	5330	6150	6880

Table 23. Tensile test results.

#5 Grade 60

Samples	Yield Strength at 0.35% strain (ksi)	Strain at 0.35% yield (in/in)	Load at 0.35% strain (kip)	Ultimate Strength (ksi)	Elongation (%)
1	62.78	0.0035	19.46	104.6	9
2	62.74	0.0035	19.45	104.8	9
Avg.	62.76	0.0035	19.46	104.7	9
COV (%)	0	0	0	0	

#7 Grade 60

Samples	Yield Strength at 0.35% strain (ksi)	Strain at 0.35% yield (in/in)	Load at 0.35% strain (kip)	Ultimate Strength (ksi)	Elongation (%)
1	63.51	0.0035	38.10	105.9	13
2	63.96	0.0035	38.37	105.9	13
Avg.	63.73	0.0035	38.24	105.9	13
COV (%)	< 1	< 1	< 1	< 1	

16 mm Stainless Steel (Heat 1)

Samples	Yield Strength at 0.2% offset (ksi)	Strain at 0.2% offset yield (in/in)	Load at 0.2% offset (kip)	Ultimate Strength (ksi)	Elongation (%)
1	93.262	0.0056	28.911	114.25	20
2	88.800	0.0055	27.528	112.79	18
Avg.	91.031	0.00555	28.220	113.52	19
COV (%)	3	1	3	1	

Table 23. Tensile test results (cont.)

16 mm Stainless Steel (Heat 2)					
Samples	Yield Strength at 0.2% offset (ksi)	Strain at 0.2% offset yield (in/in)	Load at 0.2% offset (kip)	Ultimate Strength (ksi)	Elongation (%)
1	106.2	0.0061	32.93	123.9	n/a
2	106.2	0.0062	32.92	123.7	n/a
Avg.	106.2	0.00615	32.92	123.8	n/a
COV (%)	< 1	1	< 1	< 1	

20 mm Stainless Steel					
Samples	Yield Strength at 0.2% offset (ksi)	Strain at 0.2% offset yield (in/in)	Load at 0.2% offset (kip)	Ultimate Strength (ksi)	Elongation (%)
1	100.7	0.0063	49.03	119.9	20
2	100.9	0.006	49.17	120.2	16
Avg.	100.8	0.0061	49.10	120.0	18
COV (%)	< 1	3	< 1	< 1	16

#5 MMFX					
Samples	Yield Strength at 0.2% offset (ksi)	Strain at 0.2% offset yield (in/in)	Load at 0.2% offset (kip)	Ultimate Strength (ksi)	Elongation (%)
1	123.273	0.00648	38.215	157.79	5
2	121.622	0.00650	37.703	158.50	8
Avg.	122.448	0.00649	37.959	158.14	
COV (%)	1	< 1	1	< 1	

#7 MMFX					
Samples	Yield Strength at 0.2% offset (ksi)	Strain at 0.2% offset yield (in/in)	Load at 0.2% offset (kip)	Ultimate Strength (ksi)	Elongation (%)
1	128.089	0.0066	76.854	163.12	6
2	128.073	0.0068	76.844	162.81	8
Avg.	128.081	0.0067	76.849	162.97	
COV (%)	< 1	2	< 1	< 1	

APPENDIX B

Table 24. Crack patterns, failure modes, load-slip, and stress-strain curves for GR60 steel hooked bars.

60_5_90_1

Bar yield followed by concrete splitting

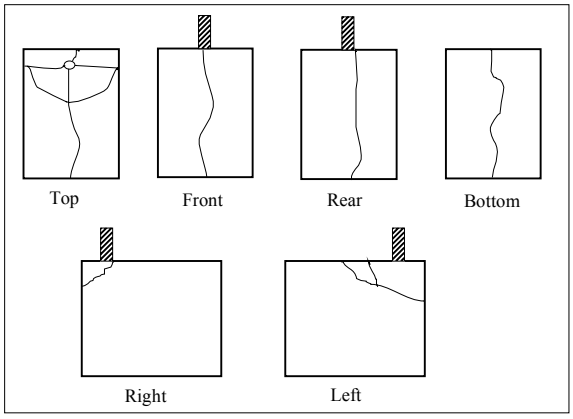

60_5_90_S

Bar Rupture

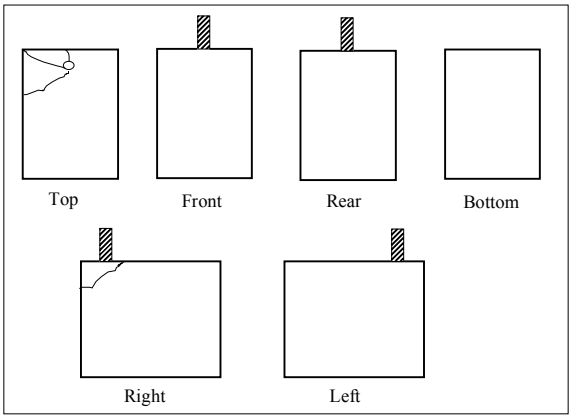

Load-Slip for Linear Pots
60_5_90_1

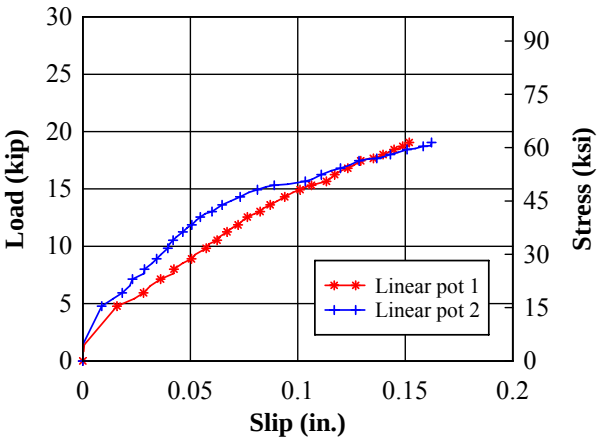

Load-Slip for Linear Pots
60_5_90_S

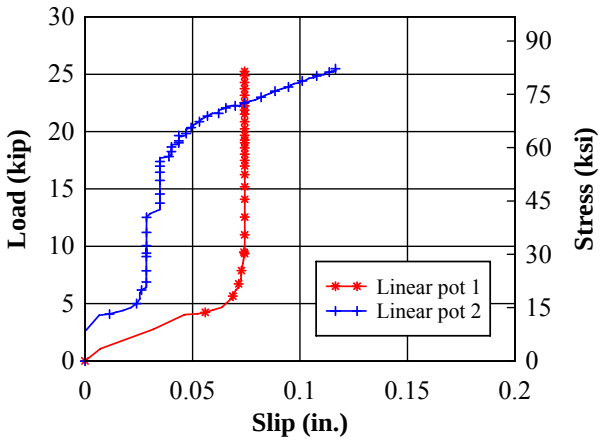

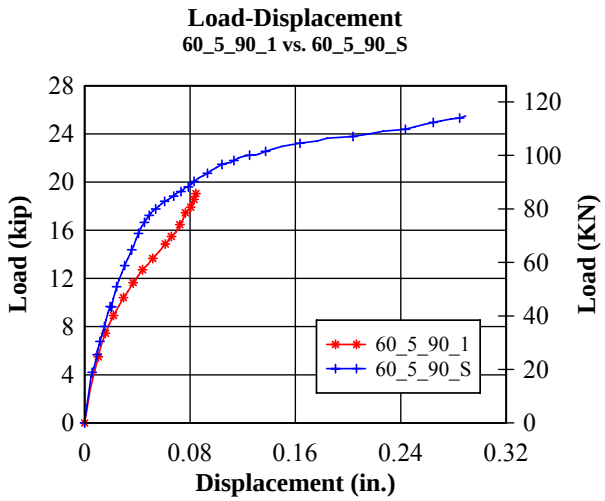
Load-Displacement
60_5_90_1 vs. 60_5_90_S
Load (kip)
Load (KN)
Displacement (in.)
28
24
20
16
12
8
4
0
120
100
80
60
40
20
0
0
0.08
0.16
0.24
0.32
60_5_90_1
60_5_90_S

60_5_90_25_1

Bar yield followed by concrete splitting

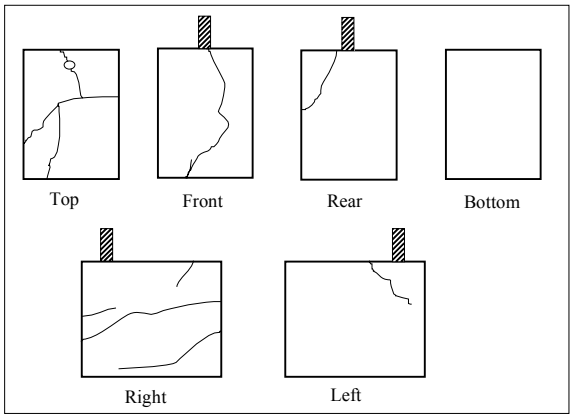

60_5_90_25_2

Bar yield followed by concrete splitting

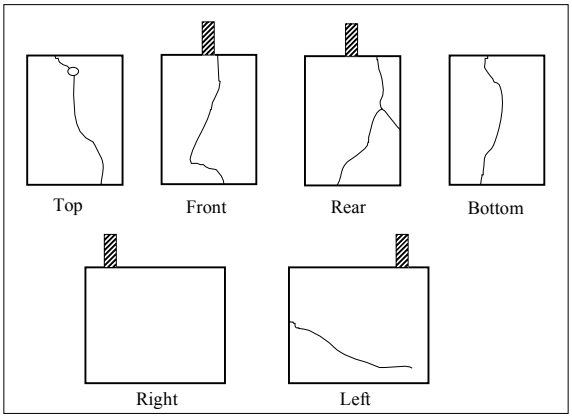

Load-Slip for Linear Pots

60_5_90_25_2

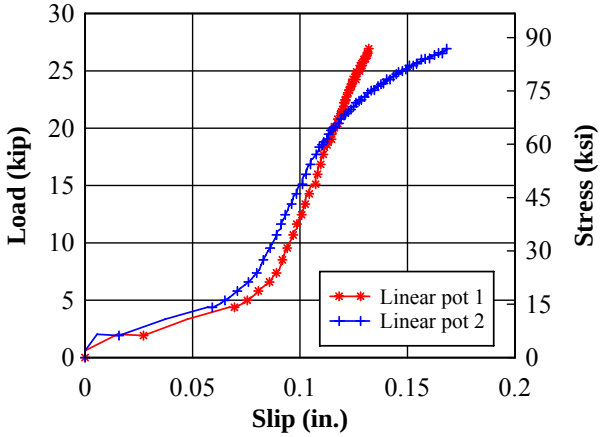

Load-Displacement

60_5_90_25_1 vs. 60_5_90_25_2

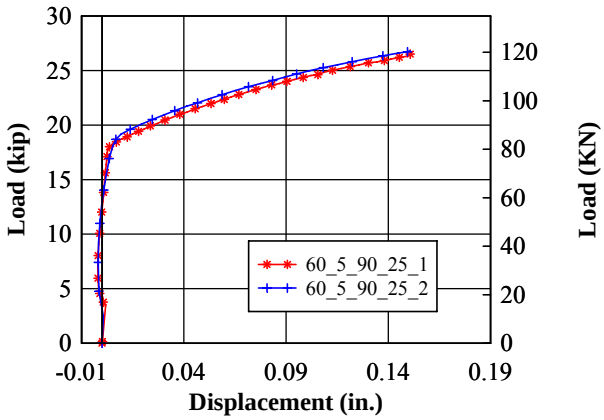

Stress-Strain

60_5_90_25_1 vs. 60_5_90_25_2

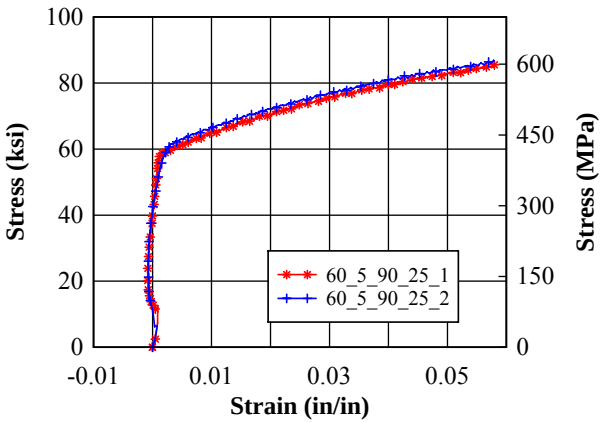

60_5_180_35_1

Bar Rupture

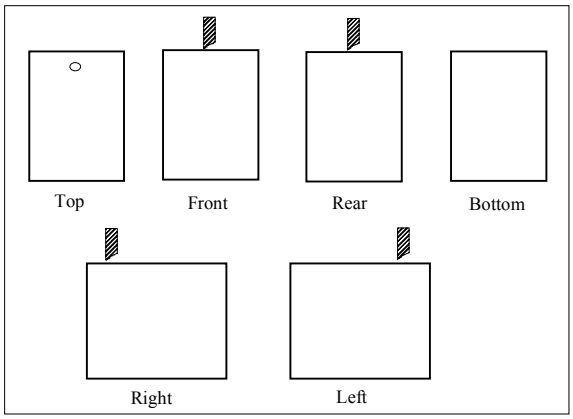

60_5_180_35_2

Bar Rupture

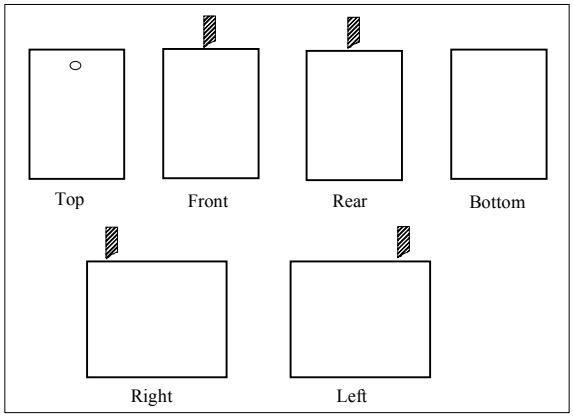

Load-Slip for Linear Pots
60_5_180_35_1

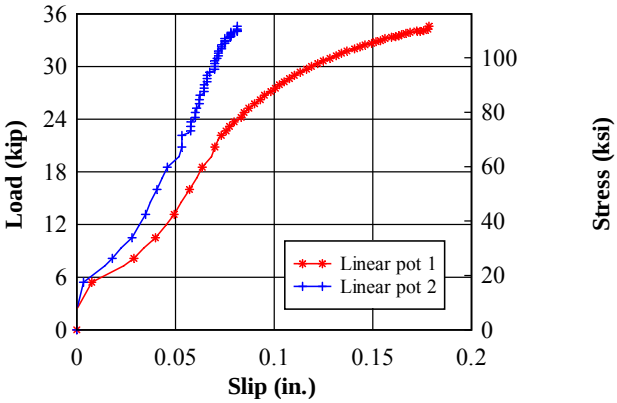

Load-Slip for Linear Pots
60_5_180_35_2

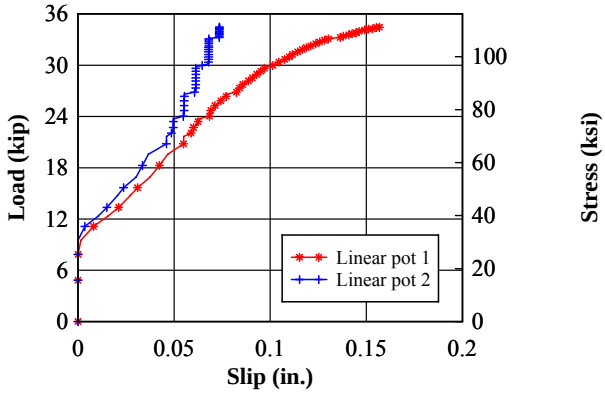

Load-Displacement
60_5_180_35_1 vs. 60_5_180_35_2

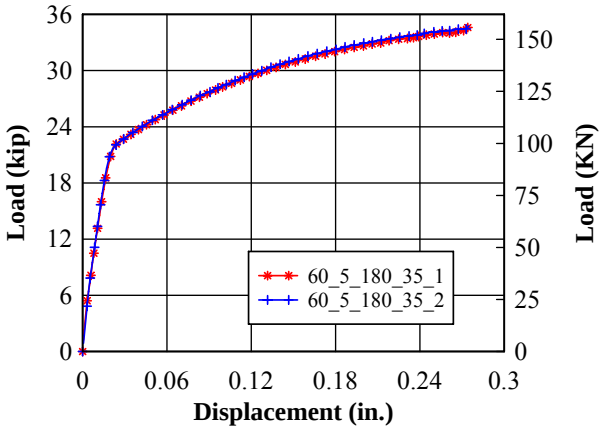

Stress-Strain
60_5_180_35_1 vs. 60_5_180_35_2

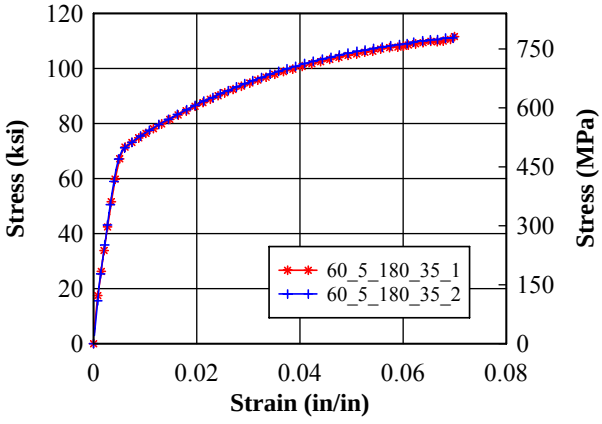

60_7_90_1

Bar yield followed by concrete splitting

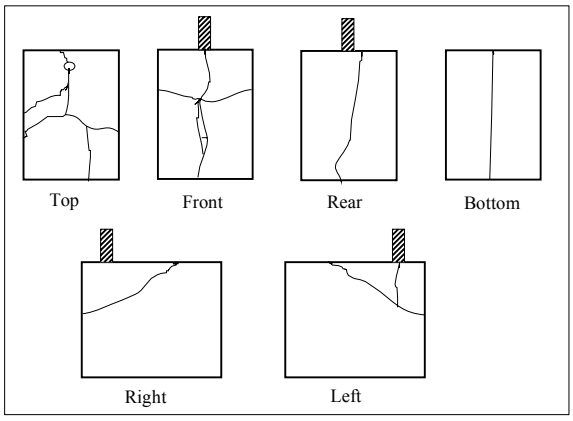

60_7_90_S

Bar yield followed by concrete splitting

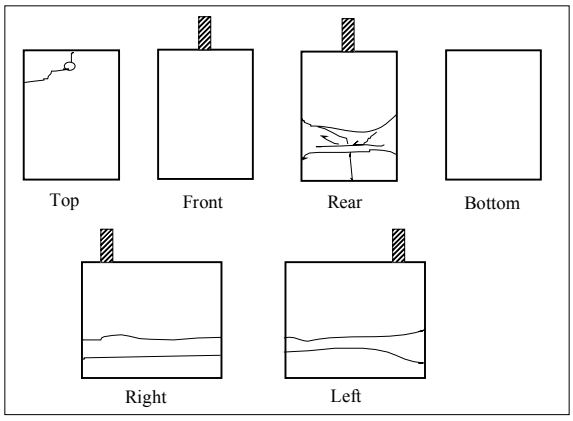

Load-Slip for Linear Pots
60_7_90_1

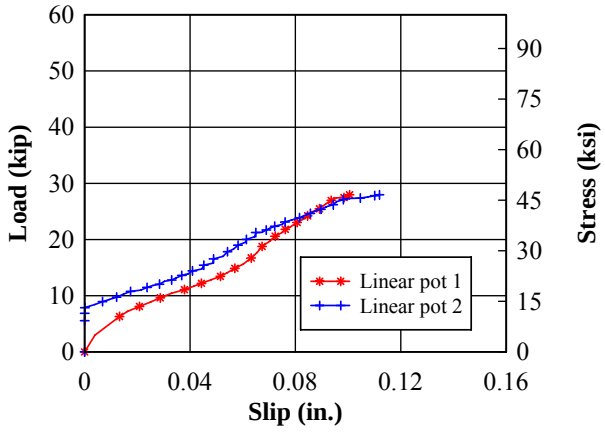

Load-Slip for Linear Pots
60_7_90_S

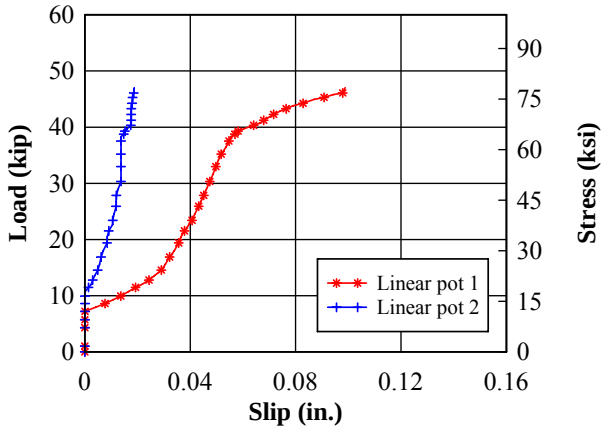

Load-Displacement
60_7_90_1 vs. 60_7_90_S

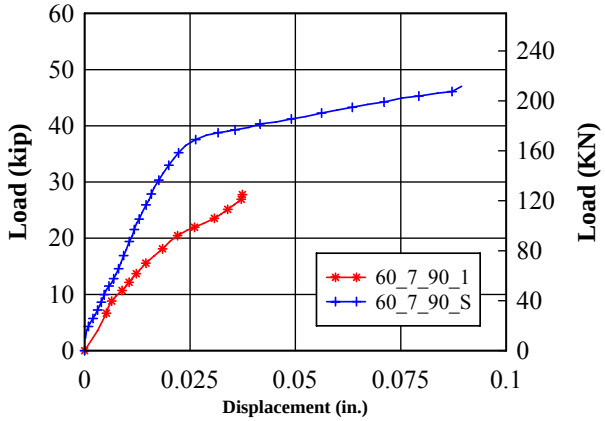

60_7_90_47_1

Bar yield followed by concrete splitting

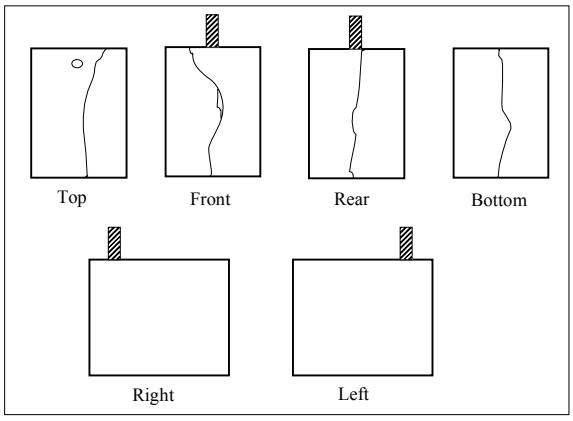

60_7_90_47_2

Bar yield followed by concrete splitting

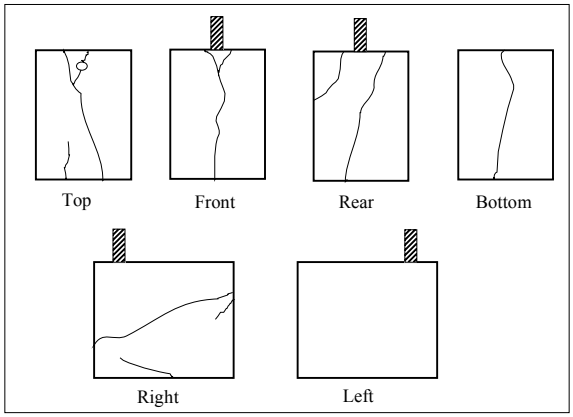

Load_Slip for Linear Pots
60_7_90_47_2

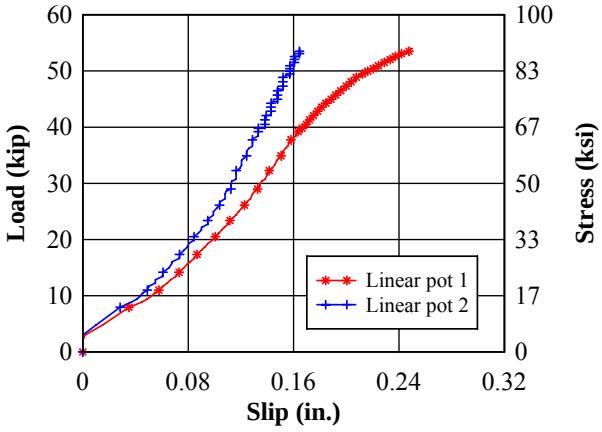

Load-Displacement
60_7_90_47_1 vs. 60_7_90_47_2

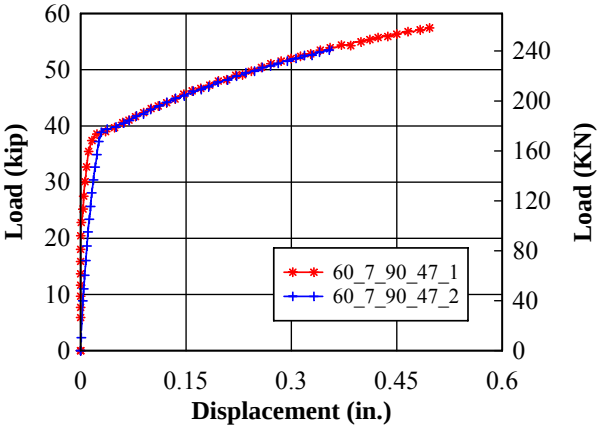

Stress-Strain
60_7_90_47_1 vs. 60_7_90_47_2

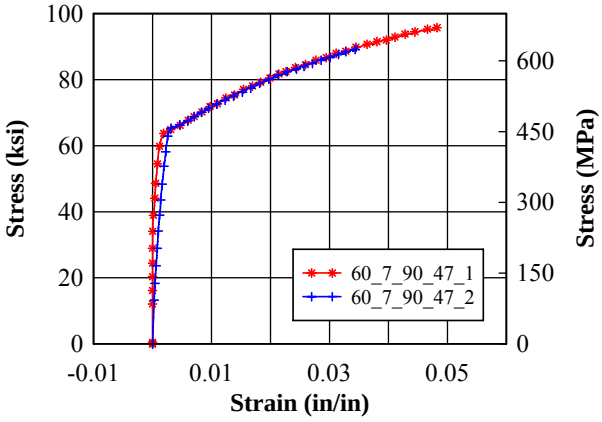

60_7_180_35_1

Bar yield followed by concrete splitting

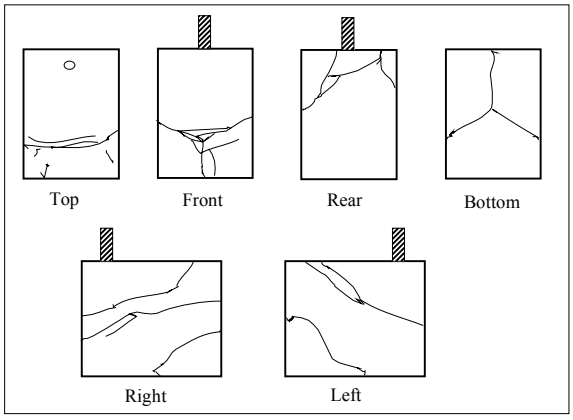

60_7_180_35_2

Bar yield followed by concrete splitting

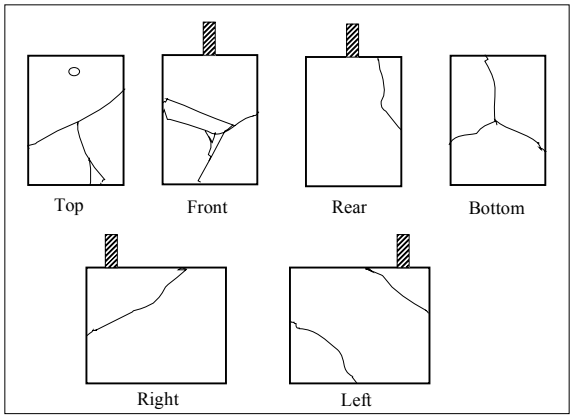

Load-Slip for Linear Pots
60_7_180_35_1

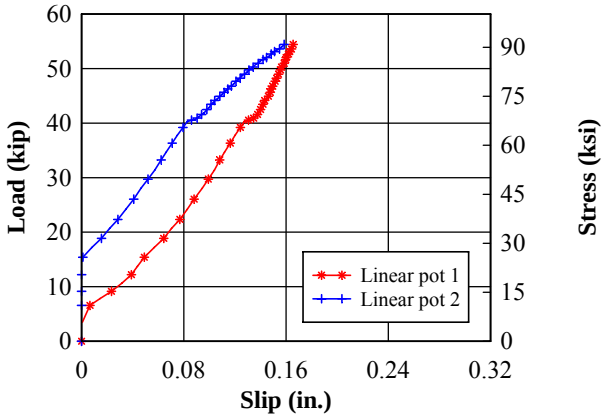

Load-Slip for Linear Pots
60_7_180_35_2

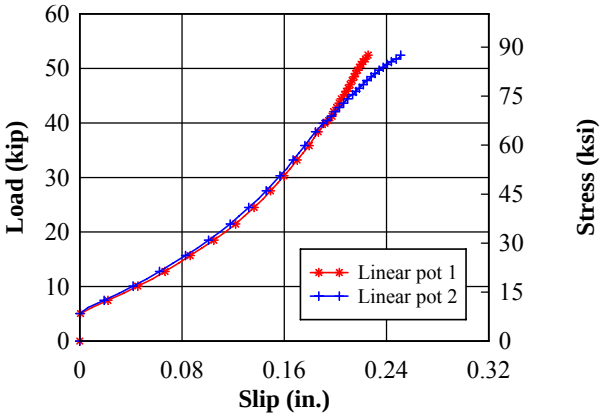

Load-Displacement
60_7_180_35_1 vs. 60_7_180_35_2

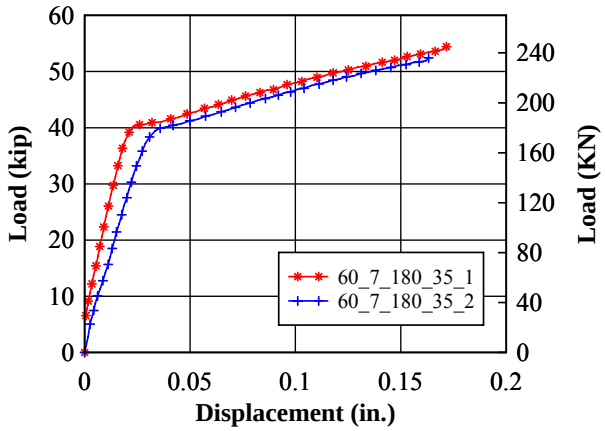

Stress-Strain
60_7_180_35_1 vs. 60_7_180_35_2

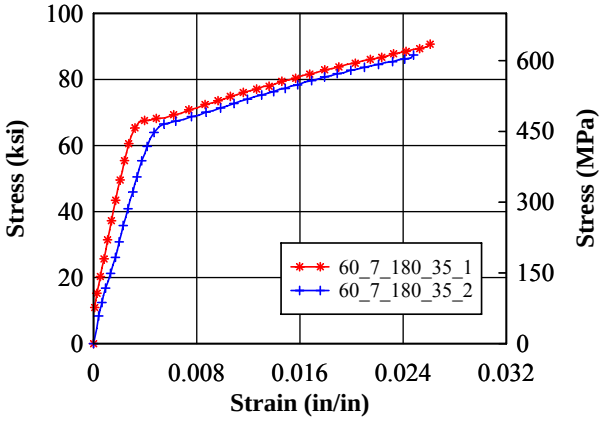

60_7_180_35_3

Bar yield followed by concrete splitting

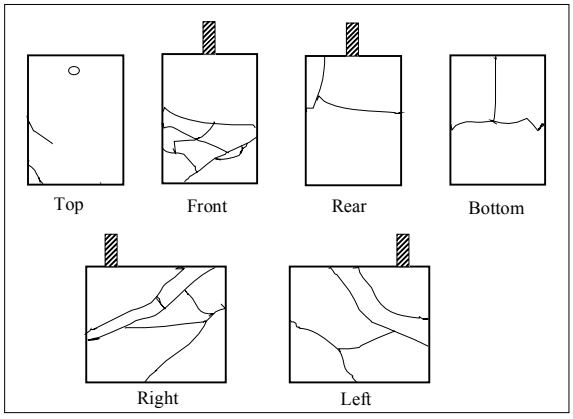

60_7_180_35_4

Bar yield followed by concrete splitting

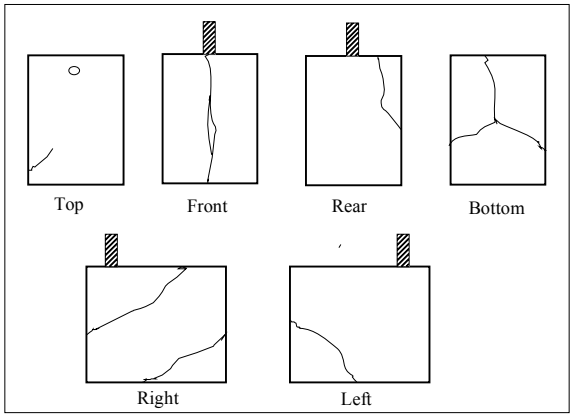

Load-Slip for Linear Pots
60_7_180_35_3

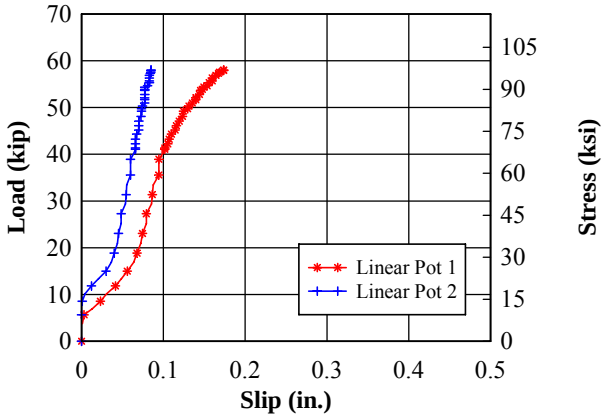

Load-Slip for Linear Pots
60_7_180_35_4

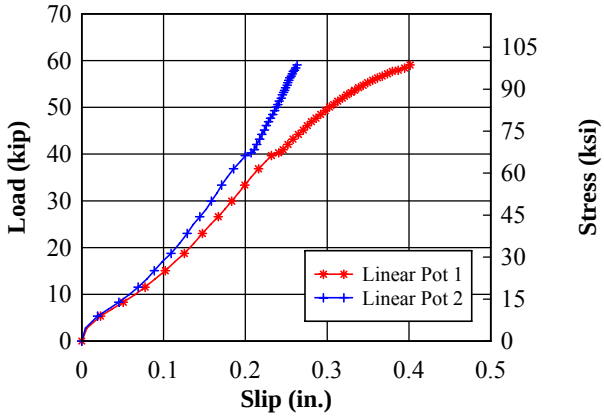

Load-Displacement
60_7_180_35_3 vs. 60_7_180_35_4

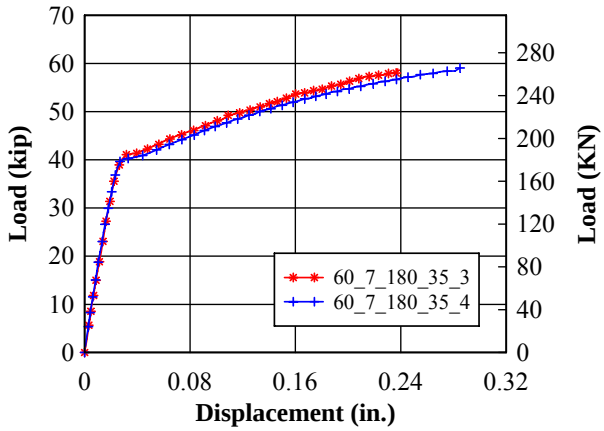

Stress-Strain
60_7_180_35_3 vs. 60_7_180_35_4

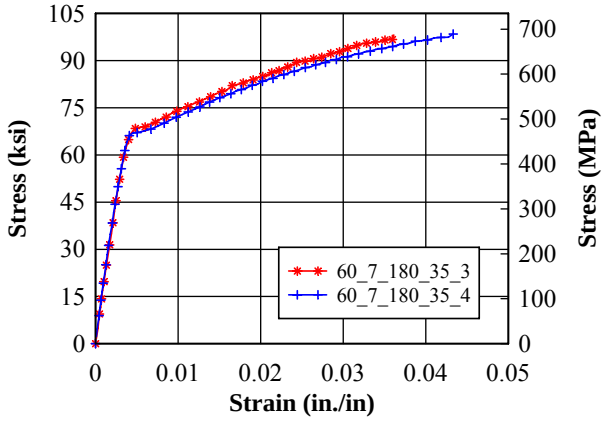

Table 25. Crack patterns, failure modes, load-slip, and stress-strain curves for stainless steel hooked bars.

SS_16_90_25_1

Bar yield no rupture stroke limit reached

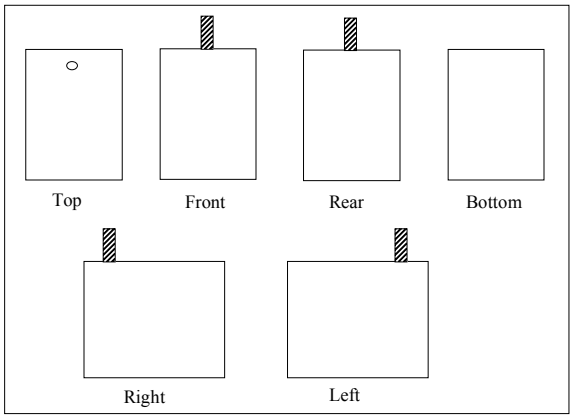

SS_16_90_25_2

Bar yield no rupture stroke limit reached

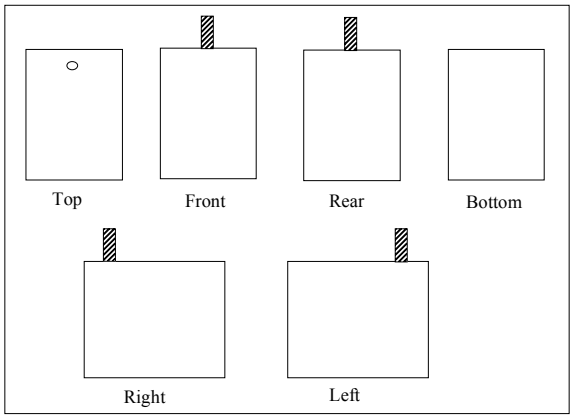

Load-Slip for Linear Pots
SS_16_90_25_1

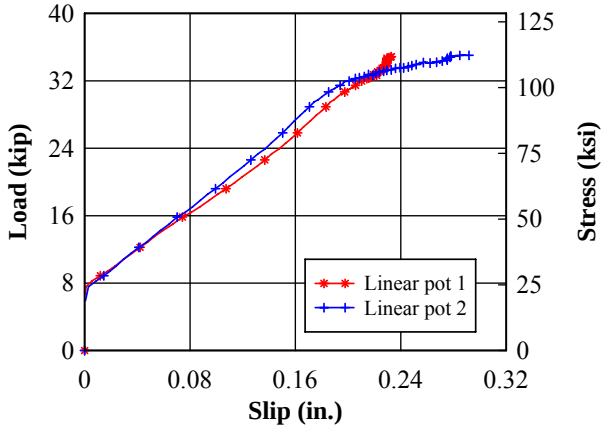

Load-Slip for Linear Pots
SS_16_90_25_2

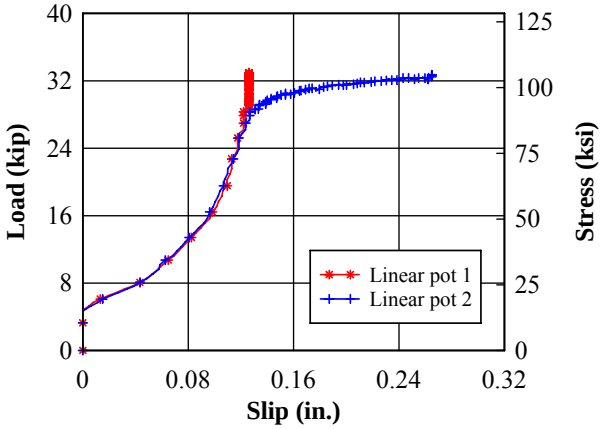

Load-Displacment
SS_16_90_25_1 vs. SS_16_90_25_2

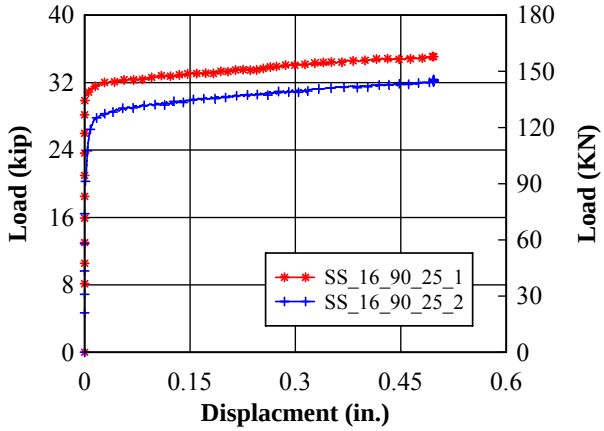

Stress-Strain
SS_16_90_25_1 vs. SS_16_90_25_2

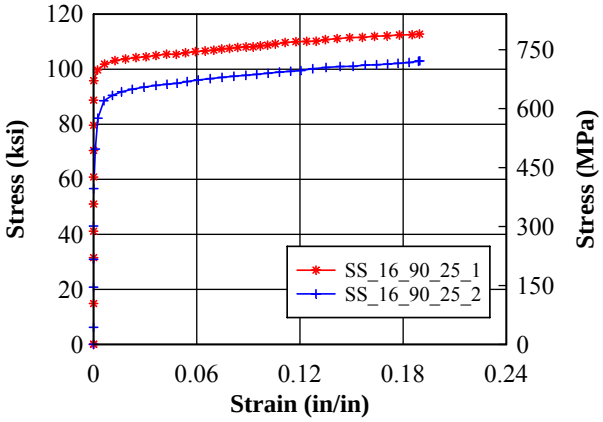

SS_16_90_35_1

Bar yield no rupture stroke limit reached

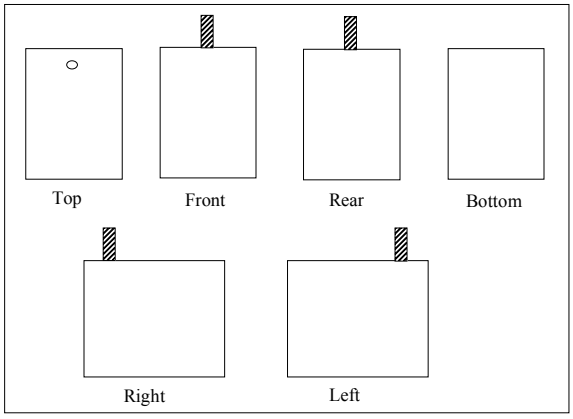

SS_16_90_35_2

Bar yield no rupture stroke limit reached

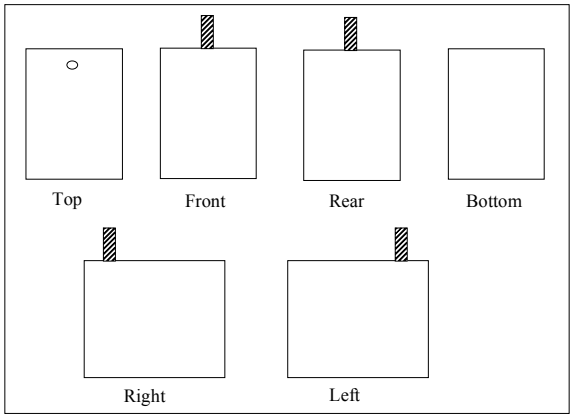

Load-Slip for Linear Pots
SS_16_90_35_1

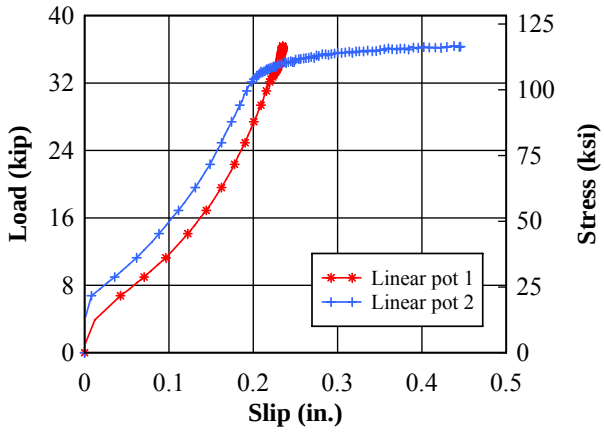

Load-Slip for Linear Pots
SS_16_90_35_2

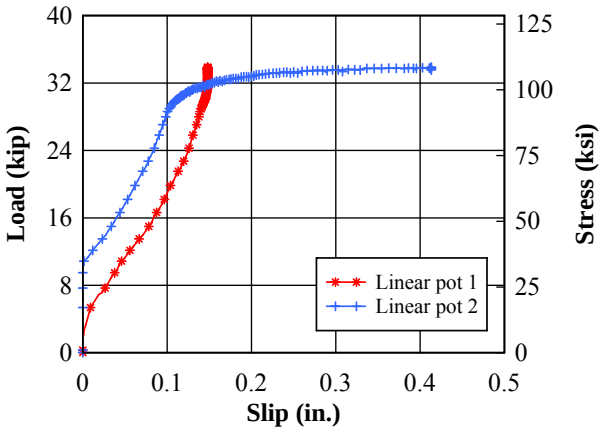

Load-Displacement
SS_16_90_35_1 vs. SS_16_90_35_2

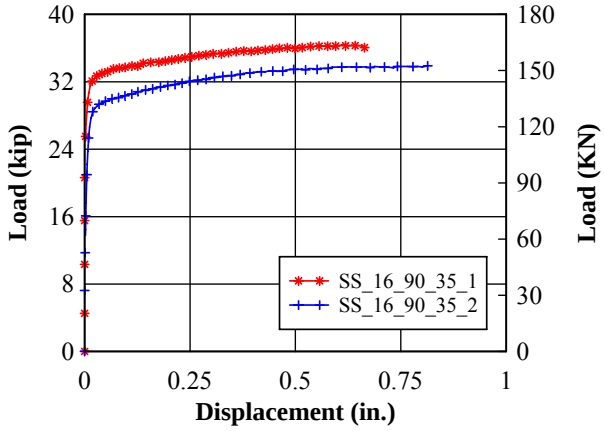

Stress_Strain
SS_16_90_35_1 vs. SS_16_90_35_2

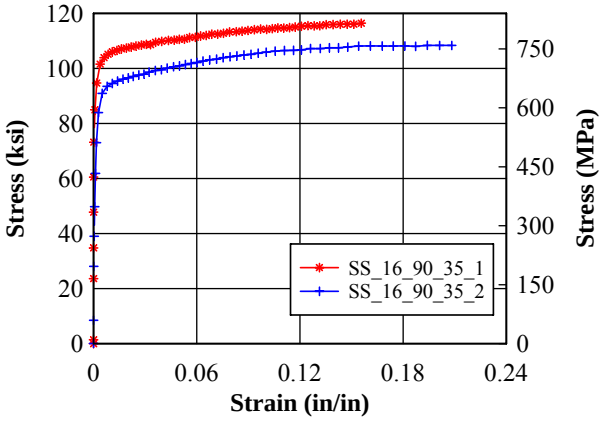

SS_16_180_35_1

Bar yield no rupture stroke limit reached

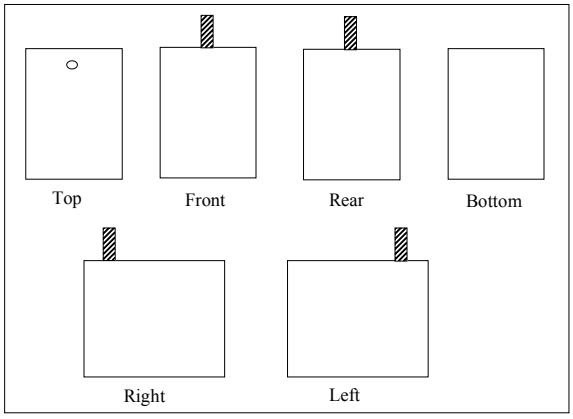

SS_16_180_35_2

Bar yield followed by concrete splitting

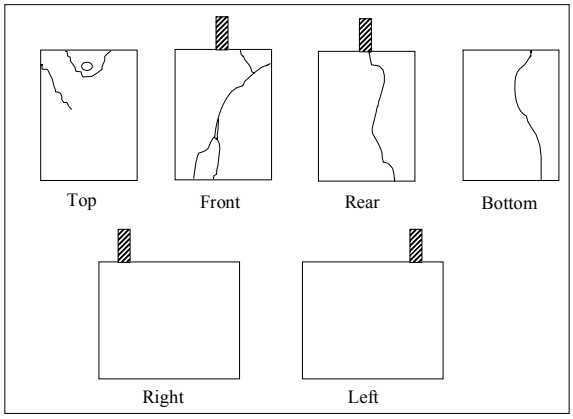

Load-Slip for Linear Pots
SS_16_180_35_1

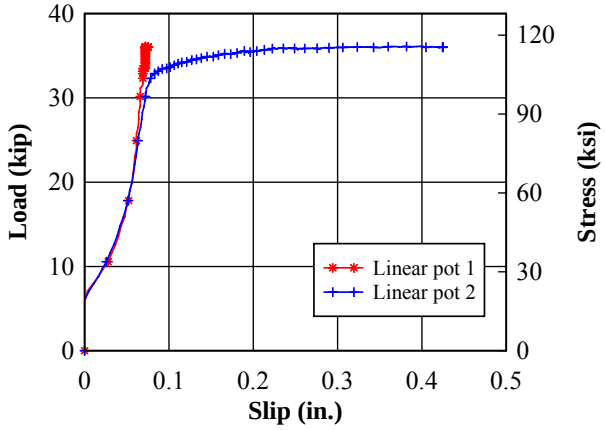

Load-Slip for Linear Pots
SS_16_180_35_2

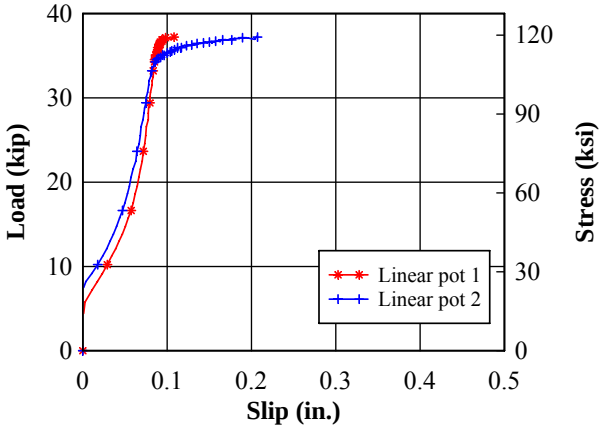

Load-Displacement
SS_16_180_35_1 vs. SS_16_180_35_2

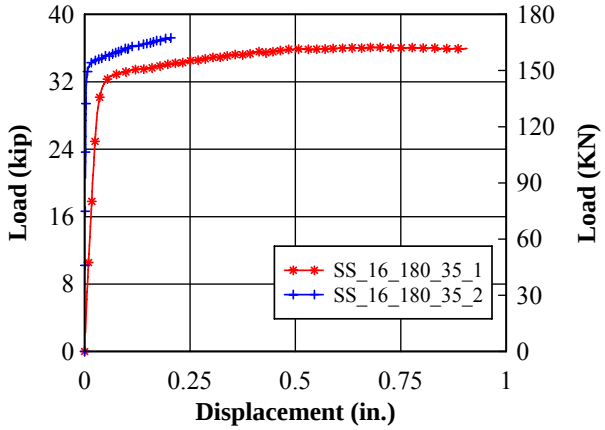

Stress-Strain
SS_16_180_35_1 vs. SS_16_180_35_2

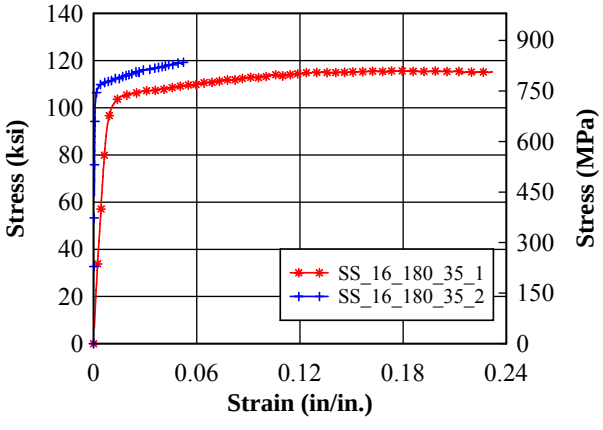

SS_16_180_35_3

Bar Rupture

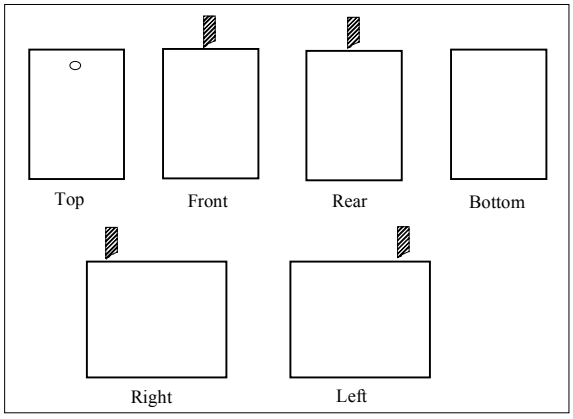

SS_16_180_35_4

Bar yield no rupture stroke limit reached

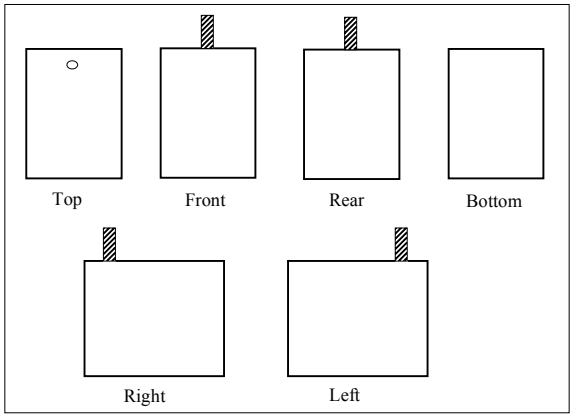

Load-Slip for Linear Pots

SS_16_180_35_3

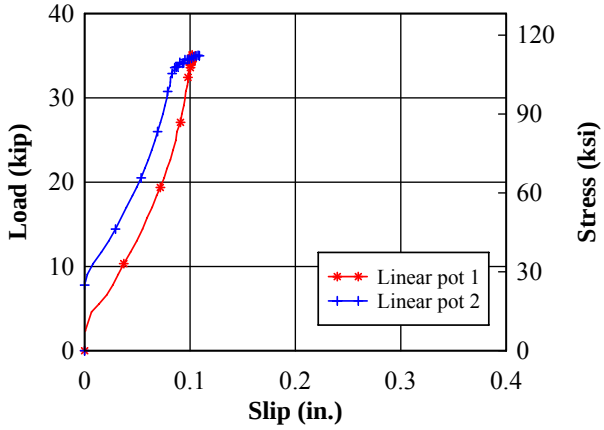

Load-Slip for Linear Pots

SS_16_180_35_4

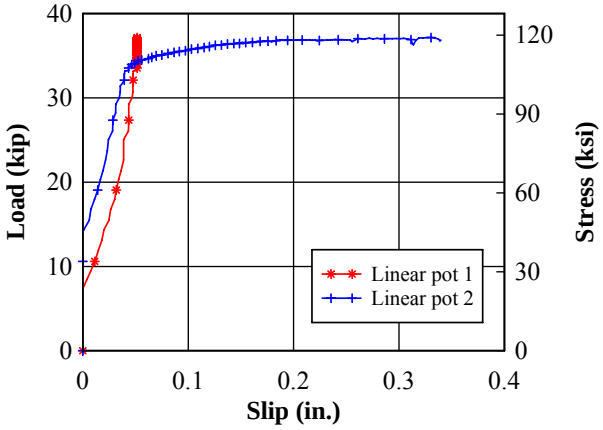

Load-Displacement

SS_16_180_35_3 vs. SS_16_180_35_4

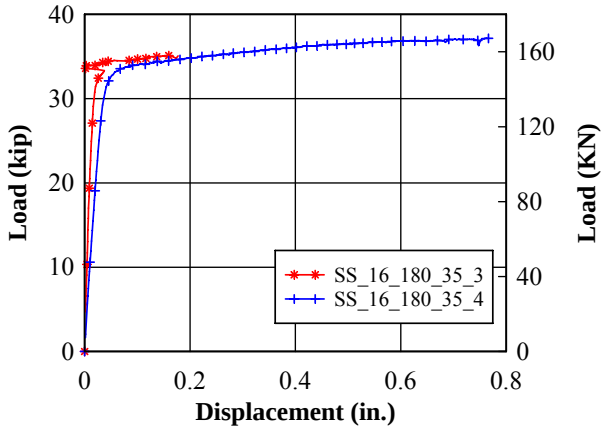

Stress-Strain

SS_16_180_35_3 vs. SS_16_180_35_4

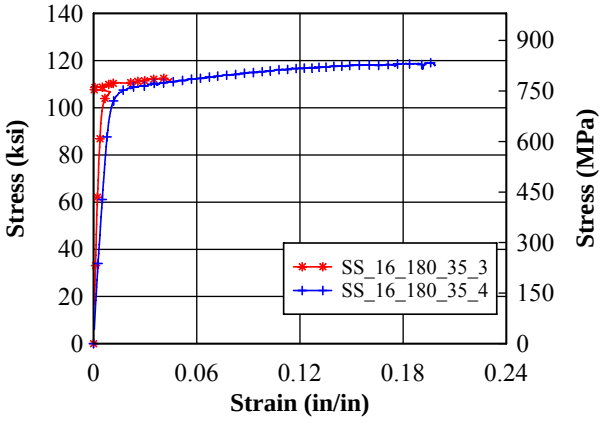

SS_20_90_35_1

Bar yield followed by concrete splitting

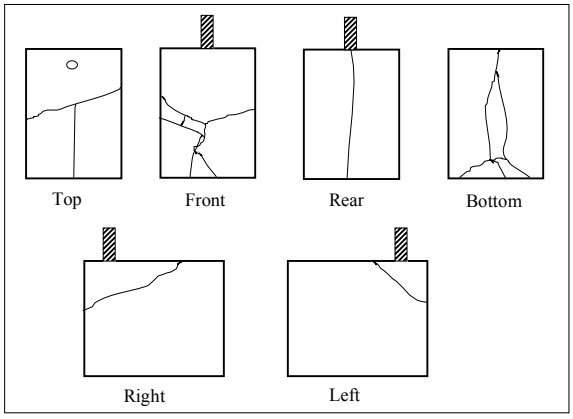

SS_20_90_35_2

Bar yield followed by concrete splitting

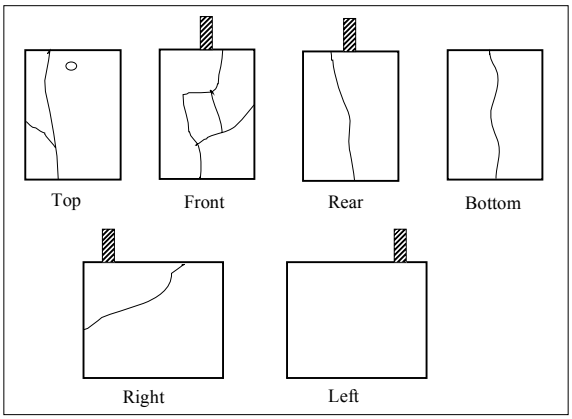

Load-Slip for Linear Pots
SS_20_90_35_1

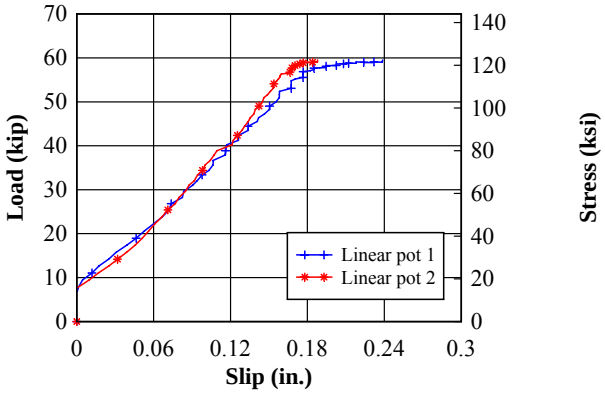

Load-Slip for Linear Pots
SS_20_90_35_2

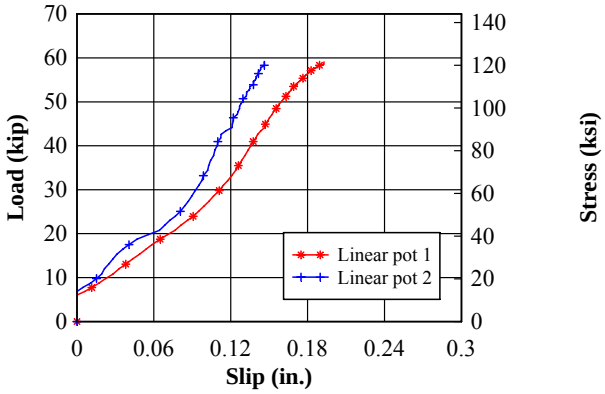

Load-Displacement
SS_20_90_35_1 vs. SS_20_90_35_2

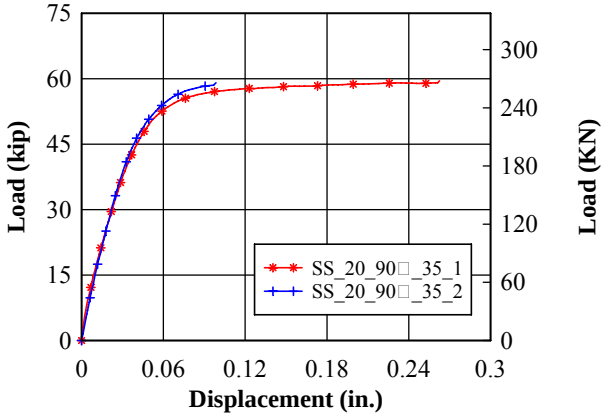

Stress-Strain
SS_20_90_35_1 vs. SS_20_90_35_2

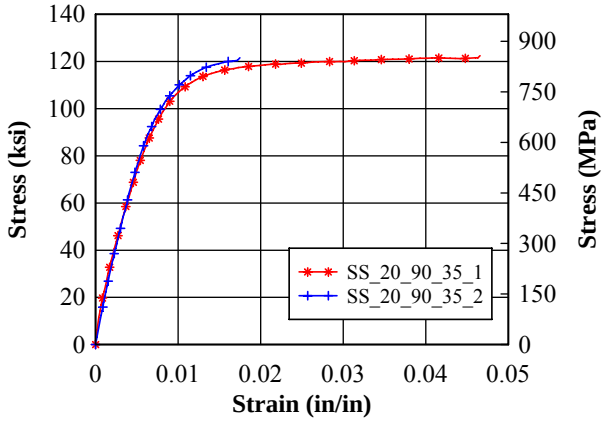

SS_20_90_35_3

Bar yield followed by concrete splitting

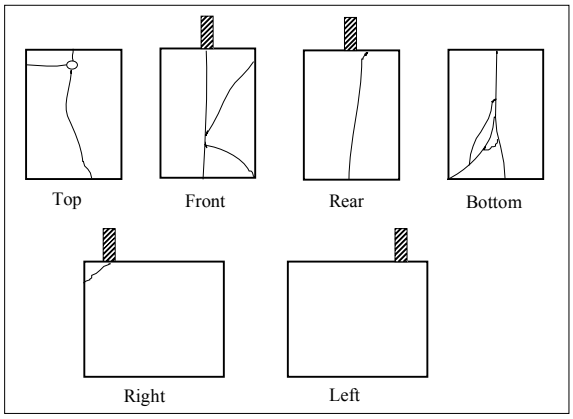

SS_20_90_35_4

Bar yield followed by concrete splitting

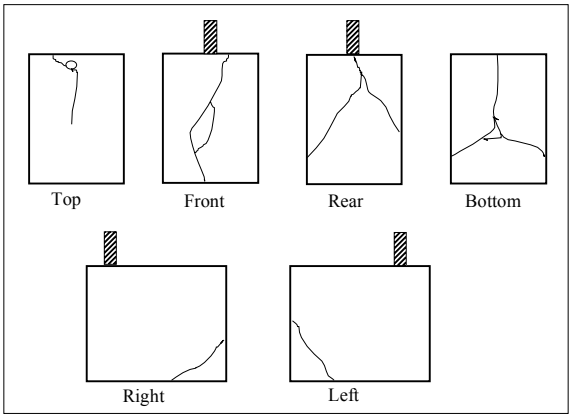

Load-Slip for Linear Pots
SS_20_90_35_3

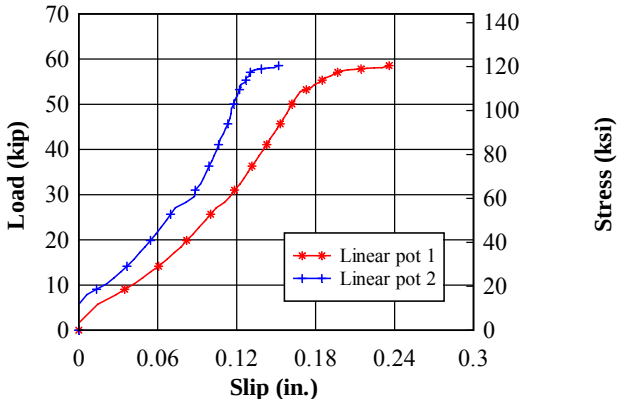

Load-Slip for Linear Pots
SS_20_90_35_4

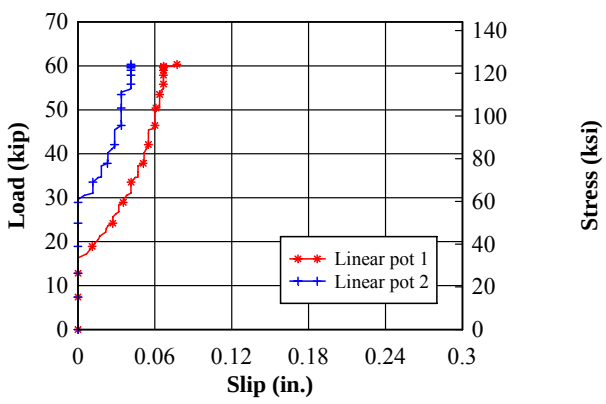

Load-Displacement
SS_20_90_35_3 vs. SS_20_90_35_4

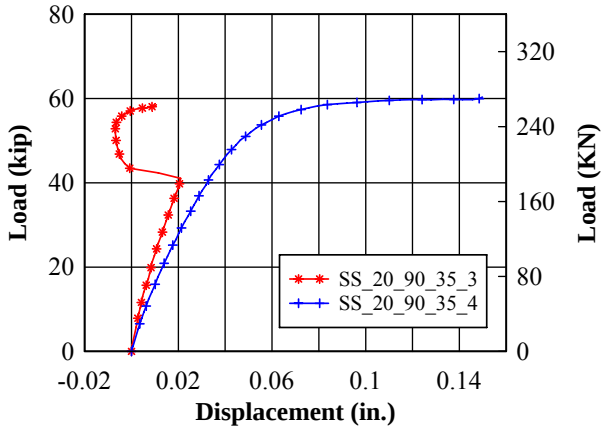

Stress-Strain
SS_20_90_35_3 vs. SS_20_90_35_4

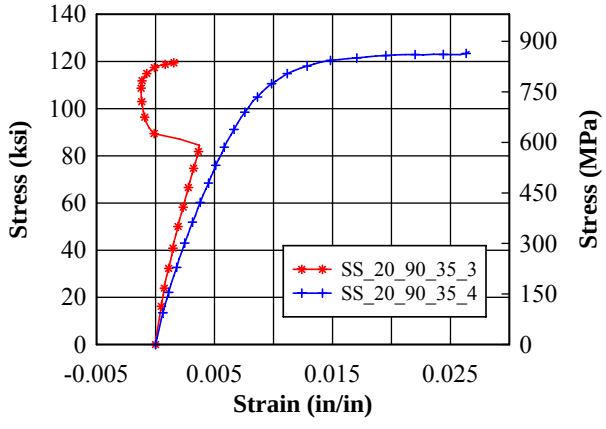

SS_20_180_35_1

Bar yield followed by concrete splitting

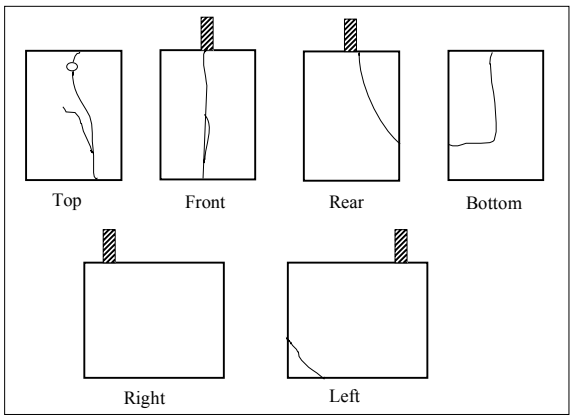

SS_20_180_35_2

Bar yield followed by concrete splitting

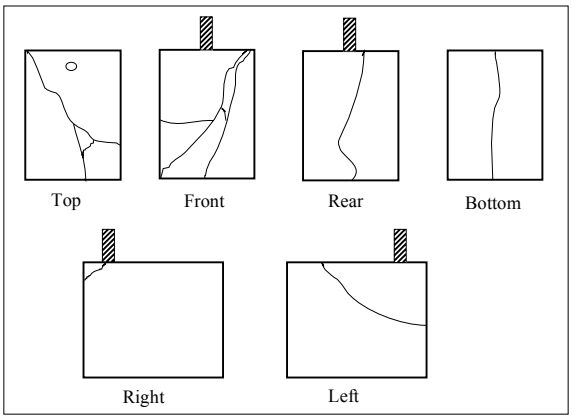

Load-Slip for Linear Pots
SS_20_180_35_1

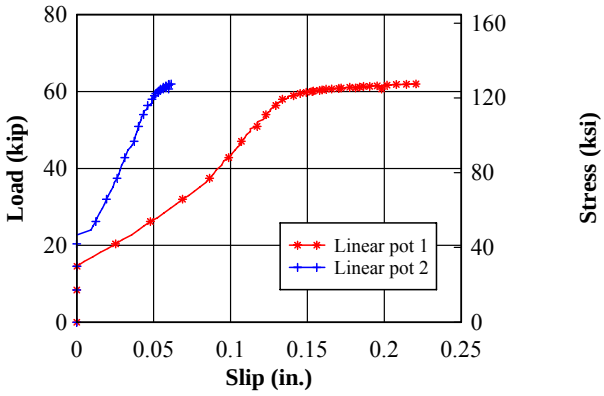

Load-Slip for Linear Pots
SS_20_180_35_2

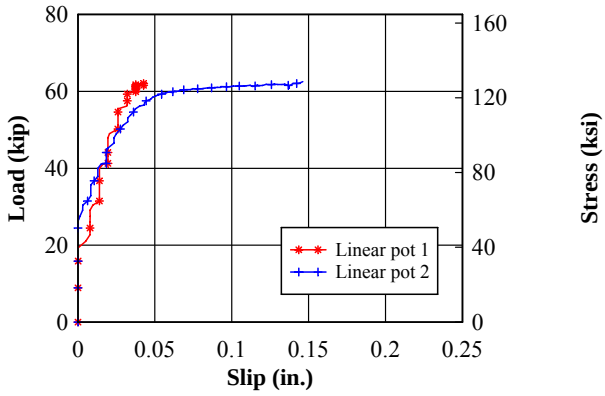

Load-Displacement
SS_20_180_35_1 vs. SS_20_180_35_2

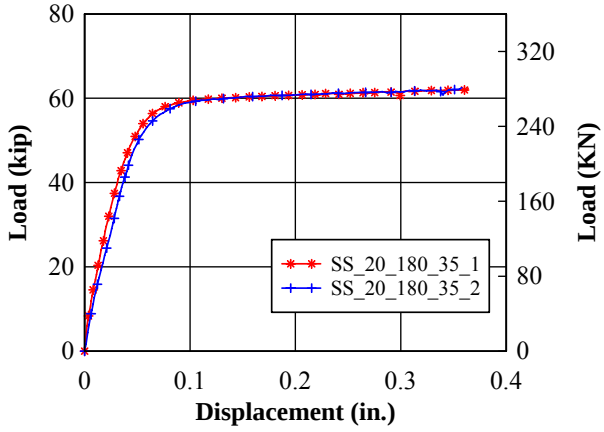

Stress-Strain
SS_20_180_35_1 vs. SS_20_180_35_2

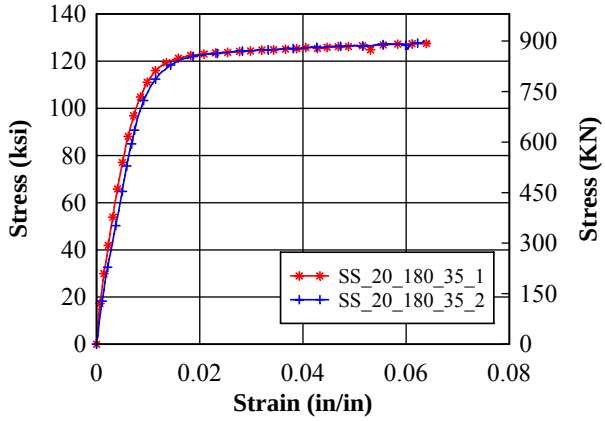

SS_20_180_35_3

Bar yield followed by concrete splitting

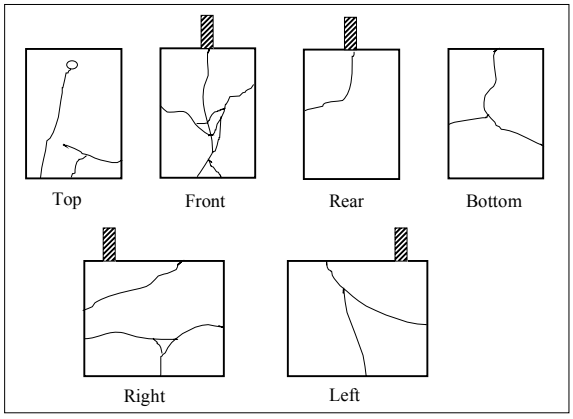

SS_20_180_35_4

Bar yield followed by concrete splitting

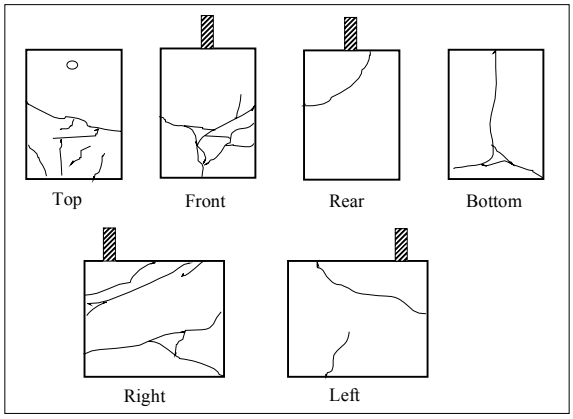

Load-Slip for Linear Pots
SS_20_180_35_3

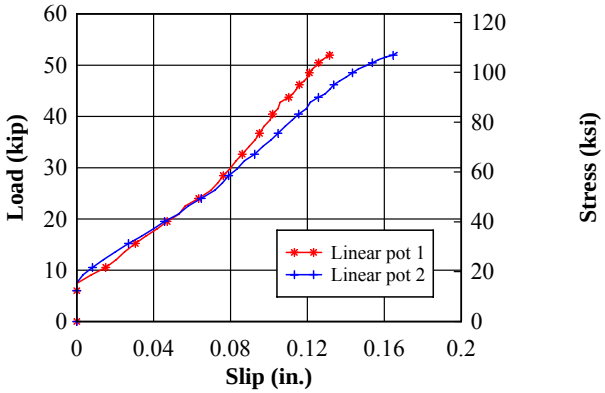

Load-Slip for Linear Pots
SS_20_180_35_4

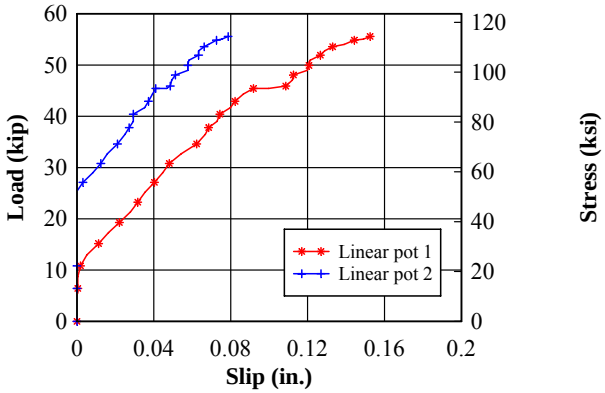

Load-Displacement
SS_20_180_35_3 vs. SS_20_180_35_4

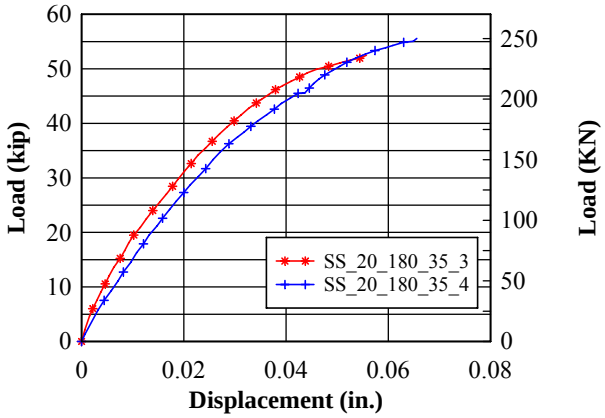

Stress-Strain
SS_20_180_35_3 vs. SS_20_180_35_4

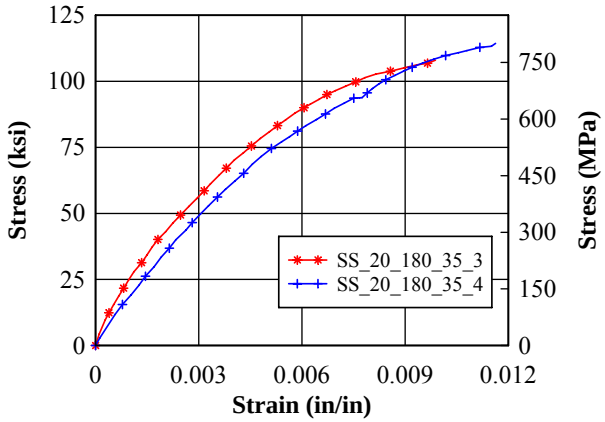

Table 26. Crack patterns, failure modes, load-slip, and stress-strain curves for MMFX hooked bars.

MM_5_90_25_1

Bar rupture

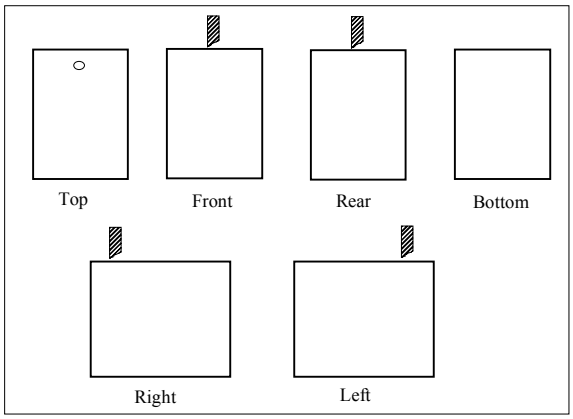

MM_5_90_25_2

Bar rupture

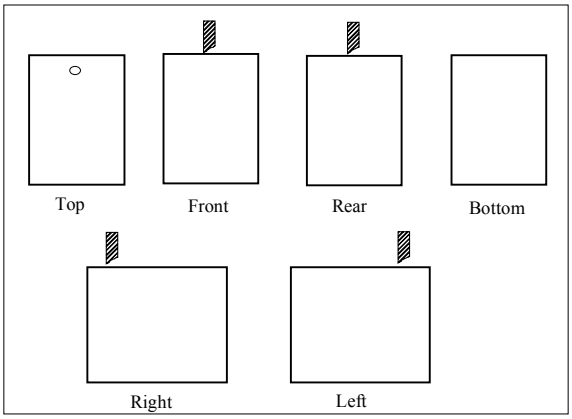

Load-Slip for Linear Pots
MM_5_90_25_1

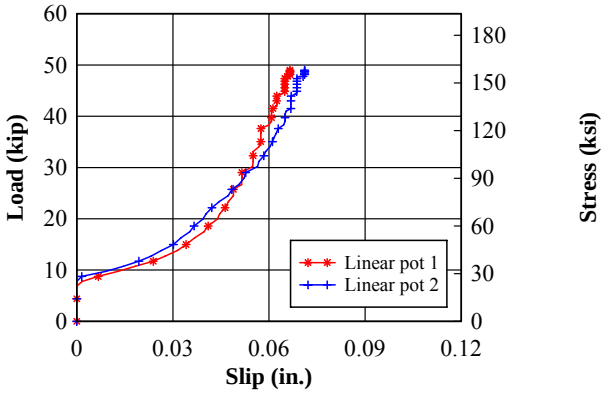

Load-Slip for Linear Pots
MM_5_90_25_2

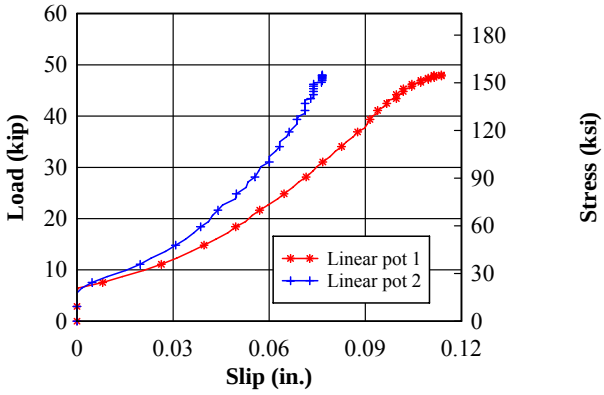

Load-Displacement
MM_5_90_25_1 vs. MM_5_90_25_2

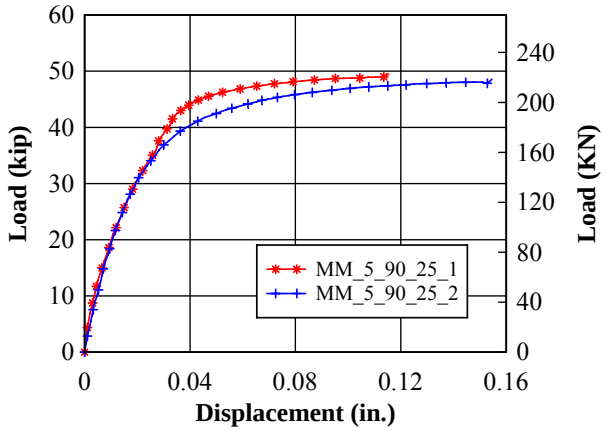

Stress-Strain
MM_5_90_25_1 vs. MM_5_90_25_2

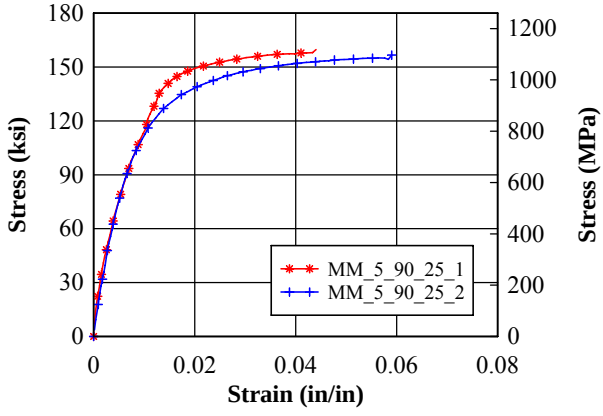

MM_5_90_35_1

Bar yield followed by concrete splitting

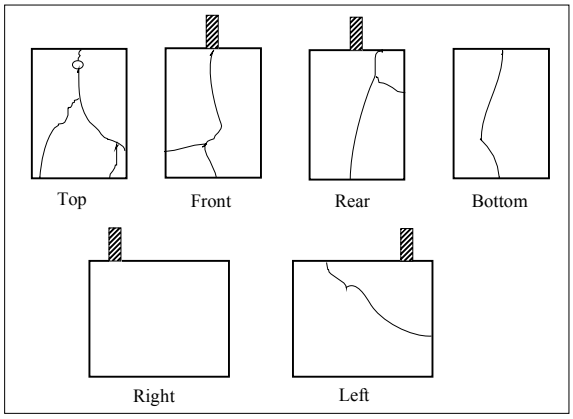

MM_5_90_35_2

Bar yield followed by concrete splitting

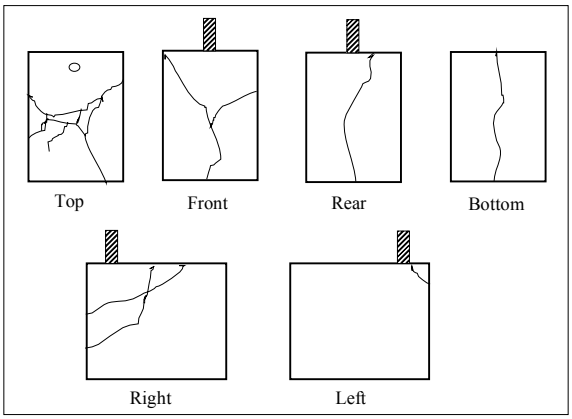

Load-Slip for Linear Pots
MM_5_90_35_1

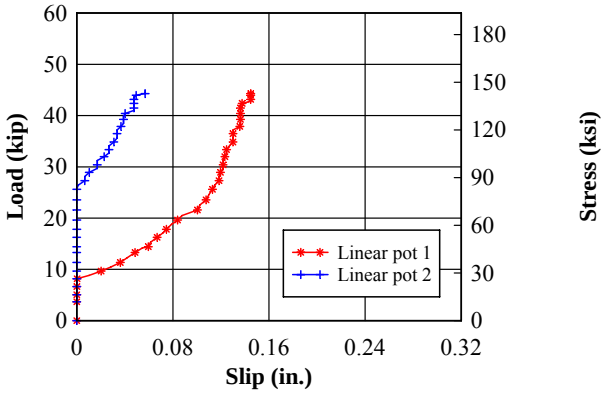

Load-Slip for Linear Pots
MM_5_90_35_2

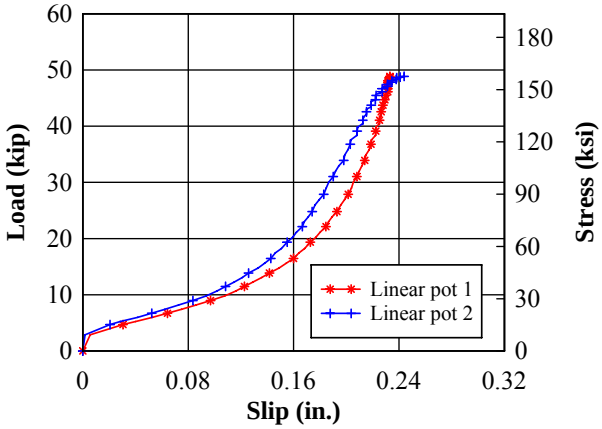

Load-Displacement
MM_5_90_35_1 vs. MM_5_90_35_2

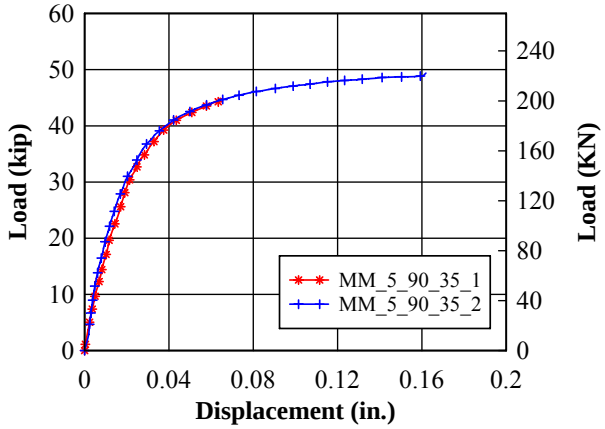

Stress-Strain
MM_5_90_35_1 vs. MM_5_90_35_2

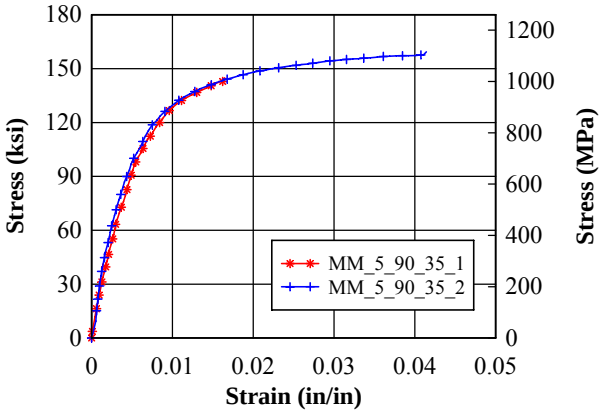

MM_5_180_35_1

Bar yield followed by concrete splitting

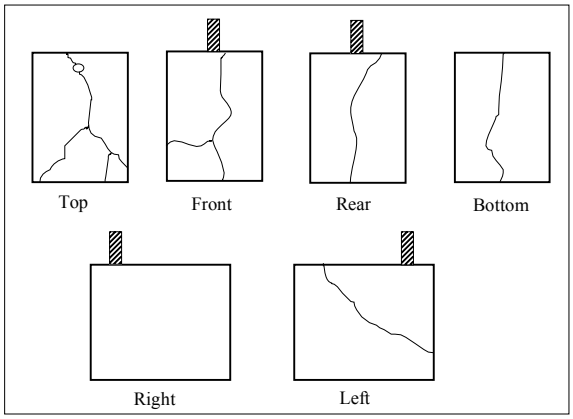

MM_5_180_35_2

Bar yield followed by concrete splitting

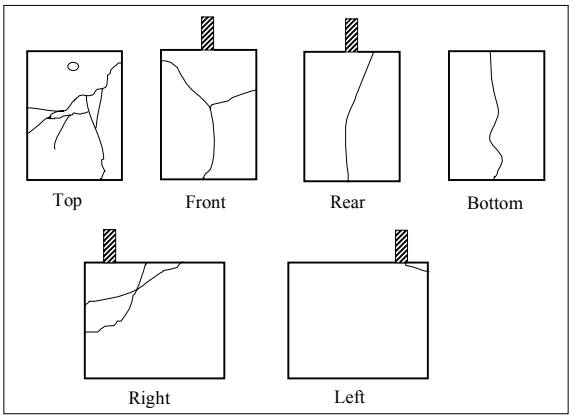

Load-Slip for Linear Pots
MM_5_180_35_1

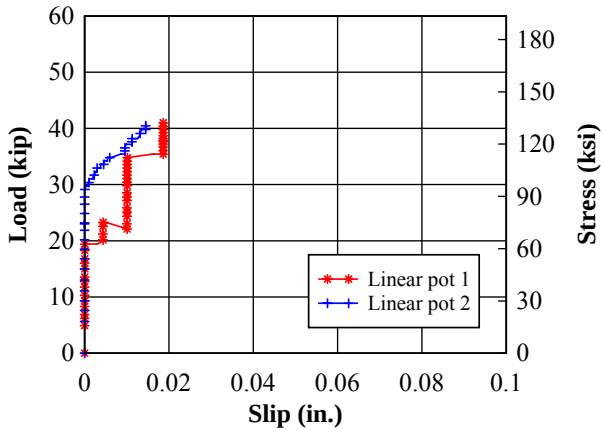

Load-Slip for Linear Pots
MM_5_180_35_2

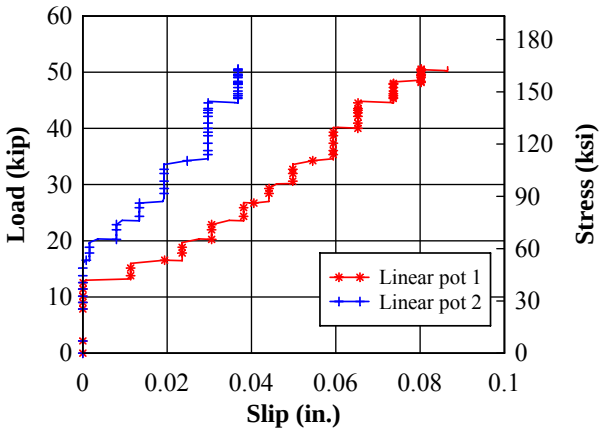

Load-Displacement
MM_5_180_35_1 vs. MM_5_180_35_2

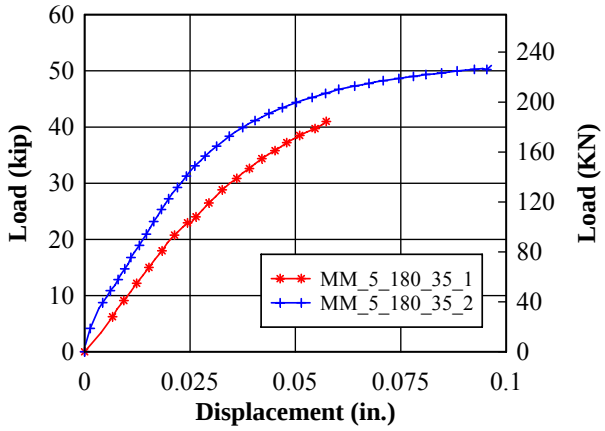

Stress-Strain
MM_5_180_35_1 vs. MM_5_180_35_2

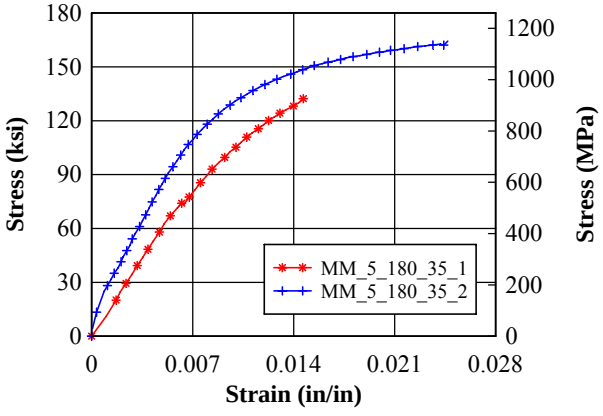

MM_5_180_35_3

Bar yield followed by concrete splitting

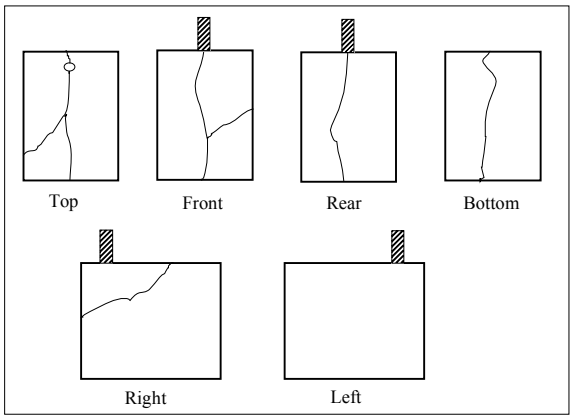

MM_5_180_35_4

Bar rupture

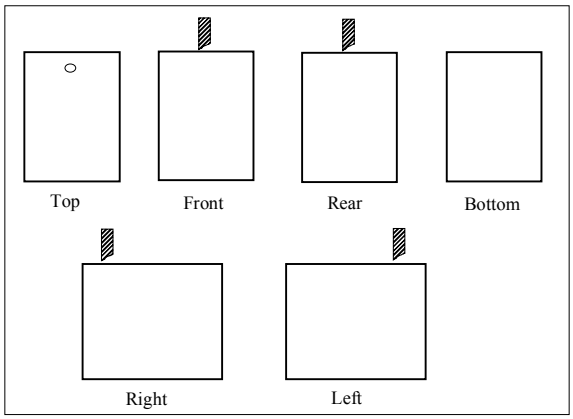

Load-Slip for Linear Pots
MM_5_180_35_3

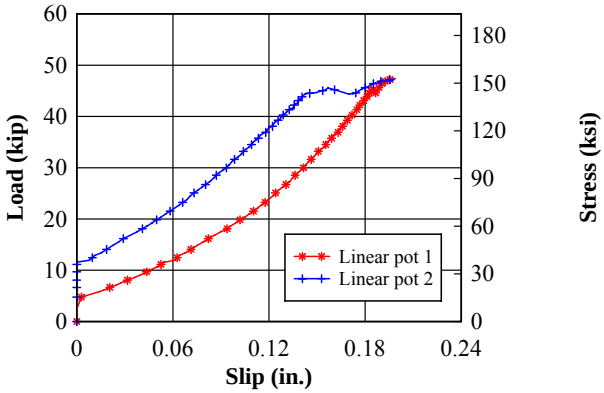

Load-Slip for Linear Pots
MM_5_180_35_4

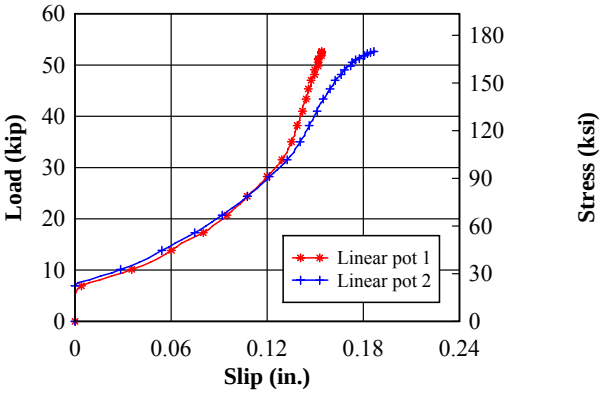

Load-Displacement
MM_5_180_35_3 vs. MM_5_180_35_4

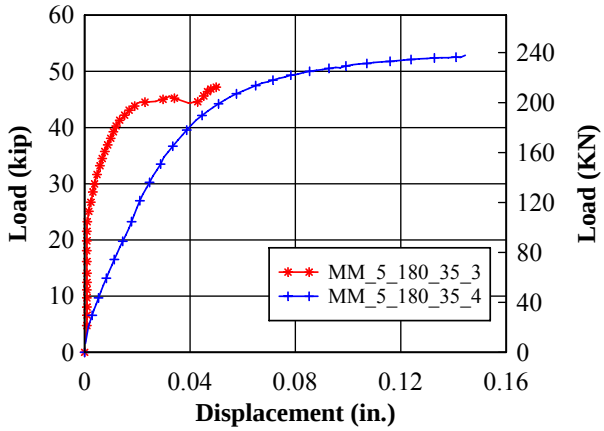

Stress-Strain
MM_5_180_35_3 vs. MM_5_180_35_4

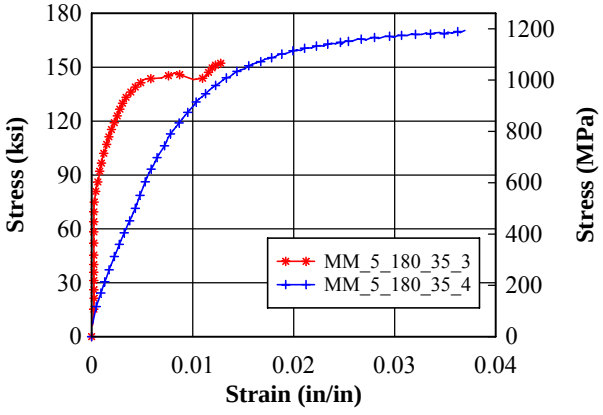

MM_7_90_25_1

Concrete splitting

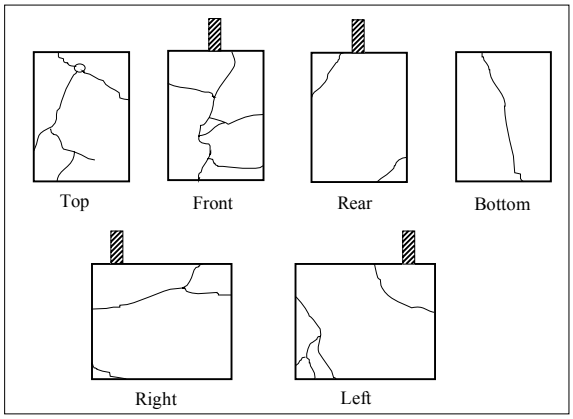

Load-Slip for Linear Pots
MM_7_90_25_1

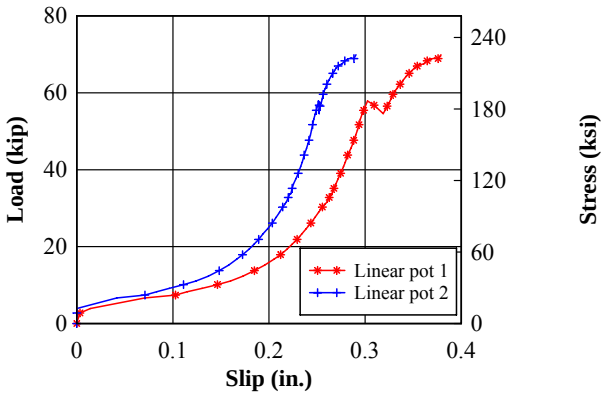

Load-Slip for Linear Pots
MM_7_90_25_2

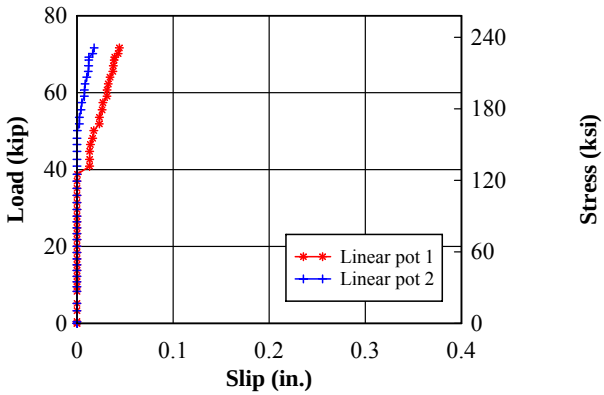

Load-Displacement
MM_7_90_25_1 vs. MM_7_90_25_2

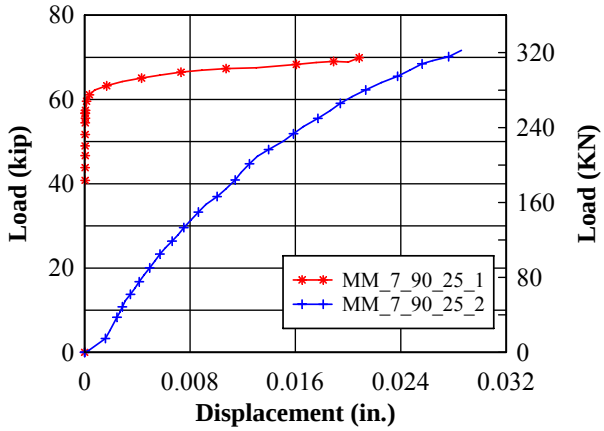

Stress_Strain
MM_7_90_25_1 vs. MM_7_90_25_2

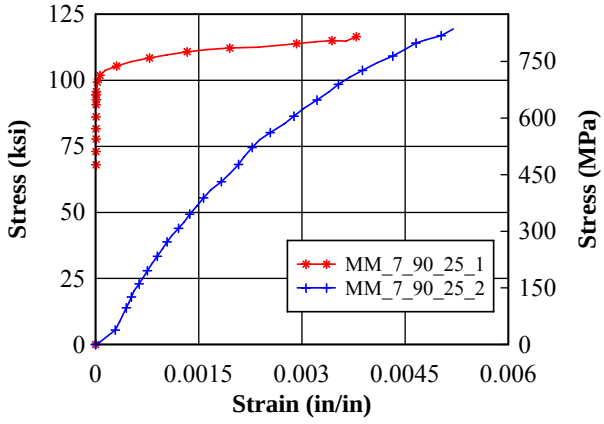

MM_7_90_35_1

Bar cast out of position

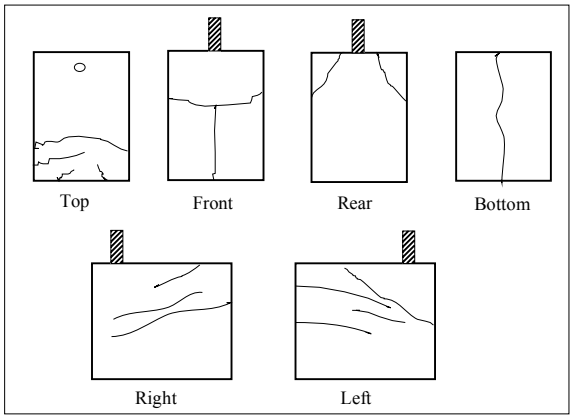

MM_7_90_35_2

Bar cast out of position

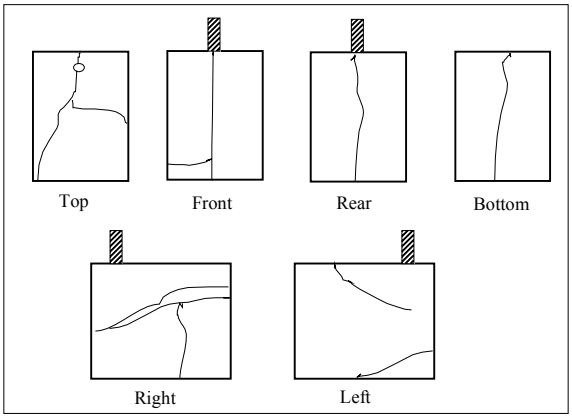

Load-Slip for Linear Pots
MM_7_90_35_1

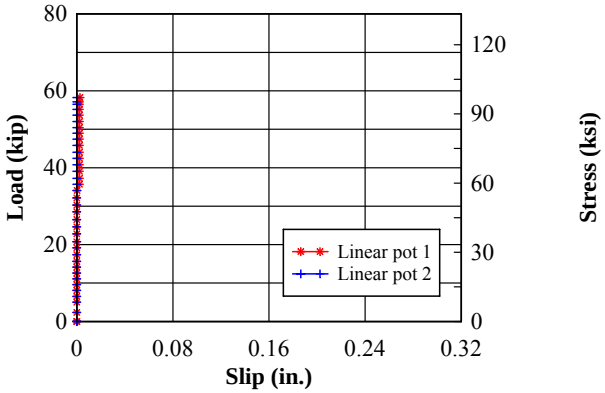

Load-Slip Comparison
MM_7_90_35_2

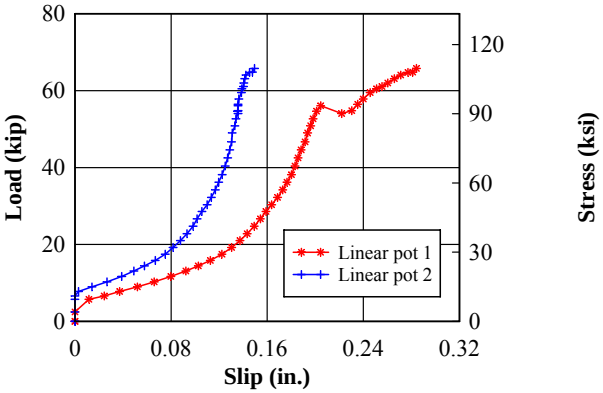

Load-Displacement
MM_7_90_35_1 vs. MM_7_90_35_2

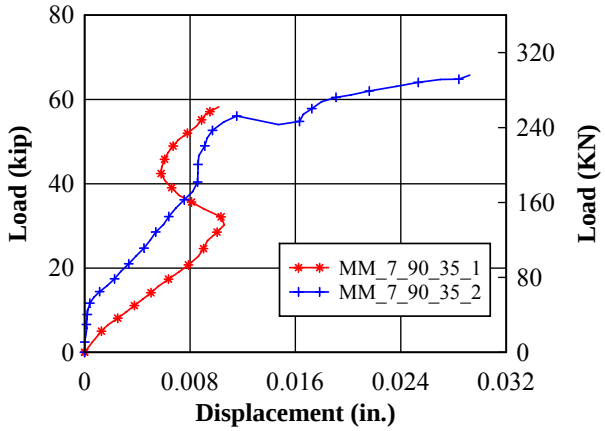

Stress-Strain
MM_7_90_35_1 vs. MM_7_90_35_2

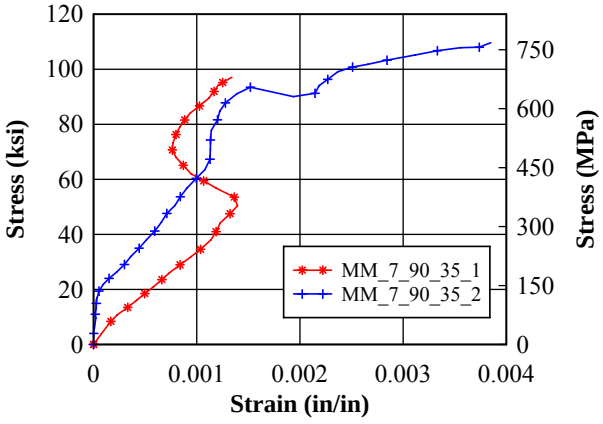

MM_7_90_35_3

Concrete splitting

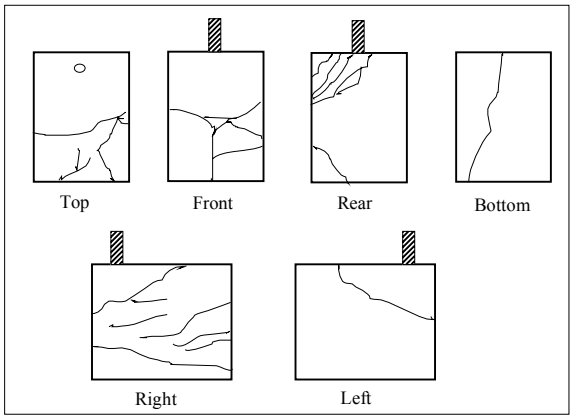

MM_7_90_35_4

Bar yield followed by concrete splitting

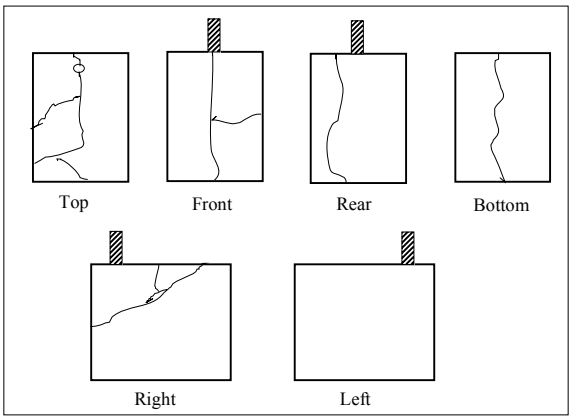

Load_Displecement

MM_7_90_35_3 vs. MM_7_90_35_4

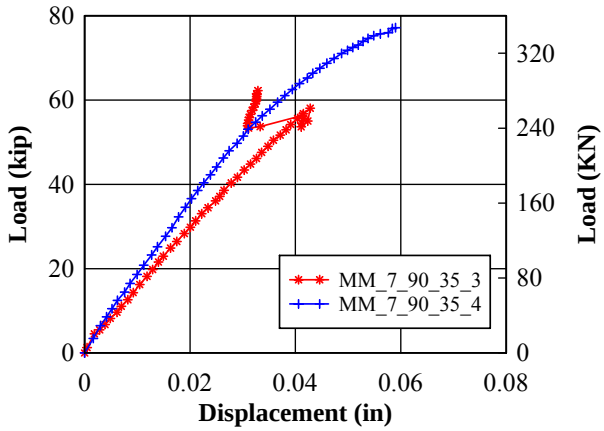

Stress-Strain

MM_7_90_35_3 vs. MM_7_90_35_4

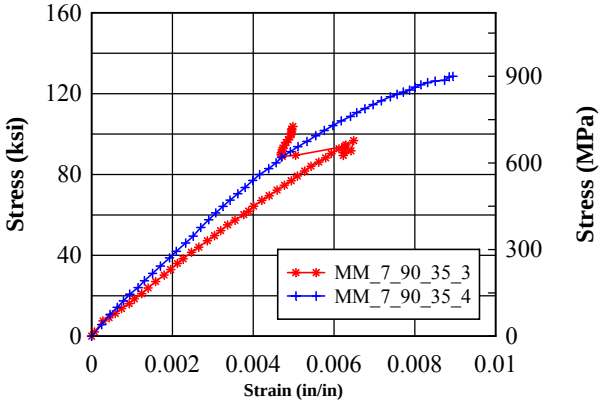

MM_7_180_35_1

Concrete Splitting

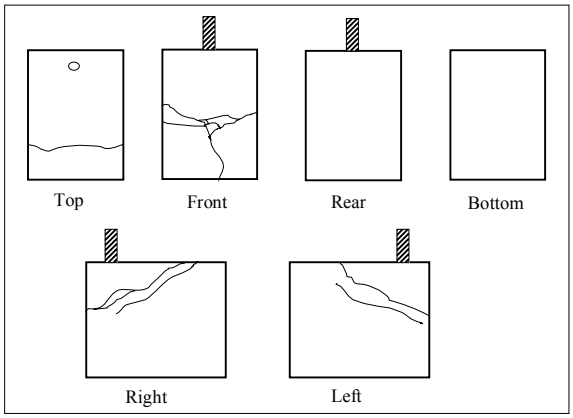

MM_7_180_35_2

Bar yield followed by concrete splitting

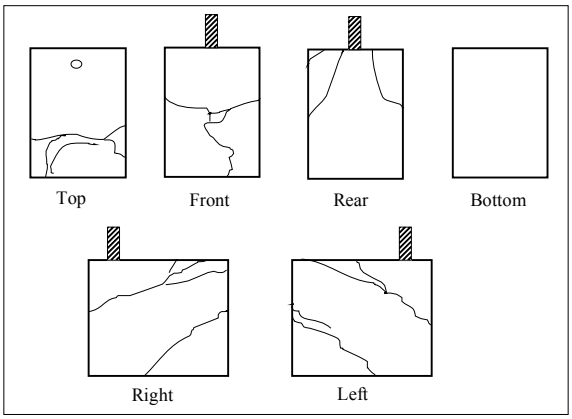

Load-Slip for Linear Pots
MM_7_180_35_1

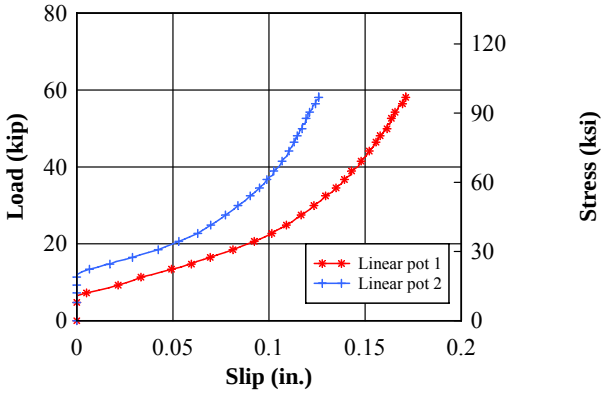

Load-Slip for Linear Pots
MM_7_180_35_2

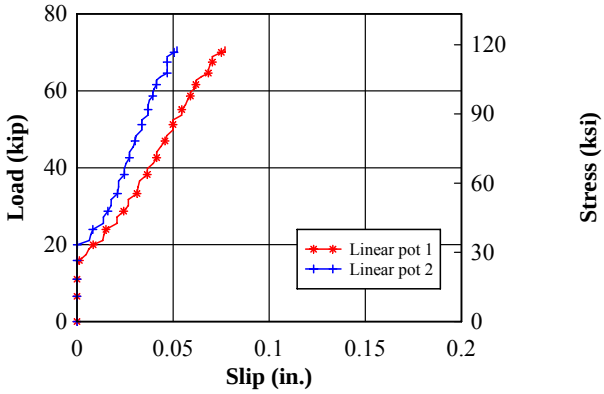

Load-Displacement
MM_7_180_35_1 vs. MM_7_180_35_2

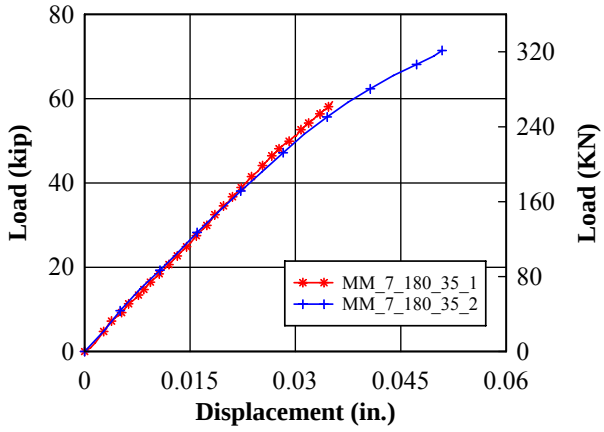

Stress-Strain
MM_7_180_35_1 vs. MM_7_180_35_2

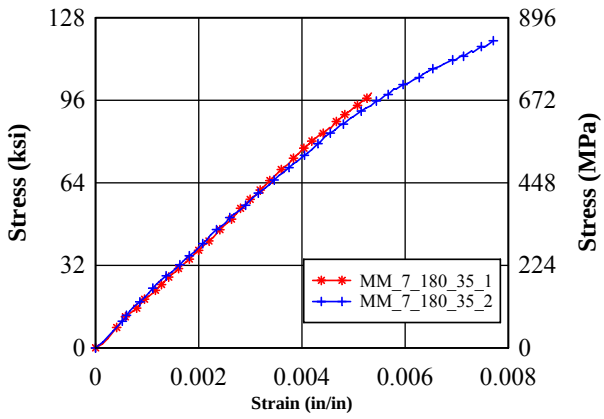

MM_7_180_35_3

Concrete Splitting

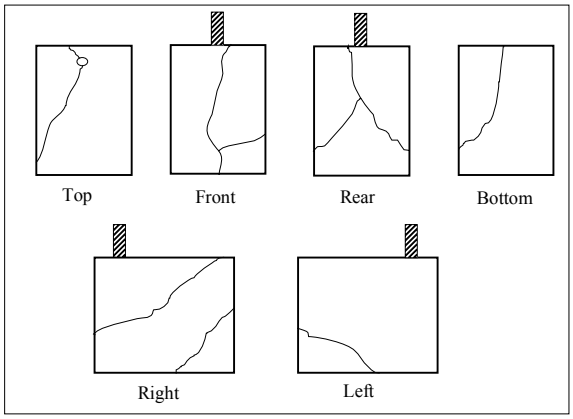

MM_7_180_35_4

Bar yield followed by concrete splitting

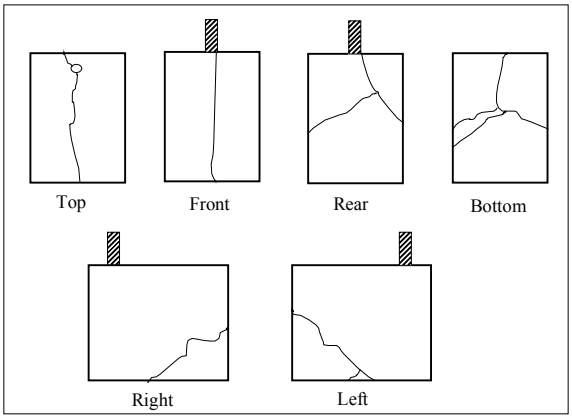

Load-Slip for Linear Pots
MM_7_180_35_3

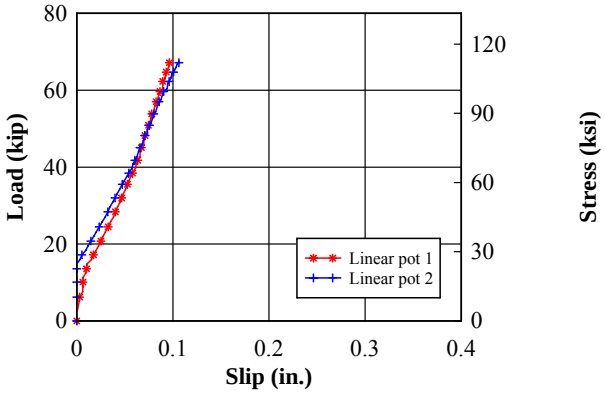

Load-Slip for Linear Pots
MM_7_180_35_4

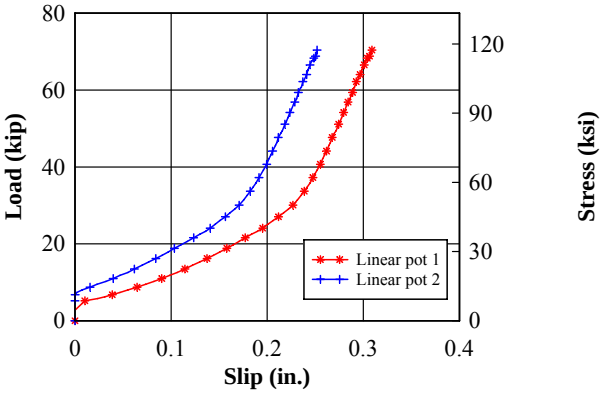

Load-Displacement
MM_7_180_35_3 vs. MM_7_180_35_4

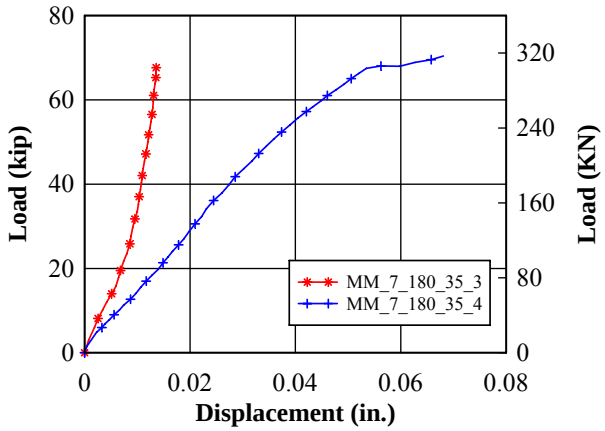

Stress-Strain
MM_7_180_35_3 vs. MM_7_180_35_4

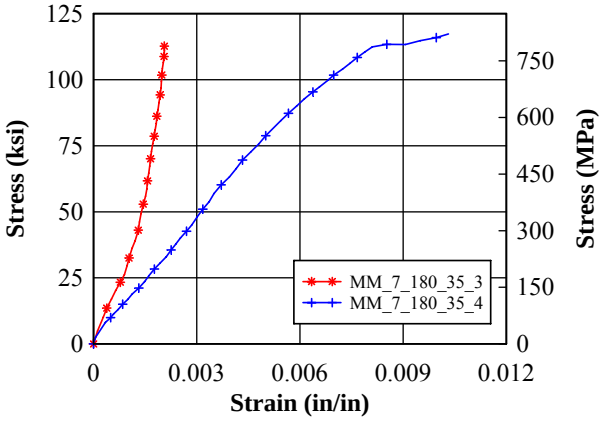

APPENDIX C

Two fully confined tests were conducted on MMFX bars. Figure 52 shows the test setup. A single #6 bar was embedded in the reinforced slab as shown. The slab for test 1 was constructed with concrete that had an average strength of 7251 psi when tested at 33 days. The slab for test 2 had an average strength of 6572 psi when tested at 29 days. The embedment provided was calculated according to ACI 318-02 section 12.5 assuming f'_c = 6000 psi and a yield strength of f_y = 120 ksi, which resulted in a development length of approximately 16.3 in. after the application of the appropriate reduction factors. Because the bar was embedded in a continuous slab with very large cover, it was decided to use a smaller development length since the goal at that time was to determine the actual development length and not to test the applicability of the ACI equation for MMFX hooked bars. Therefore, an embedment of 14 in. was selected as development length for the #6 90^0 hooked MMFX bars.

The bar was tested using two structural steel wide-flange shapes spanning between supports placed near the edge of the slab. The hydraulic jack was placed on the frame and the bar was secured with a strand chuck for a 0.6-in. diameter prestressing strand. Hydraulic pressure was applied until the bar ruptured.

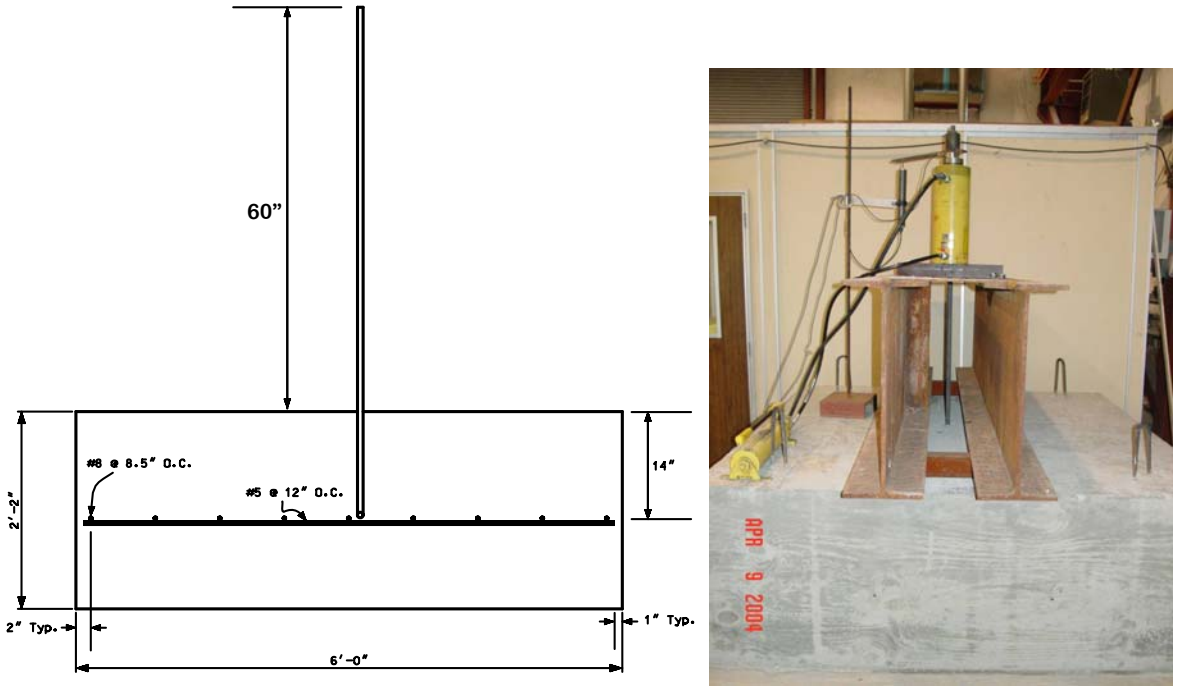

(a) (b)

(c)

Figure 52. Confined test setup (a) schematic, (b) end view photo, and (c) elevation photo.

Load was measured with a load cell mounted between the jack and chuck. Displacement was measured with an LVDT placed on the end of the bar with reference to the surface of the concrete. The resulting gage length for the elongation measurement was approximately 55 inches.

Figure 54 shows the load displacement relationship for the two tests. The load-displacement relationship remains linear up to the proportional limit at approximately 120 ksi. Beyond the proportional limit, bar test 1 and 2 reached an ultimate stress of 235 ksi and 190 ksi, respectively. Bar test 2 was paused for several minutes during loading, which may have affected the results.

The development length used was lower than that calculated by the ACI equation for a 90^0 hook. However, the bar was fully developed (ruptured) even with the lower embedment and despite the fact that the yield strength used to calculate the development length was 120 ksi in contrast to the actual ultimate tensile strength of the bars which was approximately 190 ksi and 235 ksi.

Figure 53. Bar condition after test (a) spalled concrete around base of bar and (b) rupture surface of bar.

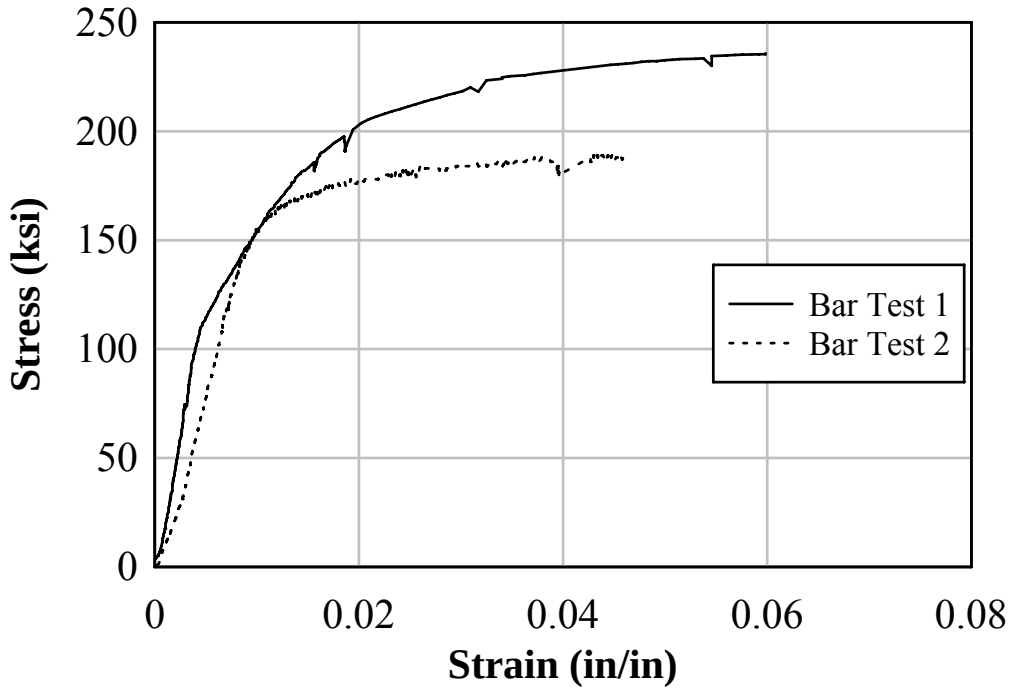

Figure 54. Load displacement of bar tests.